Resonant Inverter configurations for All-Metal Induction Cooking Applications

A Thesis
Submitted in partial fulfillment of the requirements
for the award of the degree of

Doctor of Philosophy
in
Electrical Engineering

By
Khatroth Srinivas
(Roll No. 717015)

Supervisor
Dr. S. Porpandiselvi
Associate Professor

Department of Electrical Engineering
National Institute of Technology Warangal
Warangal - 506004, Telangana State, India
June - 2022

Dedicated to

My beloved Parents and family

Shri Shivaram & Smt. Sakunabai

Shri Lingoji & Smt. Lalitha

APPROVAL SHEET

This thesis entitled **"Resonant Inverter configurations for All-Metal Induction Cooking Applications"** by **Khatroth Srinivas** (Roll No. 717015) is approved for the degree of Doctor of Philosophy.

Examiner

.....

.....

.....

Supervisor

Dr. S. Porpandiselvi
Associate Professor

Chairman

Dr. N Vishwanathan

Professor

EED, NIT Warangal

Date:.....

Department of Electrical Engineering
National Institute of Technology Warangal
Warangal - 506004, Telangana State, India

DEPARTMENT OF ELECTRICAL ENGINEERING

NATIONAL INSTITUTE OF TECHNOLOGY WARANGAL

CERTIFICATE

This is to certify that the thesis titled **"Resonant Inverter configurations for All-Metal Induction Cooking Applications"**, submitted by **Mr. Khatroth Srinivas** (Roll No. 717015), is a bonafide work submitted to National Institute of Technology Warangal in partial fulfilment of the requirements for the award of the degree of **Doctor of Philosophy** in Electrical Engineering. To the best of my knowledge, the work incorporated in this thesis has not been submitted elsewhere for the award of any degree.

Dr. S. Porpandiselvi
(Thesis Supervisor)
Assistant Professor
Department of Electrical Engineering
National Institute of Technology
Warangal-506004

Date: August 23,2022

Place: Warangal

DECLARATION

This is to certify that the work presented in the thesis entitled **"Resonant Inverter configurations for All-Metal Induction Cooking Applications"** is a bonafide work done by me under the supervision of **Dr. S. Porpandiselvi**, Assistant Professor Department of Electrical Engineering, National Institute of Technology, Warangal, India and was not submitted elsewhere for the award of any degree.

I declare that this written submission represents my ideas in my own words and where others' ideas or words have been included, I have adequately cited and referenced the original sources. I also declare that I have adhered to all principles of academic honesty and integrity and have not misrepresented or fabricated or falsified any idea / data / fact / source in my submission. I understand that any violation of the above will be a cause for disciplinary action by the Institute and can also evoke penal action from the sources which have thus not been properly cited or from whom proper permission has not been taken when needed.

Date: August 23,2022
Please: Warangal

Khatroth Srinivas
(Research Scholar - 717015)

ACKNOWLEDGMENTS

It gives me immense pleasure to express my deep sense of gratitude and thanks to my supervisor **Dr. S. Porpandiselvi**, Assistant Professor, Department of Electrical Engineering, National Institute of Technology Warangal, for her invaluable guidance, support, and encouragement. She has shown me the imaginative side of this wonderful and potential research area. Her guidance and encouragement have helped me to overcome the difficulties encountered in research as well as in my life.

I wish to express my sincere thanks to **Prof. N. V. Ramana Rao,** Director, NIT Warangal for his support and encouragement.

I am very much thankful to **Prof. M. Sailaja Kumari**, Head, Department of Electrical Engineering for her constant encouragement and support.

I also express my sincere thanks to **Prof. N. Vishwanathan** and **Prof. V. T. Somasekhar**, Former Heads, Department of Electrical Engineering for their valuable suggestions and support.

I take this opportunity to thank all my Doctoral Scrutiny Committee members, **Prof. N. Vishwanathan**, Department of Electrical Engineering, **Prof. D. M. Vinod Kumar**, Department of Electrical Engineering and **Dr. R. S. Selvaraj,** Associate Professor, Department of Mathematics for their constructive suggestions and excellent advice during the progress of this research work.

I also appreciate the encouragement from teaching and non-teaching members of Department of Electrical Engineering. They have always been encouraging and supportive.

I convey my special thanks to contemporary research scholars Mr. Madhu Babu S, Mr. Rambabu, Dr. Kasi Ramakrishna, Dr. Satyakar, Ms. Mounika Dasohari, Mr. K. Hemasundara Rao, Mr. G. Ramesh, Mr. Suman Dhara and Mr. Punna Srinivas for being with me during my research journey.

I acknowledge my gratitude to all my teachers and colleagues at various places for supporting and co-operating with me to complete the work.

I express my deep sense of gratitude and reverence to my beloved parents **Shri. Khatroth Shivaram** & **Smt. Sakunabai**, my wife **Smt. Jayasree**, my sons **Hitanshusai** & **Sheehan**, parent-in-laws **Shri. Lingoji** & **Smt. Lalitha**, my brother **Shri. Devidas**, my sister in

law **Shri. Jayasudha** for their sincere prayers, blessings, constant encouragement, shouldering the responsibilities and moral support rendered to me throughout my life, without which my research work would not have been possible. I heartily acknowledge all my relatives for their love and affection towards me.

Above all, I express my deepest regards and gratitude to **"ALMIGHTY"** whose divine light and warmth grace that showered upon me the perseverance, inspiration, faith and enough strength to keep the momentum of work high even at tough moments of research work.

Khatroth Srinivas

ABSTRACT

Induction heating (IH) applications are widely used in industrial, domestic, and medical domains due to the unique characteristics of IH such as contact-less heating, non-polluting nature and high efficiency. Advances in key supporting technologies such as switching devices, digital power control, and magnetic components have led to the advent of high-performance and higher-efficiency systems that outperform traditional heating systems. Induction heating systems are also simple and economical compared to conventional heating methods. Multiple-load domestic IH systems are becoming very popular, due to reduced number of component count, independent load power regulation, and greater conversion efficiencies.

In this thesis, various converter topologies used in IH have been discussed. This work presents multi-stage and single-stage converter topologies for multiple load, different material vessels domestic IH applications. Further, the major challenges associated with non-magnetic material induction cooking, and the possible solutions to address these challenges through higher operating frequencies, and with various power control techniques have been discussed.

This thesis proposes three converter configurations for multiple load and different material vessels domestic IH applications. The objectives are to provide high power conversion efficiency, reduced component count, powering multiple loads with independent power control, reduced size of reactive elements, power factor correction and configurations suitable for different material domestic IH applications.

The first proposed inverter configuration is a cascaded full-bridge resonant inverter configuration for different material vessel induction cooking (IC) applications. It powers three different material loads of iron, steel and aluminium. In this configuration, three different induction heating loads are simultaneously operated at their respective resonant frequencies. This inverter configuration features simultaneous heating of vessels of three different materials with independent power control. The output power control is achieved with asymmetric duty cycle control. This configuration provides an overall efficiency of 92 % at maximum duty cycle and is suitable for high power applications also. This configuration can be extended to more than three IH loads by the addition of more legs in the bridge circuit. It is suitable for domestic as well as commercial IH applications.

The second proposed inverter configuration is a three leg multi-load resonant inverter

for domestic IH which can heat vessels made of three different materials. In this configuration, three legs of the inverter are operated at three different frequencies which are suitable for iron, steel and aluminium vessels respectively. IH loads are operated at frequencies that are closer to resonant frequencies. Pulse frequency control approach is used to control the load powers. This configuration provides independent load power control. It uses only two switching devices per load. This inverter has lowest component count compared to above mentioned inverter configurations. It offers high efficiency and eliminates the use of electro mechanical switches. The overall efficiency of this inverter is greater than 93 % at maximum duty cycle. This inverter is suitable for high power applications also. It can be extended to more than three IH loads by the addition of more inverter legs.

The third proposed converter configuration is a single-stage AC-AC resonant converter for different material vessel domestic IH applications. This converter offers input power factor correction and boost operation with a multi-load integrated bridge inverter design. The inverter legs in this configuration operate at two different frequencies to power domestic IH loads of steel and aluminium vessels. This configuration provides independent power control with pulse frequency modulation (PFM) technique. It eliminates the use of electro-mechanical switches and offers the advantages of low component count compared to multi-stage inverter configurations. This inverter is suitable for high power applications also. This inverter configuration can be extended to more than three IH loads by including additional legs.

All the proposed converter configurations have been found to be suitable for multiple loads comprising different material cooking vessels used in domestic as well as commercial IH applications. These converter configurations have been studied thoroughly, designed and simulated. Hardware prototypes have been implemented for all three configurations. Experimental results have been validated with simulation results.

Contents

List of Figures

List of Tables

Abbreviations & Symbols

List of Abbreviations

AC	Alternating Current
ADC	Asymmetric Duty Cycle
AVC	Asymmetric Voltage Cancellation
CCM	Continuous Conduction Mode
C	Capacitor
DCM	Discontinuous Conduction Mode
DC	Direct Current
DSP	Digital Signal Processor
DST	Department of Science & Technology
D	Duty Ratio or Duty Cycle
EMI	Electromagnetic Interface
FBSRC	Full-Bridge Series Resonant Converter
FB	Full-Bridge
FPGA	Field-Programmable Gate Array
GoI	Government of India
HBSRC	Half-Bridge Series Resonant Converter
HB	Half-Bridge
HFAC	High Frequency Alternating Current

HF	High Frequency
HID	High Intensity Discharge
HS	Hard Switching
IC	Induction Cooking
IH	Induction Heating
JFET	Junction-gate Field-Effect Transistor
LAM	Load-Adaptive Modulation
LF	Low Frequency
LLC-RC	LLC Resonant Converter
L	Inductor
MF	Medium Frequency
PDM	Pulse Density Modulation
PFC	Power Factor Correction
PFM	Pulse Frequency Modulation
PS	Phase Shift
PWM	Pulse Width Modulation
QSW	Quasi Square Wave
Q	Quality Factor
SiC	Silicon Carbide
SMPC	Switched Mode Power Converter
SPR	Series-Parallel Resonance
SRC	Series Resonant Converter
SS	Soft Switching

T	Time period
UFAC	Utility Frequency Alternating Current
VF	Variable Frequency
ZVS	Zero Voltage Switching

List of Symbols

α_l	Control angle
δ	Skin depth
μ	permeability of the material
Φ_l	Phase angle
ρ	specific resistivity
C	Capacitor value
C_b	Boost capacitor
C_{rh}	High frequency load resonant capacitor
C_{rl}	Low frequency load resonant capacitor
C_{rm}	Medium frequency load resonant capacitor
C_s	Sunber capacitor
D	MOSFET body diode
D_{hl}	High frequency leg duty cycle
D_l	Low frequency leg duty cycle
D_{ml}	Medium frequency leg duty cycle
D_{rh}	Rectifier upper Diode
D_{rl}	Rectifier lower Diode
f_{rh}	High frequency load resonant frequency

f_{rl}	Low frequency load resonant frequency
f_{rm}	Medium frequency load resonant frequency
G	Voltage Gain
h_f	High-frequency
I	Rms current
i	Instanteous current
i_0	Output Current
I_{AC}	AC Current
i_{hf}	High frequency load current
i_{lf}	Low frequency load current
i_{mf}	Medium frequency load current
I_s	Source Current
L	Inductor value
L_b	Boost inductor
l_f	Low-frequency
L_{1lf}	Iron vessel equivalent inductance
L_{2mf}	Steel vessel equivalent inductance
L_{3hf}	Aluminium vessel equivalent inductance
L_{eq}	Equivalent inductance
L_{hf}	High frequency load equivalent inductance
L_{lf}	Low frequency load equivalent inductance
L_{mf}	Medium frequency load equivalent inductance
M	Mutual Inducatance

max	Maximum
P_{oh}	Aluminium load power
P_{ol}	Iron load power
P_{om}	Steel load power
R_{1lf}	Iron vessel equivalent resistance
R_{2mf}	Steel vessel equivalent resistance
R_{3hf}	Aluminium vessel equivalent resistance
R_{eq}	Equivalent Resistance
R_{hf}	High frequency load equivalent resistance
R_{lf}	Low frequency load equivalent resistance
R_{mf}	Medium frequency load equivalent resistance
S	MOSFET switch
t	time instant
t_d	dead time
v	Voltage
v_b	Dc-link voltage
v_o	Output voltage
V_{01}	Cascaded inverter Output Voltage
V_{AC}	AC Voltage
V_{dc1}	DC Voltage source-1
V_{dc2}	DC Voltage source-2
V_{DC}	DC Source Voltage
v_{ohf}	High frequency voltage component

v_{olf}	Low frequency voltage component
v_{omf}	Medium frequency voltage component
V_s	Source Voltage
X_{C1lf}	Low frequency capacitive reactance
X_{C2mf}	Medium frequency capacitive reactance
X_{C3hf}	High frequency capacitive reactance
X_{L1lf}	Low frequency inductive reactance
X_{L2mf}	Medium frequency inductive reactance
X_{L3hf}	High frequency inductive reactance
Z_{1lf}	Low frequency impedance
Z_{2mf}	Medium frequency impedance
Z_{3hf}	High frequency impedance
Z_{hf}	High frequency load equivalent impedance
Z_{lf}	Low frequency load equivalent impedance
Z_{mf}	Medium frequency load equivalent impedance

Chapter 1

Introduction

Chapter 1

Introduction

1.1 Introduction

Induction heating (IH) technology which was primarily developed for industrial applications has progressed to other domains such as residential, commercial and biomedical fields [1, 2]. Advances in key supporting technologies which include power electronic switching devices, converter configurations, digital power control, and magnetic components have led to the advent of high-performance and higher-efficiency systems that outperform traditional heating technologies. The induction targets are heated by two physical phenomena: eddy currents and magnetic hysteresis [3]. Eddy currents flowing through the resistance of the IH target generate heat due to Joule effect. In IH process, this is the main heat generation mechanism. Hysteresis effect also creates additional heat in ferromagnetic materials. The normal operating frequencies of these systems will range from line frequency to a few MHz. It has many advantages over traditional heating methods (such as gas and oil-fired furnaces), in terms of faster heating, faster start-up, higher energy savings, cleanliness, safety, and efficient control. The development of numerical and computational techniques, as well as the reduced cost of these systems, has led to widespread use of IH in a variety of processes and applications over the last few years [4, 5].

Heat is generated in the work piece due to I^2R losses when high frequency currents are conducted through a coil wound over an electrically conductive work piece, where R is the resistance of the work piece and I is high frequency current. In domestic applications, the conductive materials might be magnetic (such as iron or steel) or non-magnetic (such as copper or aluminium). In magnetic materials, hysteresis losses cause additional heating, but their contribution is small when compared to eddy current heating.

Eddy currents are induced on the work piece's surface with a penetration depth δ, that depends on the frequency of the induced currents. Penetration depth is expressed as $\delta = \sqrt{\frac{\rho}{\pi \mu f_s}}$ where, ρ is electrical resistivity, μ is magnetic permeability of the vessel material, and f_s is inverter switching frequency. Conduction from the surface transfers heat to the rest of the work

piece.

Advantages of induction heating:

➢ The induction heating approach is clean. It emits no smoke, fumes, dirt, ash, etc.

➢ As there are no open flames and no chance of gas leakage, this approach increases the safety of working.

➢ Compared to other heating methods, it provides a greater efficiency (90 % to 96 %) .

➢ As the heating coil will not become hot while heating the load, very large power densities and high temperature heating can be generated.

➢ Because of the high power densities and absence of thermal inertia, IH method heats the induction target (work piece) faster, reducing heating times and eliminating heat loss.

➢ It provides good control of load temperature. Precise temperature control is also possible.

Limitations of induction heating:

➢ Non sinusoidal currents are drawn from the supply which injects harmonics into the power lines which may lead to

- Failure of protective devices
- Interference with communication lines
- Audible noise from transformer

➢ Poor power factor due to inductive load.

➢ Output power dependability on the type of the material used

➢ Human beings exposed to strong magnetic fields which may cause health hazards.

Applications of induction heating:

➢ Surface hardening

➢ Melting of metals

➢ **Induction Cooking (IC)**

➢ Induction annealing and normalizing

➢ Induction brazing

➢ Induction bonding

➢ Induction forging

➢ Induction wire and cable heating

➢ Induction straightening

1.2 Power Converters for Induction Heating

Induction heating converter configurations are divided into two types based on the power conversion stages as

i. Multi-stage power converters (UFAC-DC-HFAC)

ii. Single-stage power converters (UFAC- HFAC)

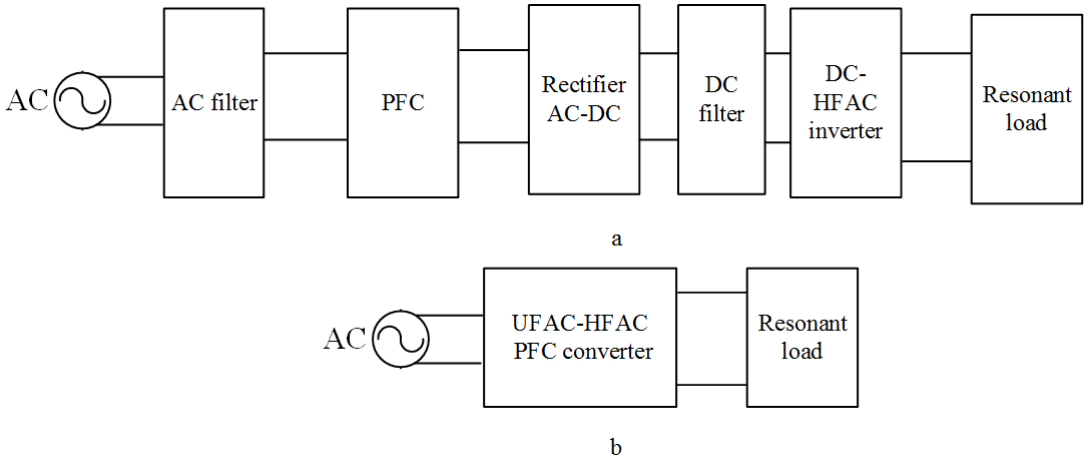

Figure 1.1: Structure of multi-stage and single-stage converters for IH applications
(a) Multi-stage power conversion
(b) Single-stage power conversion

The block diagram of the multi-stage power converter is shown in Figure. 1.1a. It contains an AC filter, a power factor correction unit, rectifier for conversion of utility frequency alternating current (UFAC) supply to DC, DC filter, and inverter for conversion of DC to high frequency alternating current (HFAC). In multi-stage power converter topologies, most commonly used inverter configurations are the single-switch, half-bridge, and full-bridge resonant inverters. However the overall efficiency of the system is low because of more number of conversion stages and cost and size are increased due to more number of components.

In the recent past, single-stage resonant converter topologies were also frequently used to convert an UFAC to HFAC without using any intermediate power conversion stages. The block

diagram of the single-stage power converter topology is shown in Figure. 1.1b. It contains only one power conversion stage. These single-stage converters offer reduced component count and higher efficiency.

1.3 Resonant Converters for Induction Heating

Resonant converters have been part of active research in power electronics field. It offers the advantages of soft switching, improved power factor and high efficiency. They are widely used in high-voltage power supply, capacitor charging circuits, power factor correction units, inductive power transfer etc.

The second-order series and parallel resonant circuits, as well as third-order LLC series parallel resonant circuit are the most popular resonant tank topologies. The series resonant circuits are used in voltage source inverters and by operating the circuit above the resonant frequency, zero voltage switching (ZVS) is ensured with snubber capacitors [6], [7]. Similarly parallel-resonant circuits [8], are used widely in current source inverters to achieve zero current switching (ZCS).

IH loads have a low power factor typically, 0.1 to 0.3 lagging. Hence, resonant inverters are good choices for IH applications, where IH load is resonated in order to compensate the reactive power requirement. Resonant inverters are designed to supply the induction coil with appropriate power at the required frequency. For heating and meting applications, frequencies of a few hundred Hz to a few kHz are used. Typical frequency range for medium power applications can range from 20 kHz to 500 kHz. For this frequency range, power MOSFETs are the preferred devices. Melting applications require higher power. Hence, SCRs or GTOs are used as switching devices. Resonant inverters improve efficiency and also reduce EMI issues.

Types of Resonant Inverters:

The following types of resonant inverters are widely used in IH applications:

i. Series Resonant Inverter: It uses LC series resonant circuit. It is a widely used inverter due to its simple design and superior performance compared to other types of inverters.

ii. Parallel Resonant Inverter: It uses LC parallel resonant circuit. Current source is mostly used with a parallel resonant inverter. The load acts as if it were capacitive in this condition. SCRs can be utilized as switching devices in high-power applications. SCRs are operated with load commutation.

iii. Series-Parallel Resonant Inverter: This inverter has positive features of both series and parallel resonant inverters. This type of inverters has limited applications since the analysis and control is slightly difficult due to multiple resonant frequencies.

Series resonant inverter is used in the proposed inverter configurations described in this thesis.

1.3.1 Overview of Domestic Induction Heating

Induction cooking is an application of induction heating, which converts electrical energy into heat in the vessels kept over the IH coil based on the principle of electromagnetic induction [9]. The power conversion stages of an IH system are shown in Fig. 1.2a. High frequency AC current supplied by the high frequency inverter flows through IH coil. The IH coil produces a high-frequency electromagnetic field which induces voltage and hence eddy currents in the bottom of the cooking vessel. Hence, the vessel is heated through Joule effect. The heat is generated in the cooking vessel directly. Hence, the system is more efficient. The equivalent circuit of induction heating load may be considered as a series combination of L_{eq} and R_{eq} as shown in Fig. 1.2b, where L_{eq} is the equivalent inductance and R_{eq} is the equivalent resistance referred to IH coil side when the vessel is kept on the cooker [10]. These values depend on the material of the vessel and also vary with switching frequencies.

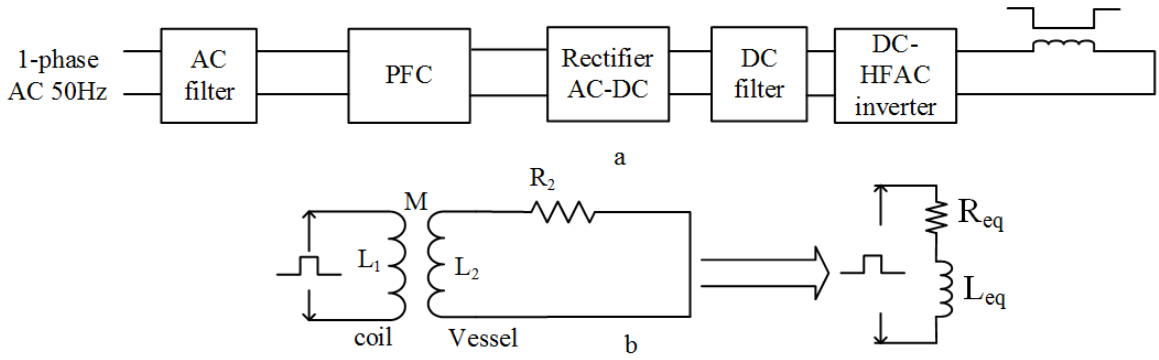

Figure 1.2: Power conversion stages and equivalent circuit of IH load
(a) Power conversion stages of domestic IH system
(b) Equivalent circuit of an IH load

1.3.2 Overview of materials used in domestic induction cookware appliances

Iron (carbon steel), stainless steel, and aluminium are the three most commonly used metals in the manufacturing of cooking appliances. Iron has been in use for a long time and has been the primary choice in the past. However, because of significant chemical interaction of iron with the food items, different types of coatings (porcelain, glass, or enamelware) must be used to inhibit the reaction. However, if the coating's integrity is compromised, the interaction between the food and the steel leads to contamination of food.

Stainless steel is a less chemically reactive material that is often used in cookware. A

combination of steel, chromium, and nickel results in long-lasting, corrosion-resistant material which is believed to be the safest choice for general-purpose cookware. However, one disadvantage of stainless steel is its poor heat conductivity. This causes uneven heat distribution. The difficulty is solved by sandwiching an aluminium plate between two layers of stainless steel plates. This additional process results in higher cost and a more difficult production process.

Aluminium cookware is the most popular and widely used appliance due to its high heat conductivity, low mass, and low cost. Anodized aluminium cookwares are also used as aluminium can stain with acidic foods.

The conventional induction cookers are suitable only for iron and steel material and are not suitable for non-ferromagnetic material like aluminium and copper.

1.4 Motivation

From the literature review on different IH converter schemes, the following observations are drawn:

- Some of the converters available in literature are not capable to power multiple IH loads
- Most of the converters available in literature are suitable only for ferromagnetic IH loads
- Most of the converter configurations use electro-mechanical switches to select the resonant capacitor combinations
- Some of the configurations are lacking of independent power control
- Many of the IH systems use Full bridge diode rectifier for first-stage AC-DC conversion which leads to high component count and low efficiency

Hence, despite the availability of different converter configurations for IH applications, due their limitations listed above, there is enough scope for further research in the area of different material Induction Heating.

1.5 Objectives of the Thesis

This research work focuses on the design of resonant converter configurations for IH applications with the following features:

i Powering multiple IH loads

ii Suitability for different material vessels

iii High power conversion efficiency

iv Low component count

v Soft switching

vi Single stage ac-ac conversion

vii Boost operation and high power factor

viii Independent load power control

1.6 Contribution

Three different inverter configurations have been proposed and implemented and are presented in this thesis. These are summarised as follows

[1] Cascaded Full-Bridge Resonant Inverter Configuration for Different Material Vessel Induction Cooking.
This inverter configuration is capable of powering multiple-loads of iron, steel and aluminium vessels. The advantages of this cascaded inverter are summarized as follows:

i Powers multiple IH loads

ii Suitable for different material vessels

iii Eliminates the use of electro-mechanical switches

iv Low component count

v Overall efficiency is high ($\geq$ 92 %)

vi Independent power control is achieved using asymmetric duty cycle control

vii Proposed scheme can be extended to more than three loads
Only limitation is the requirement of two DC sources.

[2] Frequency Controlled Multi-load Resonant Inverter for Different Material Induction Heating Applications.
It is a three leg inverter which is capable of powering multiple-loads of iron, steel and aluminium vessels:

The advantages of the proposed three leg inverter are

i Suitable for multiple IH loads

ii Suitable for different material vessel domestic induction Cooking

iii Independent power control using pulse frequency control

iv High power conversion efficiency

v Use of only two switching devices per load

vi Eliminates the need for electro-mechanical switches

Hence, it is well suitable for multiple load Induction cooking applications.

[3] Single-Stage Pulse Frequency Controlled AC-AC Resonant Converter for Different Material Vessel Induction Cooking Applications.
This inverter configuration is capable of powering two IH loads of steel and aluminium vessels.

The advantages of the proposed Single -stage converter configuration are summarized as follows:

i Eliminates the rectifier bridge

ii Achieved boost operation and high power factor

iii Suitable for two IH loads

iv Reduces the size of reactive components

v Suitable for different material vessel domestic induction Cooking

vi Independent power control is achieved using pulse frequency modulation

vii High power conversion efficiency

viii Used only two switching devices per load

ix Eliminates the use electro-mechanical switches

Thus, it is well suitable for two different vessel induction cooking.

1.7 Thesis Organization

This thesis is organized into the following six chapters.

Chapter 1 presents the basics of induction heating system and multi-output and single-stage conversion requirement. It provides a brief description of the work done and chapter-wise summary of thesis.

Chapter 2 presents review of the existing inverter topologies and power control techniques used in induction heating application. This sets the motivation for the research work carried out in this thesis.

Chapter 3 describes the first proposed inverter configuration, cascaded full-bridge resonant inverter configuration for different material induction cooking. The circuit operation, analysis and design procedure are presented. Independent power control is achieved with ADC control. Simulation and experimental results are presented. Independent power control is demonstrated.

Chapter 4 presents the second proposed inverter configuration, frequency controlled resonant inverter for different material induction heating applications. The circuit operation, analysis and design procedure are presented. Independent power control is achieved with PFM control. Simulation and experimental results are presented.

Chapter 5 presents the third proposed inverter configuration, single-stage pulse frequency controlled ac-ac resonant converter for different material induction cooking. The circuit operation, analysis and design procedure are presented. Power factor correction, boost operation and independent power control are explained. PFM control is used. Simulation and experimental results are presented.

Chapter 6 presents the main conclusions of the thesis and scope for future work.

Chapter 2

Review of Domestic Induction Heating System

Chapter 2

Review of Domestic Induction Heating System

2.1 Introduction

This chapter presents an overview of IH and high-frequency inverters for domestic IH applications. Literature review on converter configurations for IH applications is presented. Merits and limitations of these circuits are also discussed in the following sections.

2.1.1 Conventional Methods of Electric Heating

The following methods of electric heating are widely used in heating applications.

i. Resistance Heating: I^2R loss is utilised in this method. When current flows through a resistive element, heat is produced due to I^2R loss which acts as the source of heat. However, heat produced in this method may damage the insulation and other electrical components, and it also affects the lifetime of various components in the circuit.

ii. Conduction Heating: In the process of conduction, heat energy is transferred through collision between nearby atoms or molecules. As the particles in solids and liquids are closer together, conduction is greater in solids when compared with gases.

iii. Infrared Radiation Heating: Infrared heaters comprises of two parts: a heating system and a reflector. Electrical energy is converted into thermal energy via the heating system. The reflector then distributes the thermal energy produced by the heating system to objects in its vicinity as radiant heat. The human eye is susceptible to all of the radiation in the electromagnetic spectrum, especially at very high intensities.

iv. Dielectric hysteresis Heating: Dielectric Heating is an electric heating procedure that raises the temperature of a dielectric (non-conducting) substance by applying an alternating electric field (high voltage ac signal). The material that is in touch with the external field gets heated as

the temperature rises. Its efficiency is around 50 %, which is regarded as major disadvantage.

v. Electric Arc Heating: An electric arc can be used to heat materials. The substances that can be heated includes solid, liquid, or gases. When direct heating is used, an electrode is heated to produce the necessary heat while in indirect heating, heat is transferred from the arc by convection or radiation.

vi. Induction Heating: Induction heating is more popular and has many advantages compared to above heating methods, as discussed in Chapter 1.

2.2 Converter Configurations for Induction Heating

Many domestic and industrial applications of IH have emerged since the late 1980s, and induction cookers are now used in several countries. There has been a growth in use of IH for medical applications [11], due to its precise and local heating ability for hyperthermia therapy.

Lucía, Oscar and Maussion, Pascal and Dede, Enrique J and Burdío, José M have researched extensively on the IH technology and have proposed different IH converters and presented the key developments.

Lichan Meng, et al., proposed a commercial high-power induction cooker [10]. Power control, self frequency tracking, and ZVS implementation were performed. The resonant converter was designed with power control through PFM and PDM techniques.

S. Llorente, et al., proposed a resonant inverter for induction cooker [12]. This article has compared commonly used inverter topologies for induction cookers. Full-bridge inverters, half-bridge inverters, and single-switch inverters were some of the most common inverter configurations [13]. They were compared in terms of power device stresses, efficiency, frequency management, and electromagnetic emissions.

Acero, et al., presented a simple method for determining the winding resistance of a litz-wire coil in an induction cooking appliance by considering the eddy-current, conduction and proximity-effect losses [14].

Kim, et al., designed IH and inductive power transfer (IPT) dual functional apparatus [15]. Power stage design limitations and other practical implementation issues were addressed to enhance compatibility of the system with IH system.

The inverter configurations most commonly used in IH applications are single-switch [16, 17], half-bridge [18–22], and full-bridge [23–25] resonant inverters. The full bridge configuration is widely used for output powers greater than 5 kW and is the preferred configuration for industrial applications. Half-bridge inverter configuration is recommended for domestic in-

duction heating applications below 5 kW, whereas single switch inverter is used in small IH generators and domestic cooking applications up to 2 kW. Koertzen, et al., proposed a comparative study of single switch induction heating converter topologies in [26, 27] and addressed power handling capabilities of components, switching losses and overall efficiency of the configuration.

2.2.1 Power Control Techniques for Induction Heating

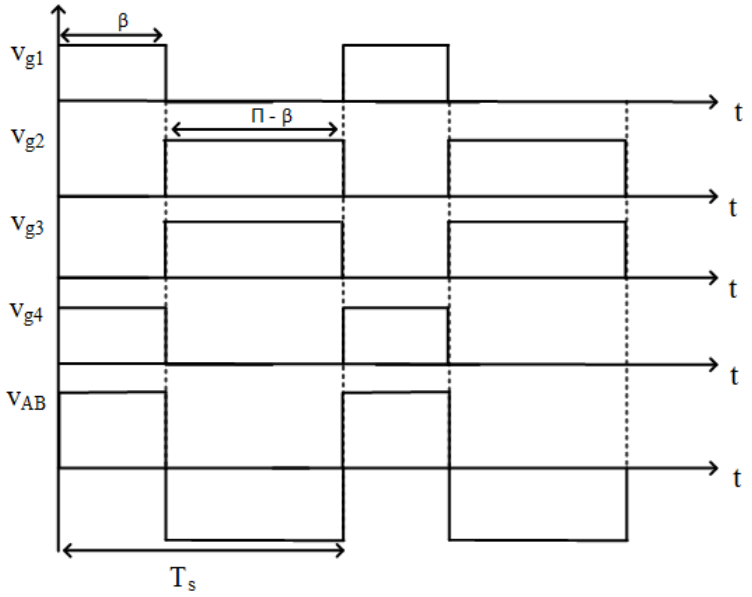

Figure 2.1: ADC control operating waveforms [28]

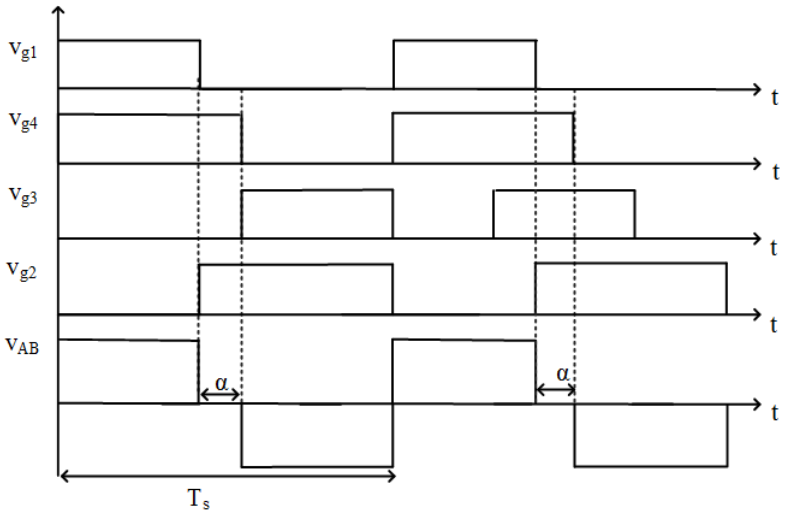

Figure 2.2: AVC control operating waveforms [29]

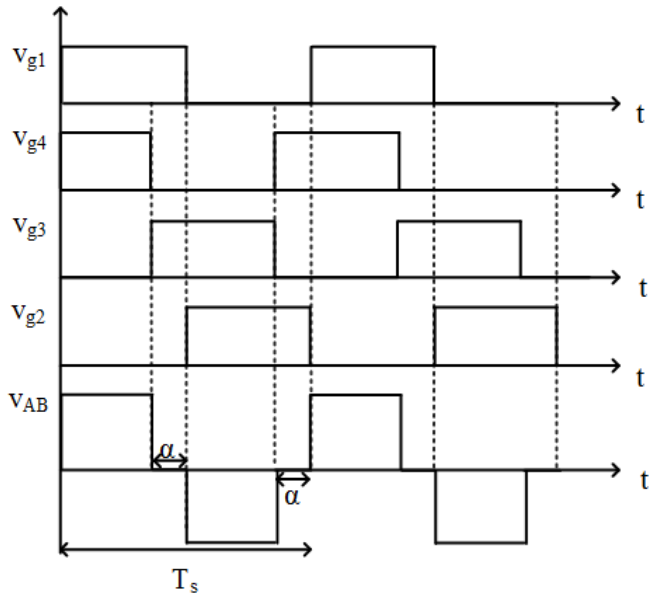

Figure 2.3: Phase shift control operating waveforms [30, 31]

The IH system's performance is defined not only by its design, but also by the control schemes used to regulate the output power. It is essential for load-based temperature regulation. Various power control strategies presented in the literature are discussed in this section.

Pulse width modulation (PWM) is the widely used technique for controlling output power [32]. The major drawback of this control scheme is that it employs hard switching and hence increases switching losses.

Variable frequency (VF) control scheme is proposed in [33, 34] to overcome the limitations of PWM control. As the load varies, the control is achieved with tracking the resonant frequency. However, the variation in frequency generates EMI and acoustic noise into the system. Constant frequency control methods are preferred to overcome EMI and acoustic noise problems. Asymmetrical duty cycle (ADC) control [28] is a constant frequency control method used to regulate output power without EMI issues. The width of the positive and negative cycles of the output voltage is asymmetric in this control scheme. Figure. 2.1 shows the ADC control operating waveforms. The main drawback of ADC control is that it injects more harmonics into the source.

Asymmetrical voltage cancellation (AVC) control technique uses a significant dead band in either the positive or negative cycle of the output voltage waveform [29]. It provides wider range of soft switching. AVC control operating waveforms are shown in Figure. 2.2. The asymmetric operation produces even harmonics in voltage and current. This problem is overcome with pulse density modulation (PDM) control . The density of the switching pulses is controlled using this approach without affecting the switching frequency. It ensures precise and smooth

control operation, and also provides a wider range of power control [35]. In Phase shift control scheme (PS), inverter pulses are generated to create a phase difference between voltage and current [30, 31]. The output power can be regulated without EMI, and the waveforms are symmetric. PS control operating waveforms are shown in Figure. 2.3. However, the power factor in this system remains poor. In addition, hybrid control techniques are proposed in [36–41] to achieve the advantages of different control schemes together.

2.2.2 Inverter Configurations for Multiple Load Induction Heating

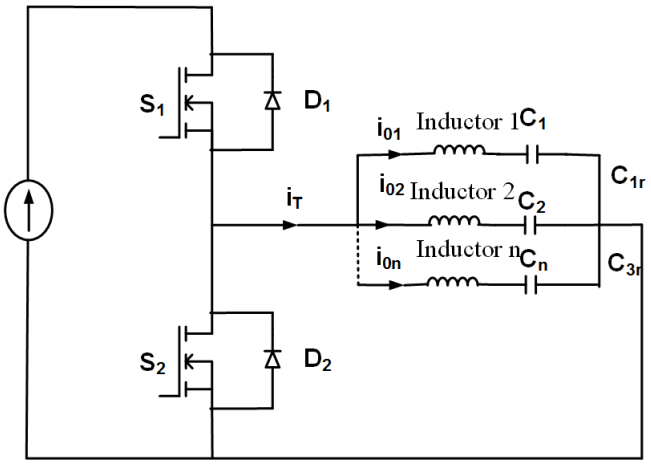

Figure 2.4: Multi-load single converter for IH [42]

Nowadays multiple-load induction cooking (IC) systems are becoming more popular. The main requirements of this system are reduced component count, improved conversion efficiency, and independent power regulation of loads. In the past, some inverter topologies have been proposed for multiple load induction heating. In [42], a multi-output inverter configuration with variable frequency control is proposed. This multi-output single converter circuit diagram is shown in Figure. 2.4. It is suitable for low power applications as it uses a half bridge configuration. An analytical investigation of a two resonant-load circuit was done using an R, L model of the inductor, followed by simulation on a complete model and subsequent practical testing; the study proved the possibility of setting the power of two inductors in a single inverter while maintaining parallel ZVS mode. Independent power control of multiple loads is obtained through variable frequency control method. Electro-mechanical switches are used to connect the loads and resonant capacitors. The use of mechanical switches and use of more number of capacitors are the major limitations of this method.

José M. Burdío et al. proposed an inverter topology with three legs in [43] for powering two IH loads. One leg is common for both loads. The circuit diagram of this three leg two-output

series resonant inverter is shown in Figure. 2.5. It was designed using a synthesis approach and asymmetrical voltage-cancellation control strategy. When compared with the full bridge equivalent circuit, the synthesised converter allows two inductive loads up to their rated values simultaneously and independently using only one converter thereby saving two transistors. The installation of two low-cost relays allows quick heating and optimal power use. It offers fewer component count, high efficiency and independent control with AVC.

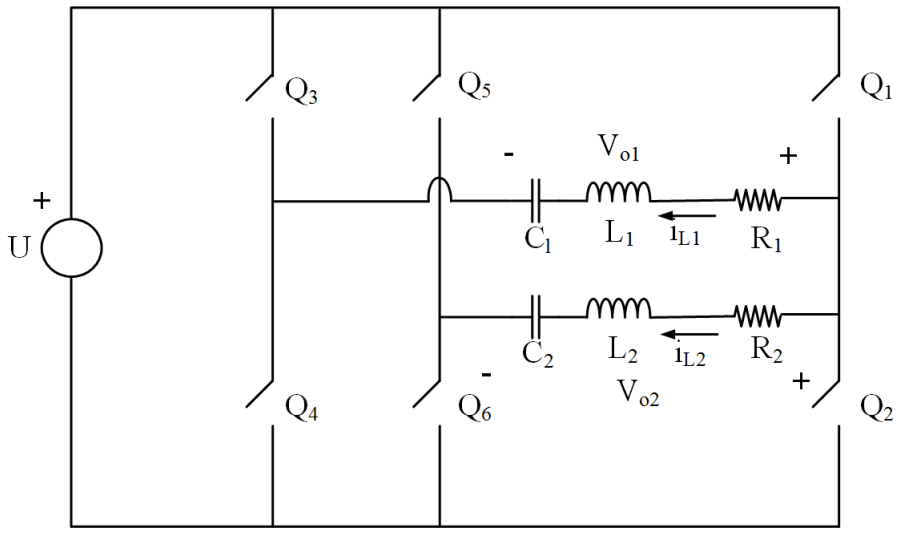

Figure 2.5: Three leg two output series resonant inverter for IH [43]

Two multi coil systems were proposed and investigated in [44]; proximity effects were considered between the coil and the distribution of eddy currents and power losses were investigated using finite-element technique. The thermal performance of two multi coil systems was also evaluated. A multiple-output ZVS resonant inverter for versatile induction heating appliances was proposed in [45]. The proposed converter features a matrix structure, which offers low-cost implementation with fewer power components, high performance and minor switching losses. In [46], a direct ac–ac converter scheme with a multiple-output resonant matrix converter was proposed to power multiple loads. The proposed configuration reduces the number of devices and complexity, leading to an efficient, adaptable, and cost-effective solution. In [47], a multi-output inverter with independent on-off control is proposed. In [48], a multiple load inverter with dual-frequency operation is proposed. ADC control technique is used for independent power control of each load.

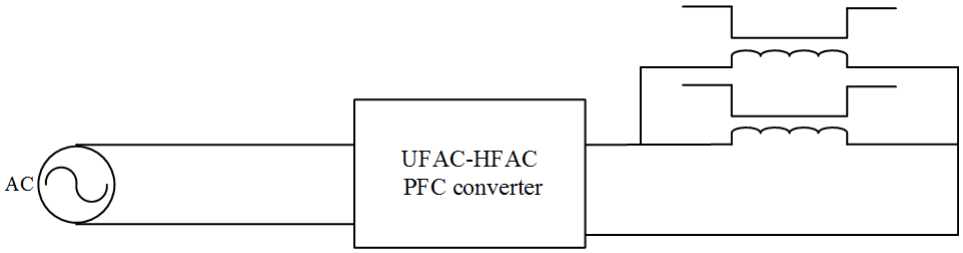

Figure 2.6: Structure of single-stage IC system with multiple loads

2.2.3 Single-Stage AC-AC Resonant Converter Configurations for IH Applications

The structure of a single stage ac-ac induction cooking system is shown in Figure. 2.6. Single-stage resonant ac-ac converter topologies have been proposed for induction heating applications in [49–51]. Totem-pole bridge-less PFC boost rectifier is used in these topologies. They offer advantages of fewer component count, high efficiency, power factor correction and boost operation. However most of these topologies are of half bridge and full bridge configurations and are suitable for single load. In [52], a half bridge boost rectifier based ac-ac converter is proposed. In [53], single-phase boost-type PFC rectifier is analysed with different modulation strategies for domestic IH applications. In [54], a multiple output multi phase resonant inverter is proposed with coupled coils. In [55], ZVS multi-output resonant inverter architecture for IH is proposed.

In [56], a high-efficiency multiple-output resonant converter for IH applications using wide band gap devices is proposed. The circuit diagram of the proposed converter is shown in Figure. 2.7. It consists of a three-leg ac-ac boost converter which can power two similar IH loads. The loads are operated at the same frequency and optimum AVC control is employed. Wide band gap devices are used to increase the efficiency. The common branch of the converter (S_H, S_L) provides the boost function, while diodes D_H and D_L rectify the input voltage. The boost inductor is L_s and boost output capacitor is C_b. Hence, the dc output voltage of the half-bridge boost rectifier stage , V_b, is proportional to the inverter's common branch duty cycle, D. The multi output inverter powers each IH load with a common inverter branch, (S_H, S_L), and a number of additional branches, N. Compared to conventional designs, the required number of switches in this configuration (N_{sw} = 2 + 2 N) is fewer, resulting in lower component count. The proposed converter was implemented for multiple-loads using SiC JFET devices. This configuration achieves high-performance and high-efficiency.

The above mentioned single-stage topologies are limited to heating only ferromagnetic vessels. Low relative permeability and low specific resistance of non-magnetic vessels pose a

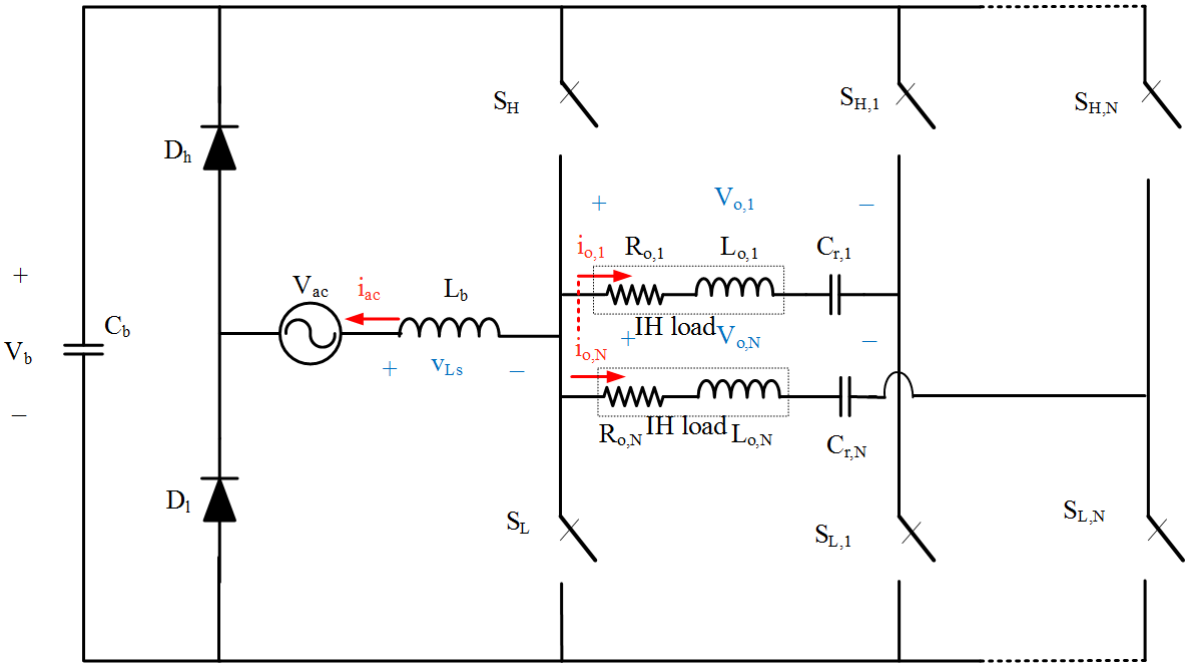

Figure 2.7: High- efficiency multi-output resonant converter for IH [56]

challenge in the induction heating of non-ferromagnetic vessels.

2.2.4 Different Material Vessel Domestic Induction Heating

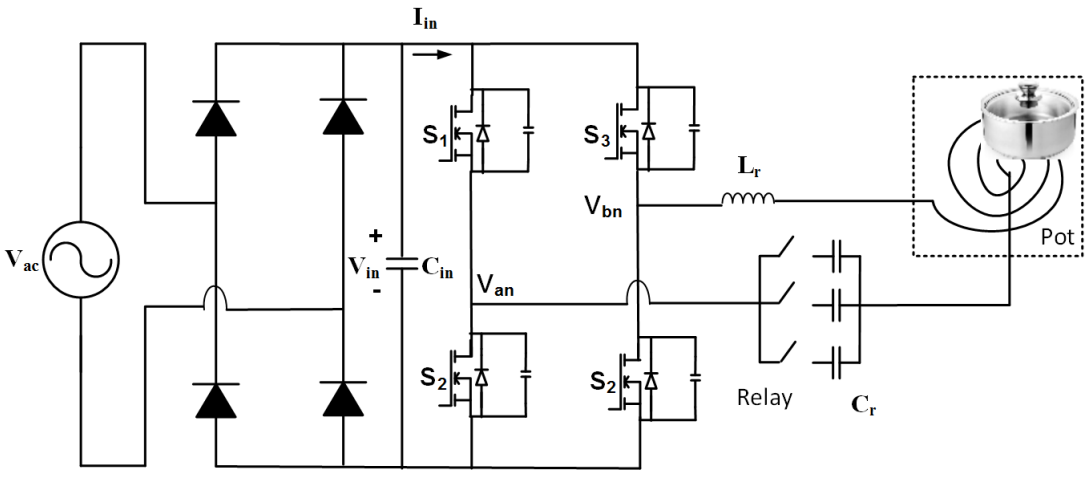

Figure 2.8: Series resonant inverter for all metal IH [57]

Most of the available multi-load IH configurations are suitable for ferromagnetic materials only. Hence, non-ferromagnetic vessels such as aluminium and copper cannot be used with IC, though they have good thermal properties and are commonly used in traditional cooking applications. In recent past, some inverter configurations suitable for vessels made from ferro

and non-ferro magnetic materials, have been proposed [58, 59].

Load-Adaptive Modulation (LAM) of a Series-Resonant inverter for all-metal induction heating applications was proposed by Hwa-Pyeong Park et al in [57]. Figure. 2.8 depicts its circuit diagram. LAM method has been proposed in order to achieve IH capability for vessels made of ferromagnetic as well as non-ferromagnetic materials. In this method, the voltage varies with full-bridge and half-bridge operating modes. The frequency doubler and frequency tripler modes increase the frequency of the eddy currents induced in the vessel which increases its equivalent resistance.

In [60,61], a high-frequency time-sharing dual resonant inverter is proposed for domestic all-metal induction cooking applications. In [62], double heating coil driven induction cooker is proposed. In these topologies, due to frequency selection and time sharing, additional switching losses occur which reduces heating efficiency. A dual-layer coil topology is proposed in [63] for different IH load applications. Each coil has half of the total turns-density. Hence, it reduces the effective ampere-turns available from each winding. In [64], selective harmonic operation is used in half-bridge inverter-based topology. This topology suffers from the limitations of low power factor and high conduction losses in body diode of the switching device.

A dual-resonant topology-re-configurable inverter for all-metal IH is developed and implemented using a novel series-parallel resonance (SPR) topology [65] with automatic load sensing and impedance matching characteristics. In this inverter configuration, two different control techniques are used for different material loads. This method suffers from the drawback of unbalanced switching losses. All these converter topologies come with their own merits and demerits.

2.3 Conclusions

In this chapter, an overview of domestic IH system has been presented. Different power control techniques have been discussed. Th existing converter configurations for single-output and multi-output IH applications have been discussed. The main requirements of multi-output IH applications are independent control of individual load, low component count and high efficiency. Single stage ac-ac converter topologies have been discussed.

Few topologies which are available in the literature that are suitable for both ferromagnetic and non-ferromagnetic materials have been presented. The advantages and limitations of these topologies also have been discussed.

It is observed that many of the existing topologies suffer from the limitations of compatibility for ferro-magnetic loads only. Some of the topologies which are suitable for different material IH also have the drawbacks of high component count, complex control, reduced effi-

ciency and lack of independent power control.

In order to overcome the above mentioned limitations, three different IH resonant inverter configurations have been proposed in this thesis and are explained in detailed in the following chapters.

Chapter 3

Cascaded Full-Bridge Resonant Inverter Configuration for Different Material Induction Cooking

Chapter 3

Cascaded Full-Bridge Resonant Inverter Configuration for Different Material Induction Cooking

3.1 Introduction

This chapter proposes a cascaded full bridge resonant inverter topology which is suitable for different material vessel IC.

In literature, cascaded multi-level inverter topologies [66–72] are proposed for different applications like photovoltaic, AC Power distribution and industrial applications. In these configurations, cascaded bridges are operated at single frequency to supply single load. Different modulation control techniques are used for load power control. Cascaded multi-level inverter configurations have been proposed for induction heating applications in [73, 74]. Dual-frequency multilevel inverter topology has been proposed with equal and unequal voltage sources. In [75], a cascaded multi level inverter topology has been proposed for high power induction heating application. These cascaded inverter configurations have been proposed for single ferro magnetic induction heating loads [76]. These proposed multi level inverter configurations have their own merits and demerits.

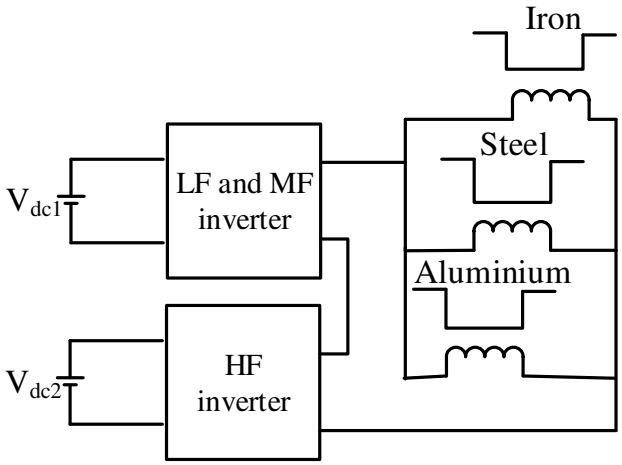

Figure 3.1: Block diagram of cascaded multi-load inverter for Induction Cooking

In this chapter, a cascaded full-bridge resonant inverter configuration, which is suitable

for three different material vessels, has been proposed. It can power multiple-loads of iron, steel and aluminium vessels. These three IH loads are simultaneously operated at their respective resonant frequencies. The output power of multiple loads are independently controlled by asymmetric duty cycle control. This configuration provides advantages of a reduced component count, high efficiency, and independent control. The block diagram of the proposed inverter configuration is shown in (Fig. 3.1). The outputs of two full-bridge inverters are cascaded and connected to three IH resonant loads. First inverter is operated at low and medium frequencies suitable for iron and steel loads. Second inverter is operated at high frequency suitable for aluminium loads. ADC control is used for output power control. Circuit operation, design, implementation, and result analysis are presented in the following sections.

In section 3.2, proposed circuit configuration and principle of operation are described. Section 3.3 presents different modes of operation. Section3.4 describes prototype implementation, simulation, and experimental results. Analysis of results is presented in Section 3.5. Section 3.6 summarizes the work performed and conclusions have been drawn.

3.2 Proposed cascaded converter configuration

3.2.1 Circuit configuration

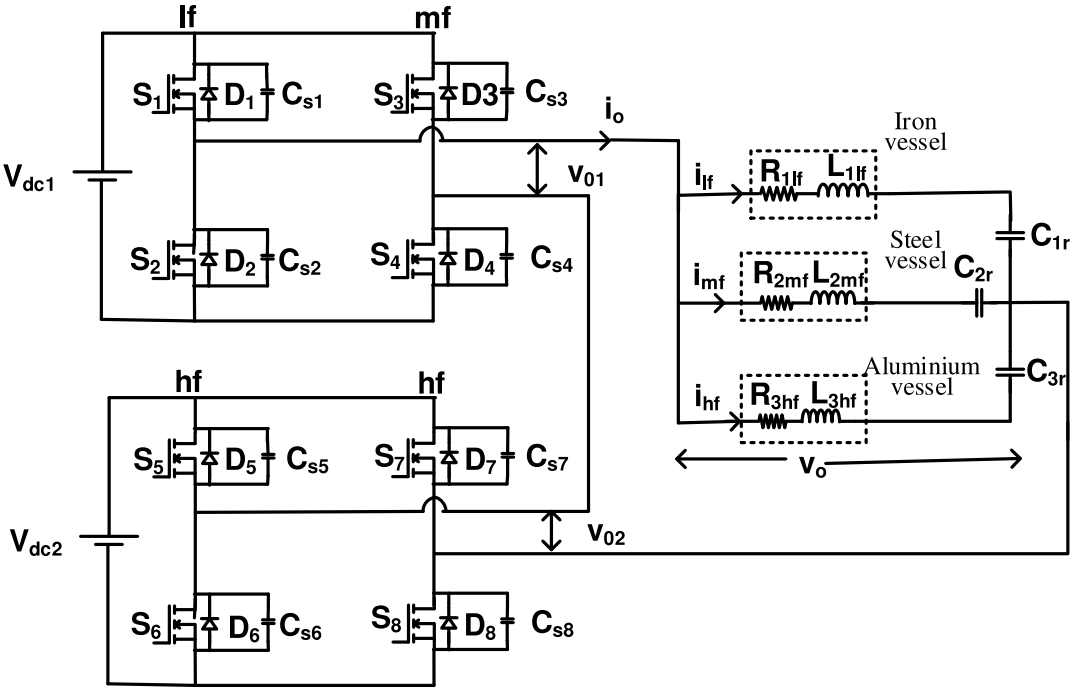

Figure 3.2: Proposed cascaded multi-load inverter configuration

The circuit diagram of the proposed multi-load inverter topology is shown in (Fig. 3.2).

This configuration consists of two full-bridge inverters connected in cascade. S_1 to S_4 are the four MOSFET switches of first inverter with body diodes D_1 to D_4 and snubber capacitors C_{S1} to C_{S4} respectively. First leg devices, S_1 and S_2 are switched at low frequency, f_l. Second leg devices, S_3 andS_4 are switched at medium frequency, f_m. S_5 to S_8 are the four MOSFET switches of second inverter with body diodes D_5 to D_8 and snubber capacitors C_{S5} to C_{S8} respectively. These inverter devices are switched at high frequency, f_h. Lossless snubber capacitors C_{S1}-C_{S8} are connected across switching devices S_1-S_8 respectively to provide ZVS operation. V_{dc1} and V_{dc2} are supply voltages of first and second inverters respectively. Three different IH resonant loads are connected across output terminals of cascaded inverters. The output voltage of cascaded inverters is v_o=v_{01}+v_{02} where v_{01} and v_{02} are output voltages of first and second inverter respectively, i_o is the output current of the cascaded inverter.

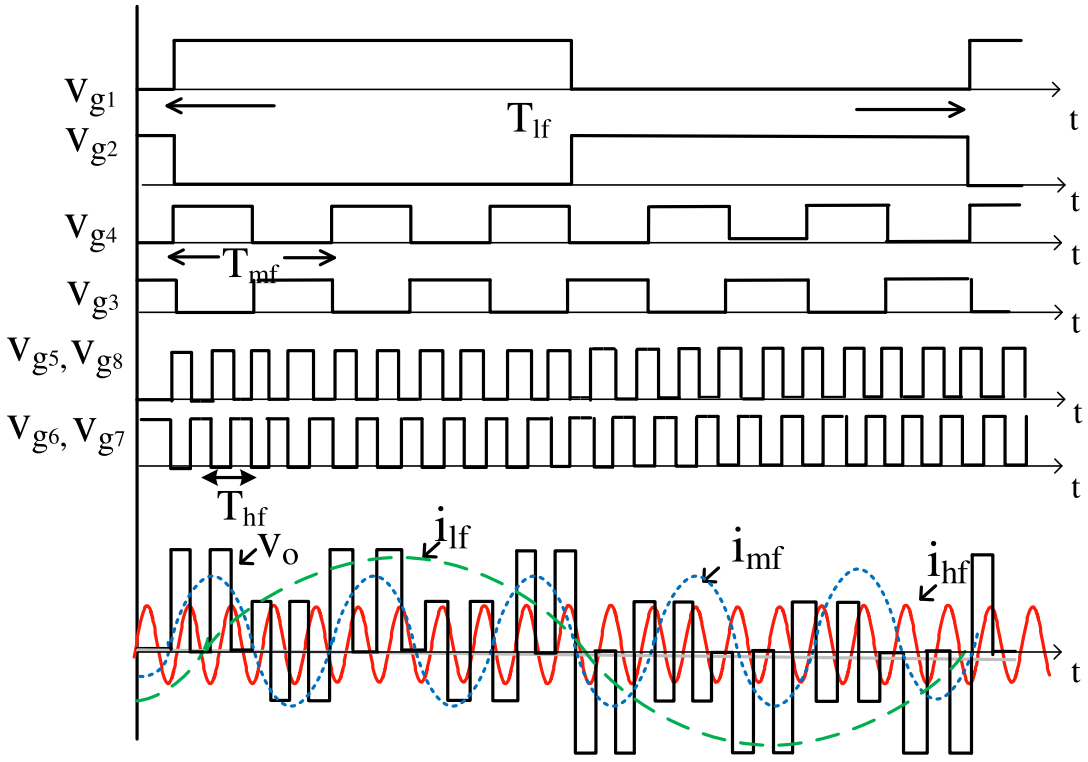

Figure 3.3: Switching pulses, output voltage and load currents

This induction cooking system consists of three burners, each one suitable for iron, steel, and aluminium vessels respectively. L_{1lf} and R_{1lf} are respectively the equivalent inductance and resistance of iron load at low frequency, f_l. An external capacitor C_{1r} is connected in series to resonate this load at low resonant frequency. The equivalent inductance and resistance of steel load are respectively f_{rl}. L_{2mf} and R_{2mf} at medium frequency. An external capacitor f_m. C_{2r} is connected in series to resonate this load. At medium resonant frequency, f_{rm}. L_{3hf} and R_{3hf} are respectively the equivalent inductance and resistance of aluminium load at high

frequency, f_h.An external capacitor C_{3r} is connected in series to resonate this load at high resonant frequency. The currents through iron, steel and aluminium resonant loads are f_{rh}. i_{lf}, i_{mf}, i_{hf}, respectively. The low, medium and high switching frequencies are selected as f_l=20 kHz, f_m=100 kHz and f_h= 400 kHz respectively. Switching pulses of the inverter devices, corresponding output voltage v_o and load currents i_{lf}, i_{mf}, and i_{hf} are shown in (Fig. 3.3). i_o is the sum of low, medium and high-frequency current components.

3.2.2 Selection of switching frequencies

The induction cooking system needs a higher frequency AC supply ($\geq$20 kHz). Low frequency utility supply voltage (50 Hz) is converted into higher frequency voltage and applied to induction cooker. This conversion stage consists of a bridge rectifier, filter circuit and a high frequency inverter. The heat generated in the vessel concentrates in a peripheral layer at a skin depth (δ) of,

$$\delta = \sqrt{\frac{\rho}{\pi \mu f_s}} \tag{3.1}$$

where, ρ is electrical resistivity and μ is magnetic permeability of the vessel material, and f_s is switching frequency of the inverter. Ferromagnetic materials have higher values of permeability and resistivity. The equivalent circuit of induction heating load may be considered as a series combination of L_{eq} and R_{eq}, where L_{eq} is the equivalent inductance and R_{eq} is the equivalent resistance, as referred to IH coil side when the vessel is kept on the cooker. These values depend on the material of the vessel and they vary with switching frequency.

In this proposed work, three vessels made of iron, steel and aluminium are considered. Iron is ferromagnetic material. Steel and aluminium are non-ferromagnetic materials. The variation of L_{eq} and R_{eq} of these three different IH loads with inverter switching frequency are shown in (Fig. 3.4). (Fig. 3.4a) shows L_{eq} and R_{eq} variation of iron load with frequency and (Fig. 3.4b) and (Fig. 3.4c) show the same for steel and aluminium vessels. It is observed that iron load has higher values of L_{eq} and R_{eq} at around 20 kHz. Hence, the switching frequency, f_l of iron IH load is selected as 20 kHz. Steel and aluminium loads are having less values of L_{eq} and R_{eq} at this frequency. Beyond 80 kHz, the equivalent resistance of steel load increases above 2 Ω and similarly beyond 300 kHz equivalent resistance of aluminium increases above 2 Ω. Hence by increasing switching frequency, the equivalent resistance and thereby output power may be increased. The switching frequency of steel IH load is selected at a medium frequency of 100 kHz and that of aluminium is selected at a high frequency of 400 kHz. External capacitors are connected to IH loads to resonate the load at resonant frequency f_r. To facilitate ZVS operation, $f_s \div f_r$ ratio has to be selected closer to 1.1. Hence f_{rl}, f_{rm} and f_{rh} are selected as 18.4 kHz 98

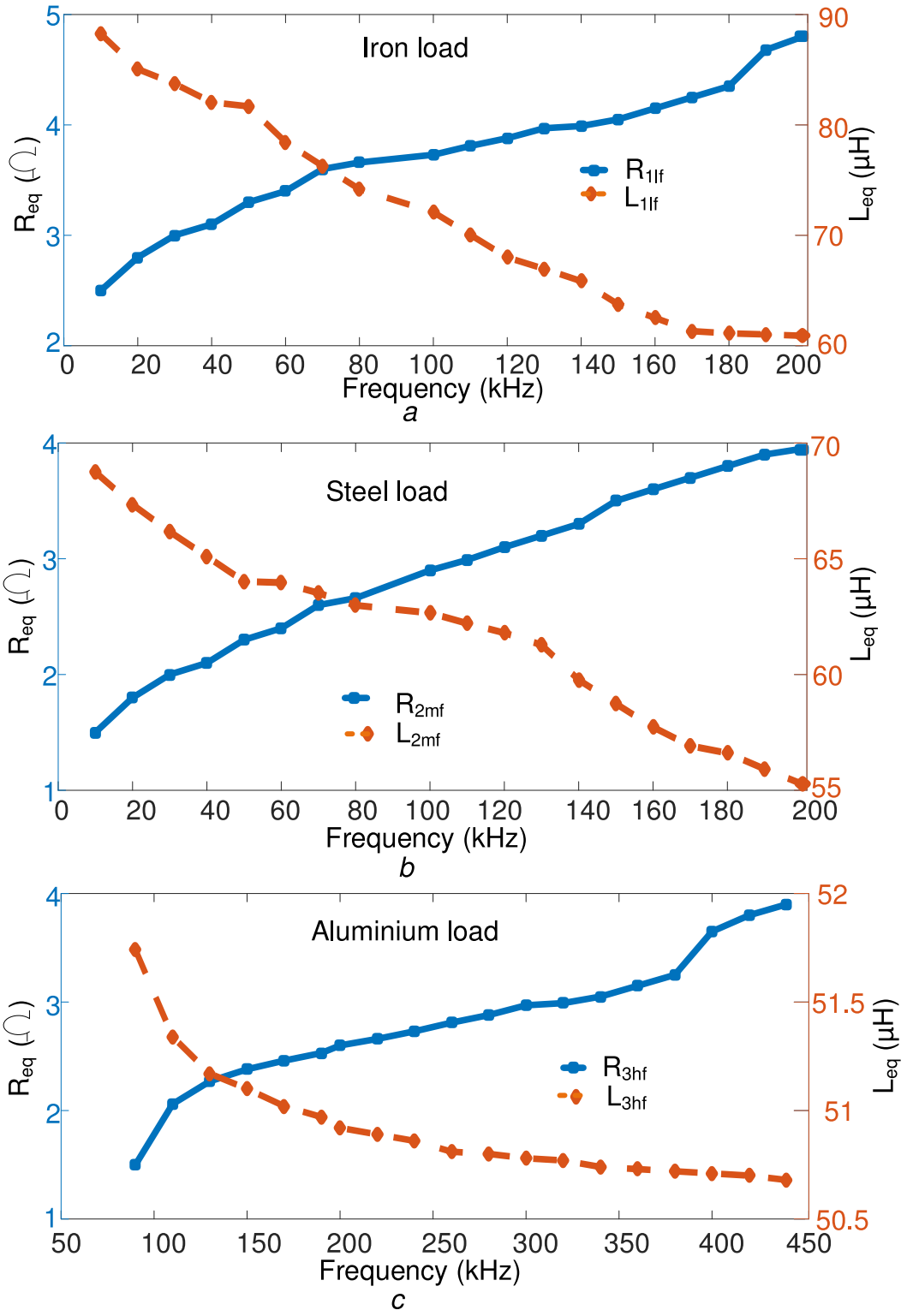

Figure 3.4: variation of R_{eq} and L_{eq} with frequency
(a)Iron load
(b)Steel load
(c)Aluminium load

kHz and 395 kHz respectively. The resonant capacitors are selected based on the expressions for f_{rl}, f_{rm} and f_{rh}, where

$$f_{rl} = \frac{1}{2\pi\sqrt{L_{1lf}C_{1r}}}, f_{rm} = \frac{1}{2\pi\sqrt{L_{2mf}C_{2r}}} and\, f_{rh} = \frac{1}{2\pi\sqrt{L_{3hf}C_{3r}}} \tag{3.2}$$

respectively.

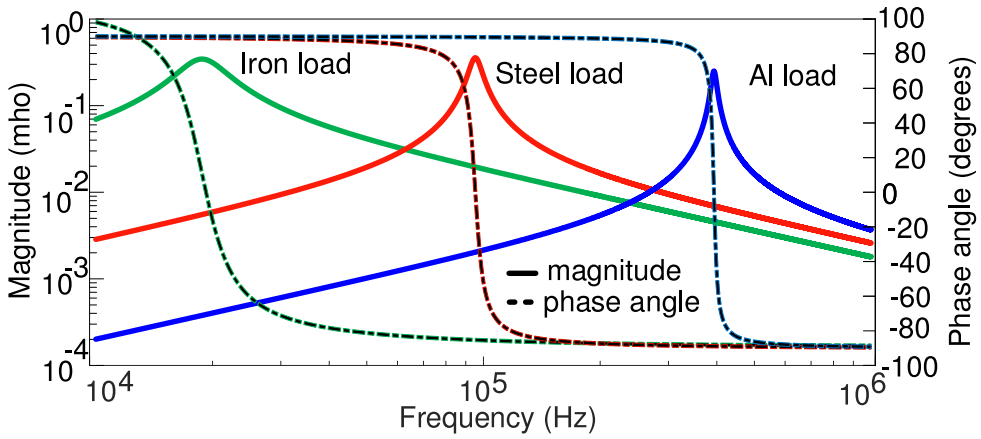

Figure 3.5: Admittance curves of different IH resonant loads

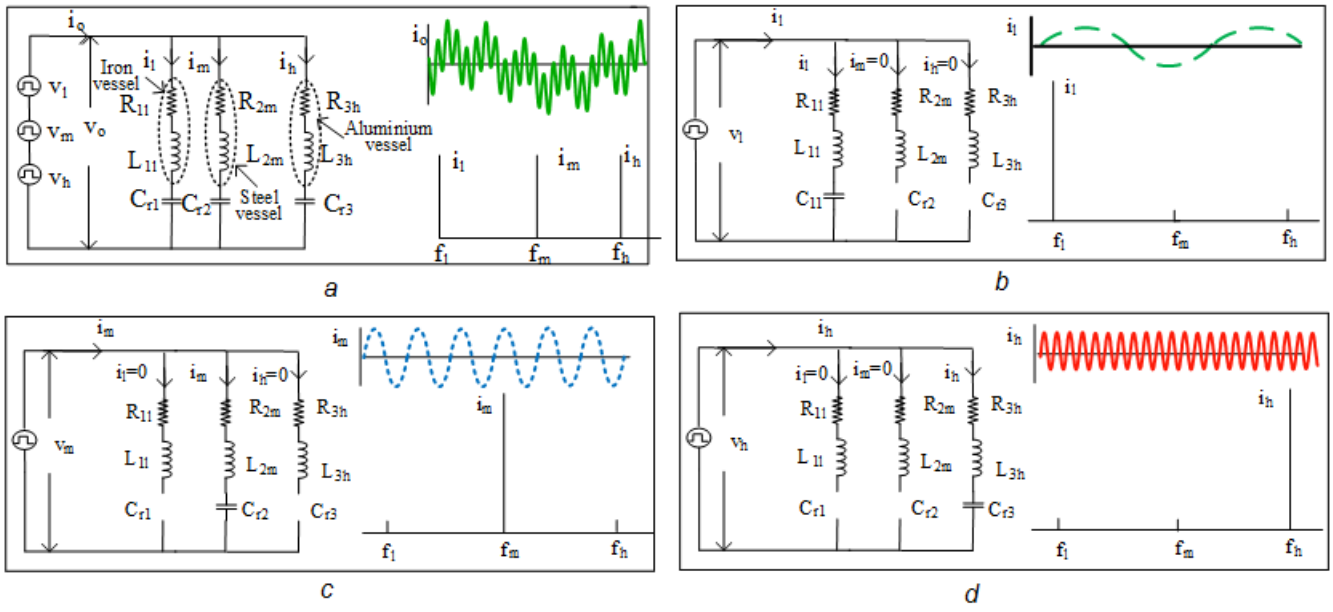

Figure 3.6: Equivalent circuits of the load, load current and their FFTs
(a) Equivalent circuit of multiple frequency inverter, load currents and FFT
(b) Equivalent circuit of load for v_{olf} and load current FFT
(c) Equivalent circuit of load for v_{omf} and load current FFT
(d) Equivalent circuit of load for v_{ohf} and load current FFT

Admittance characteristics of the three IH loads are shown in (Fig. 3.5). It shows that the iron, steel and aluminium resonant loads offer maximum admittance to low, medium and high-frequency currents respectively.

3.2.3 Operating principle

The output voltage of the proposed cascaded inverter v_o is the sum of first and second inverter output voltages v_{01} and v_{02}. First inverter is operated at low and medium frequencies. The second inverter is operated at high frequency. Hence cascaded inverter output voltage v_o is the combination of low, medium and high-frequency voltage components, v_{olf} , v_{omf} and v_{ohf} as shown in (Fig. 3.3).

$$v_0 = v_{01} + v_{02} = v_{olf} + v_{omf} + v_{ohf} \tag{3.3}$$

Fig. 3.6a shows the equivalent circuit of inverter loads. Inverter output current waveform and its FFT are also shown. It depicts i_o as a combination of low, medium and high-frequency currents.The behaviour of loads for low frequency component of output voltage v_{olf} is shown in(Fig. 3.6b). At low-frequency f_l, the resonant capacitors C_{2r} and C_{3r} offer very high reactance and act like open circuit and hence low frequency current component i_{1lf} does not flow through medium and high frequency loads. Now the impedance of iron vessel resonant load can be expressed as

$$Z_{1lf} = R_{1lf} + j(X_{L1lf} - X_{C1lf}) \tag{3.4}$$

where

X_{L1lf}=$2\pi f_l L_{1lf}$,X_{c1lf}=$1/(2\pi f_l C_{1r})$.

However, X_{L1lf}≈X_{C1lf} and hence Z_{1lf}≈R_{1lf}. Thus, iron resonant load provides least resistance path for i_{1lf} and it flows through the iron load. The behaviour of loads for medium frequency component of output voltage v_{omf} is shown in(Fig. 3.6c). At medium frequency f_m, the inductive reactance of L_{1mf} and capacitive reactance of C_{3r} are very high and hence they behave like open circuits. At medium frequency, steel vessel resonant load impedance can be expressed as

$$Z_{2mf} = R_{2mf} + j(X_{L2mf} - X_{C2mf}) \tag{3.5}$$

where

X_{L2mf}=$2\pi f_m L_{2mf}$, and X_{c2mf}=$1/(2\pi f_m C_{2r})$

However, X_{L2mf}≈X_{C2r} and hence Z_{2mf}≈R_{2mf}. Thus, steel resonant load provides least resistance path for i_{mf} and it flows through the steel load. The behaviour of loads for high frequency component of output voltage v_{ohf} is shown in(Fig. 3.6d). At high frequency f_h,

the inductive reactance of L_{1hf} and capacitive reactance of C_{2r} are very high and hence they behave like open circuits. At high frequency, aluminium vessel resonant load impedance can be expressed as

$$Z_{3hf} = R_{3hf} + j(X_{L3hf} - X_{C3hf}) \tag{3.6}$$

where

X_{L3hf}=$2\pi f_h L_{3hf}$, and X_{C3hf}=$1/(2\pi f_h C_{2r})$

However, X_{L3hf}≈X_{C3r} and hence Z_{3hf}≈R_{3hf}. Thus, aluminium resonant load provides least resistance path for high frequency current component i_{hf}. Hence high frequency current flows through the aluminium load.

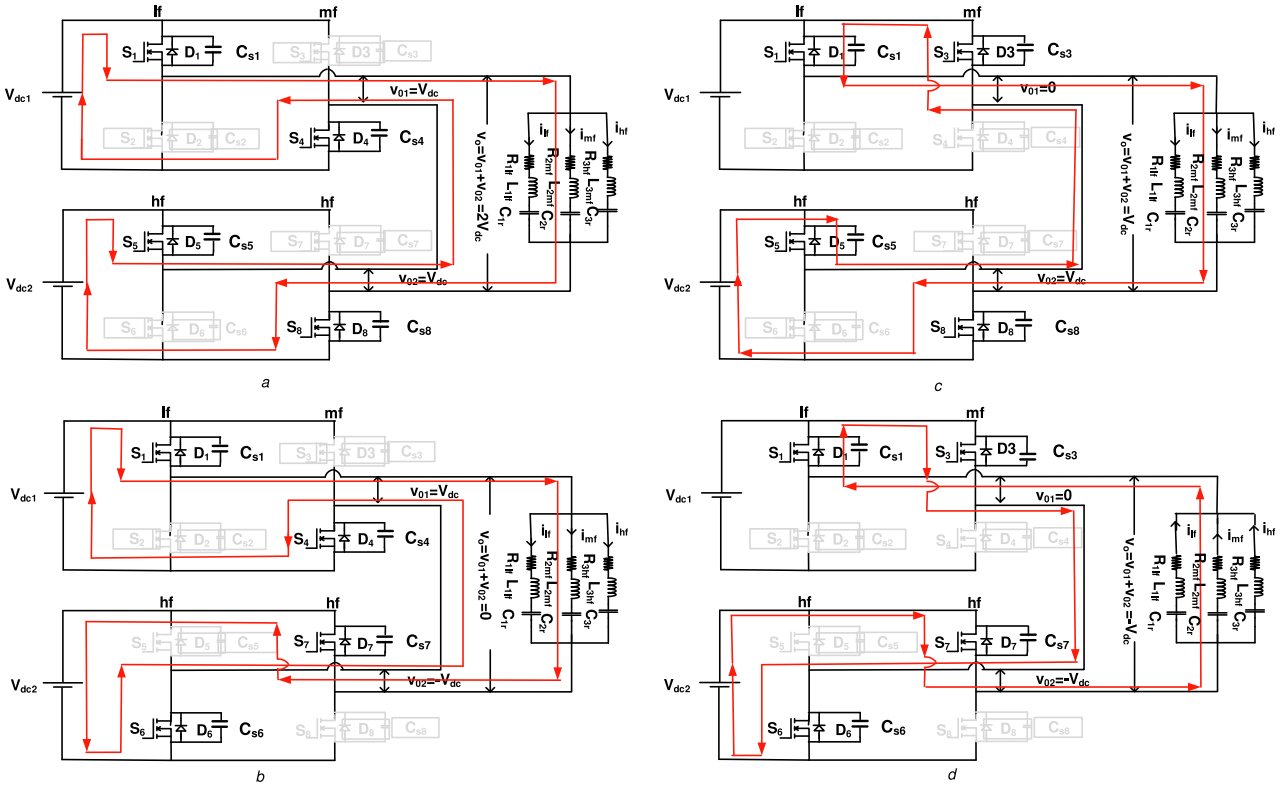

Figure 3.7: Inverter equivalent circuits for different modes of operation with S_1 is ON
(a) Mode-1:S_1,S_4, S_5 and S_8 are ON
(a) Mode-2: S_1, S_4, S_6 and S_7 are ON
(b) Mode-3: S_1, S_3, S_5 and S_8 are ON
(c) Mode-4: S_1, S_3, S_6 and S_7 are ON

3.2.3.1 Output power control

The total output power of this multi-load induction heating inverter configuration is expressed as

$$P_0 = P_{ol} + P_{om} + P_{oh} \tag{3.7}$$

where

P_{ol} = iron load output power $= {I_{lf}}^2 R_{lf}$

P_{om} = steel load output power $= {I_{mf}}^2 R_{mf}$ and

P_{oh} = aluminium load output power $= {I_{hf}}^2 R_{hf}$

I_{lf}, I_{mf} and I_{hf} are RMS values of iron, steel and aluminium load currents. These output powers delivered to different vessel loads are controlled independently using Asymmetric duty cycle control. P_{ol} is controlled through ADC control in first inverter low-frequency leg devices.

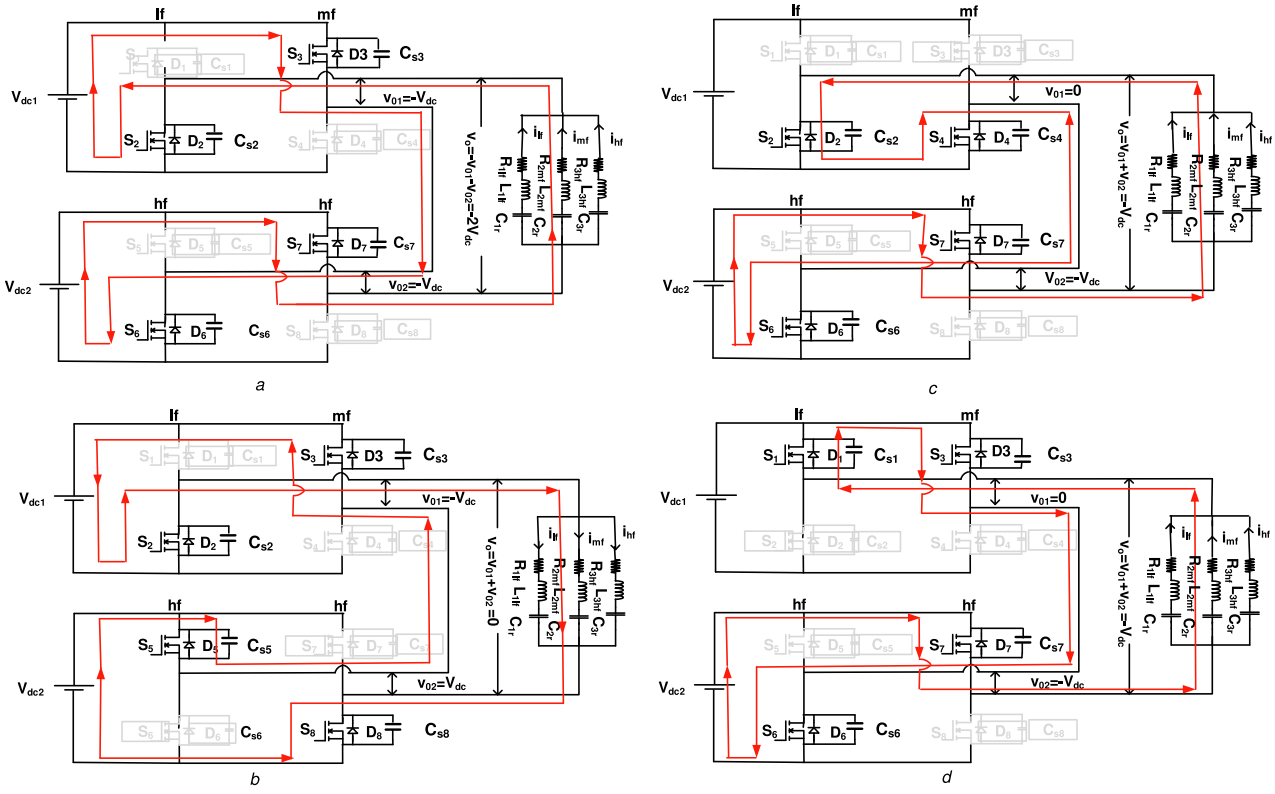

Figure 3.8: Inverter equivalent circuits for different modes of operation with S_1 is ON
(a) Mode-1:S_1,S_4, S_5 and S_8 are ON
(a) Mode-2: S_1, S_4, S_6 and S_7 are ON
(b) Mode-3: S_1, S_3, S_5 and S_8 are ON
(c) Mode-4: S_1, S_3, S_6 and S_7 are ON

P_{ol} can be expressed as

$$P_{ol} = \frac{2V_{dc}^2 \cos^2 \phi_l}{\pi^2 R_{1lf}} \cos^2 \frac{\alpha_l}{2} \tag{3.8}$$

where

ϕ_l=$\tan^{-1}(\frac{X_{L1lf}-X_{C1lf}}{R_{1lf}})$

α_l = control angle

ϕ_l = phase angle

At a fixed frequency, all parameters are constant except the control angle α_l. By varying this control angle, the low frequency duty cycle and output power P_{ol} are controlled. Similarly, first inverter medium-frequency leg (leg-2) devices are operated with ADC. The output power P_{om} can be controlled by varying the medium frequency control angle α_m. This output power P_{om} is expressed as,

$$P_{om} = \frac{2V_{dc}^2 \cos^2 \phi_m}{\pi^2 R_{2mf}} \cos^2 \frac{\alpha_m}{2} \tag{3.9}$$

where

ϕ_m=$\tan^{-1}(\frac{X_{L2mf}-X_{C2mf}}{R_{2mf}})$

Switching pulses of second inverter devices S_5 and S_8 are always in phase and S_6 and S_7 are in phase. This inverter output is also controlled by α_h is the control angle. ϕ_h is the phase angle between fundamental components of v_{hf} and i_{hf}. P_{oh} can be expressed as

$$P_{oh} = \frac{2V_{dc}^2 \cos^2 \phi_h}{\pi^2 R_{3hf}} \cos^2 \frac{\alpha_h}{2} \tag{3.10}$$

where

ϕ_h=$\tan^{-1}(\frac{X_{L3hf}-X_{C3hf}}{R_{3hf}})$

P_{oh} can be controlled by varying the high frequency control angle α_h. Thus, independent control of the individual load currents and load powers is achieved through ADC control.

3.3 Modes of operation

With the equal source voltages, V_{dc1}=V_{dc2}=V_{dc}, the inverter operation can be explained through eight different modes. When low-frequency device S_1 is ON, four operating modes are possible depending on the switching states of medium and high frequency devices. These modes are explained as below:

Mode-1: In this mode, switches S_1, S_4, S_5 and S_8 are in on-state. The corresponding equivalent circuit is shown in (Fig. 3.8a). Output voltages of first and second inverters are respectively V_{01}

= V_{dc} and V_{02} = V_{dc}. The output voltage across the loads (v_o) is the sum of V_{01} and V_{02}.

$$v_o = v_{01} + v_{02} = 2V_{dc} \tag{3.11}$$

the instantaneous value of inverter load current

$$i_o(t) = i_{lf}(t) + i_{mf}(t) + i_{hf}(t) \tag{3.12}$$

Mode-2: In this mode, switches S_1, S_4, S_6 and S_7 are in on-state. The corresponding equivalent circuit is shown in (Fig. 3.8b). Output voltages of first and second inverters are respectively V_{01} = V_{dc} and V_{02} = -V_{dc}. Output voltage across the loads is expressed as

$$v_o = v_{01} + v_{02} = 0 \tag{3.13}$$

Mode-3: In this mode, switches S_1, S_3, S_5 and S_8 are in on-state. The corresponding equivalent circuit is shown in (Fig. 3.8c). Output voltages of first and second inverters are respectively V_{01}

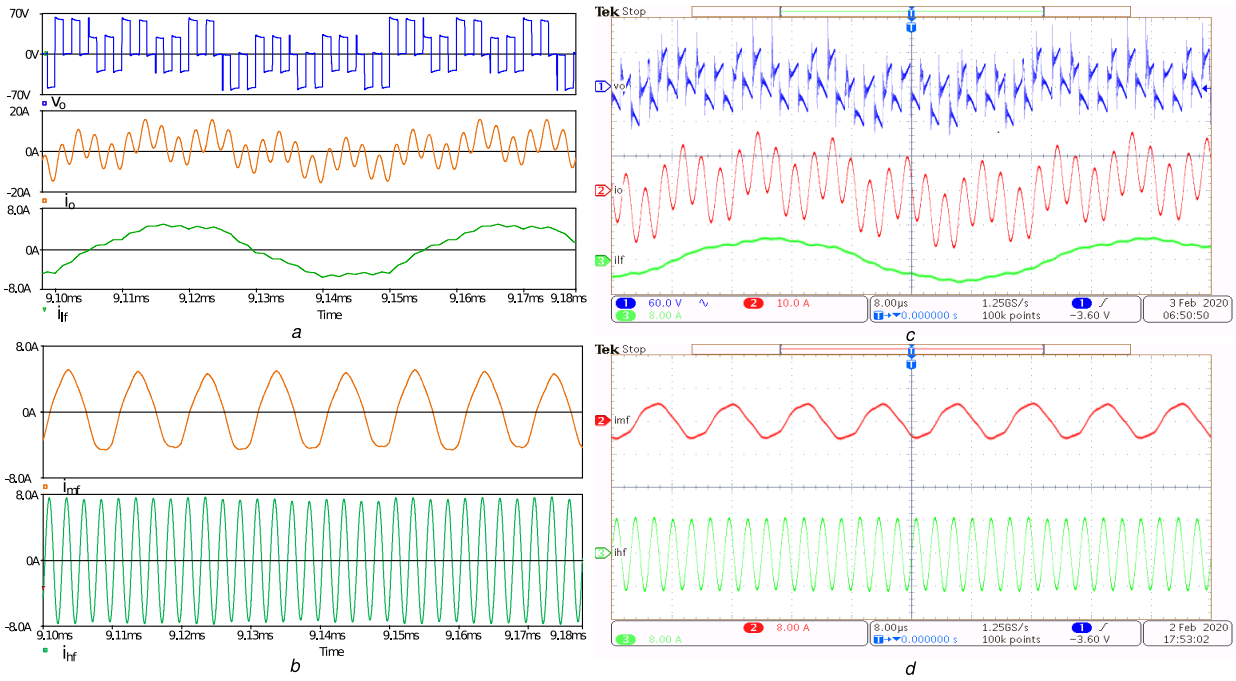

Figure 3.9: Load voltage (v_o), inverter output current (i_o) and load currents at D_l=0.95, D_m=0.95 and D_h=0.95
(a) Simulated waveforms of v_o, i_o and i_{lf}
(b) Simulated waveforms of i_{mf} and i_{hf}
(c) Experimental waveforms of v_o, i_o and i_{lf}
(d) Experimental waveforms of i_{mf} and i_{hf}

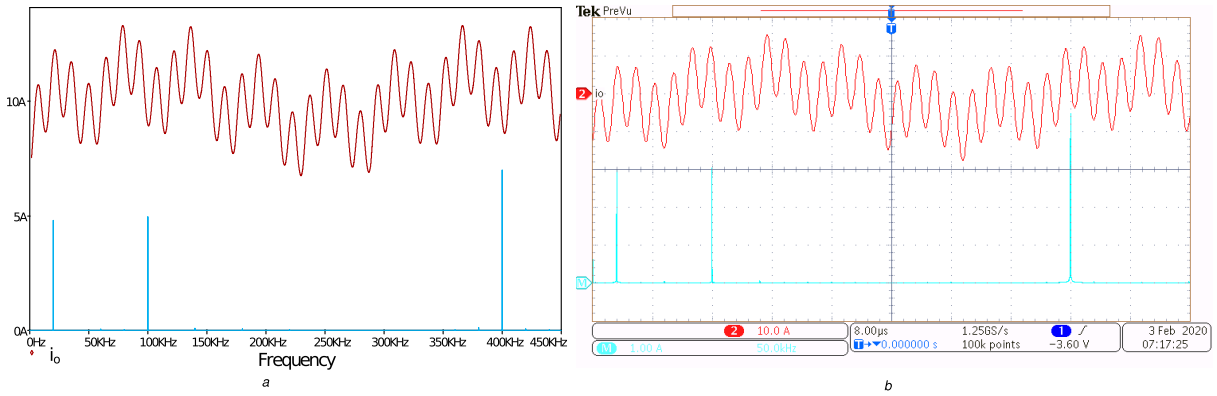

Figure 3.10: Inverter output current i_o and its FFT at D_l=0.95, D_m=0.95 and D_h=0.95
(a) Simulated waveforms
(b) experimental waveforms

= 0 and V_{02}= V_{dc}. The output voltage across the loads is expressed as

$$v_o = v_{01} + v_{02} = V_{dc} \tag{3.14}$$

Mode-4: In this mode, switches S_1, S_3, S_6 and S_7 are in on-state. The corresponding equivalent circuit is shown in (Fig. 3.8d). Output voltages of first and second inverters are respectively V_{01} = 0 and V_{02} = -V_{dc}. The output voltage across the loads is expressed as

$$v_o = v_{01} + v_{02} = -V_{dc} \tag{3.15}$$

When S_2 is ON, more four operating modes are possible as explained below
Mode-5: In this mode, switches S_2, S_3, S_6 and S_7 are in on-state. Output voltages of first and second inverters are respectively V_{01} = - $V_{dc}$and V_{02} = -V_{dc}. The output voltage across the loads is expressed as

$$v_o = v_{01} + v_{02} = -2V_{dc} \tag{3.16}$$

Mode-6: In this mode, switches S_2, S_3, S_5 and S_8 are in on-state. Output voltages of first and second inverters are respectively V_{01} = - V_{dc} and V_{02} = V_{dc}. The output voltage across the loads is expressed as

$$v_o = v_{01} + v_{02} = 0 \tag{3.17}$$

Mode-7: In this mode switches S_2, S_4, S_6 and S_7 are in on-state. Output voltages of first and second inverters are respectively V_{01} = 0 and V_{02} = -V_{dc}. The output voltage across the loads is expressed as

$$v_o = v_{01} + v_{02} = -V_{dc} \tag{3.18}$$

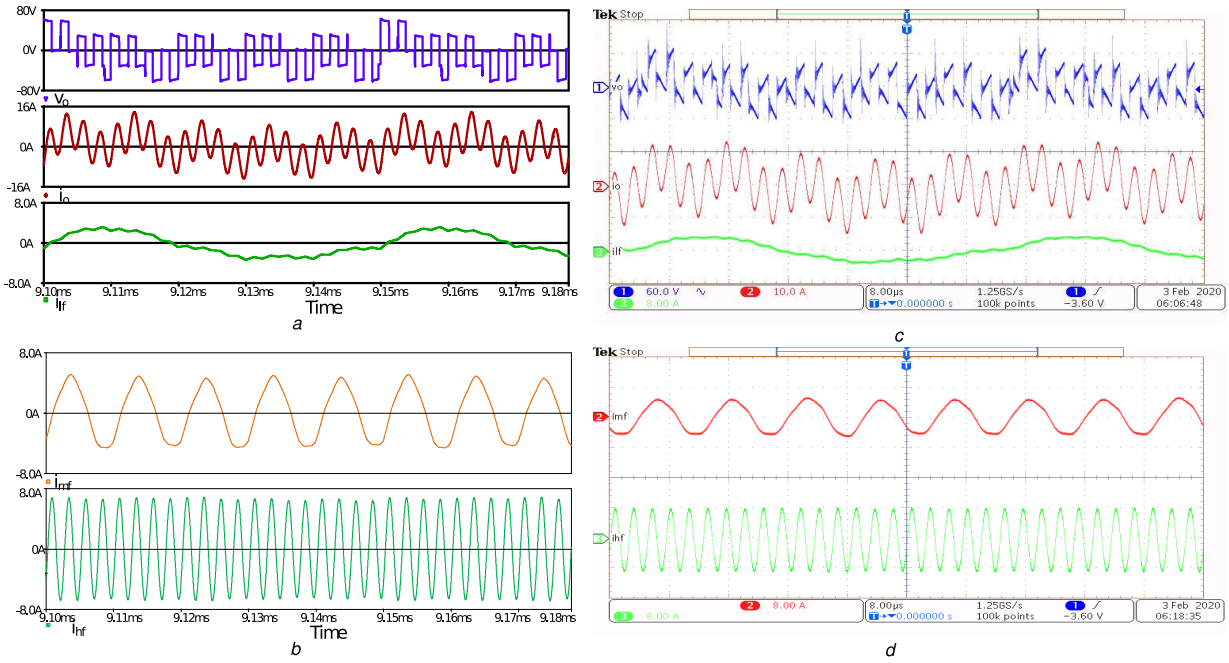

Figure 3.11: Load voltage (v_o), inverter output current (i_o) and load currents at D_l=0.2, D_m=0.95 and D_h=0.95 (a) Simulated waveforms of v_o, i_o and i_{lf}
(b) Simulated waveforms of i_{mf} and i_{hf}
(c) Experimental waveforms of v_o, i_o and i_{lf}
(d) Experimental waveforms of i_{mf} and i_{hf}

Mode-8: In this mode switches S_2, S_4, S_5 and S_8 are in on-state. Output voltages of first and second inverters are respectivelyV_{01} = 0 and V_{02} = V_{dc}. Output voltage across the loads is expressed as

$$v_o = v_{01} + v_{02} = V_{dc} \tag{3.19}$$

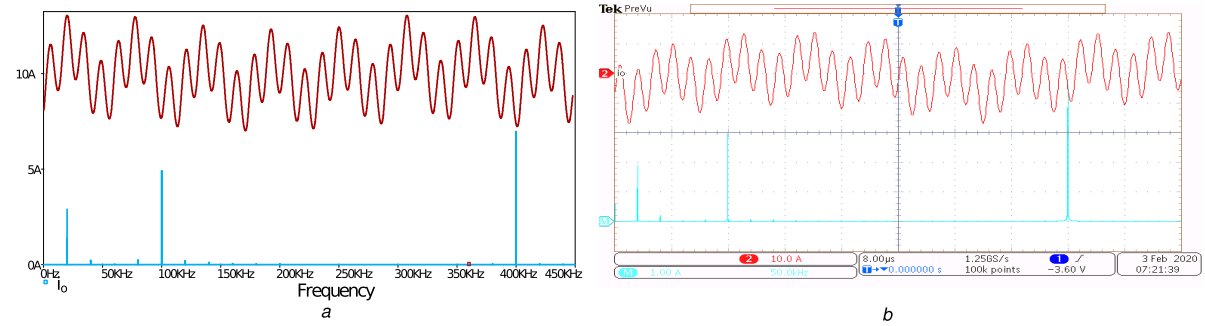

Figure 3.12: Inverter output current i_o and its FFT at D_l=0.2, D_m=0.95 and D_h=0.95
(a) Simulated waveforms
(b) experimental waveforms

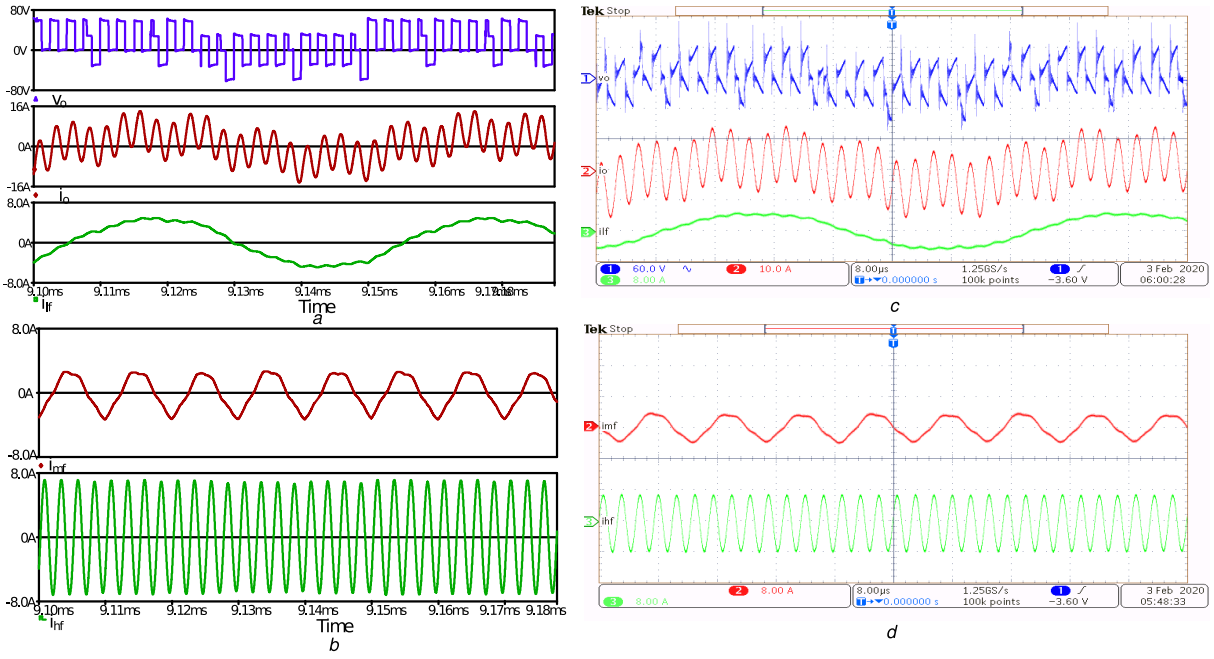

Figure 3.13: Load voltage (v_o), inverter output current (i_o) and load currents at D_l=0.95, D_m=0.2 and D_h=0.95
(a) Simulated waveforms of v_o, i_o and i_{lf}
(b) Simulated waveforms of i_{mf} and i_{hf}
(c) Experimental waveforms of v_o, i_o and i_{lf}
(d) Experimental waveforms of i_{mf} and i_{hf}

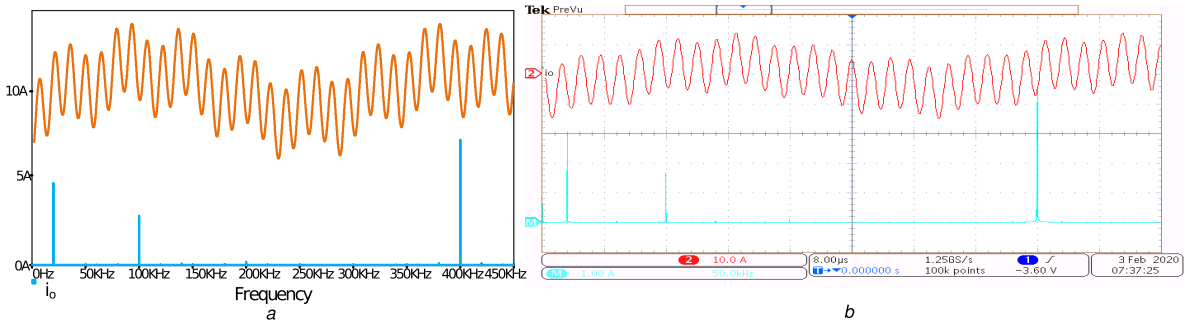

Figure 3.14: Inverter output current i_o and its FFT at D_l=0.95, D_m=0.2 and D_h=0.95
(a) Simulated waveforms
(b) Experimental waveforms

3.4 Simulation and experimental results

A 150 W prototype of the cascaded resonant inverter has been implemented for three different material vessel induction-cooking applications. The circuit parameters are presented in Table 3.1. Two isolated, equal DC voltage sources of V_{dc1} = 30 V and V_{dc2} = 30 V are used. The IH load parameters are measured from the coil side with the different material vessels of

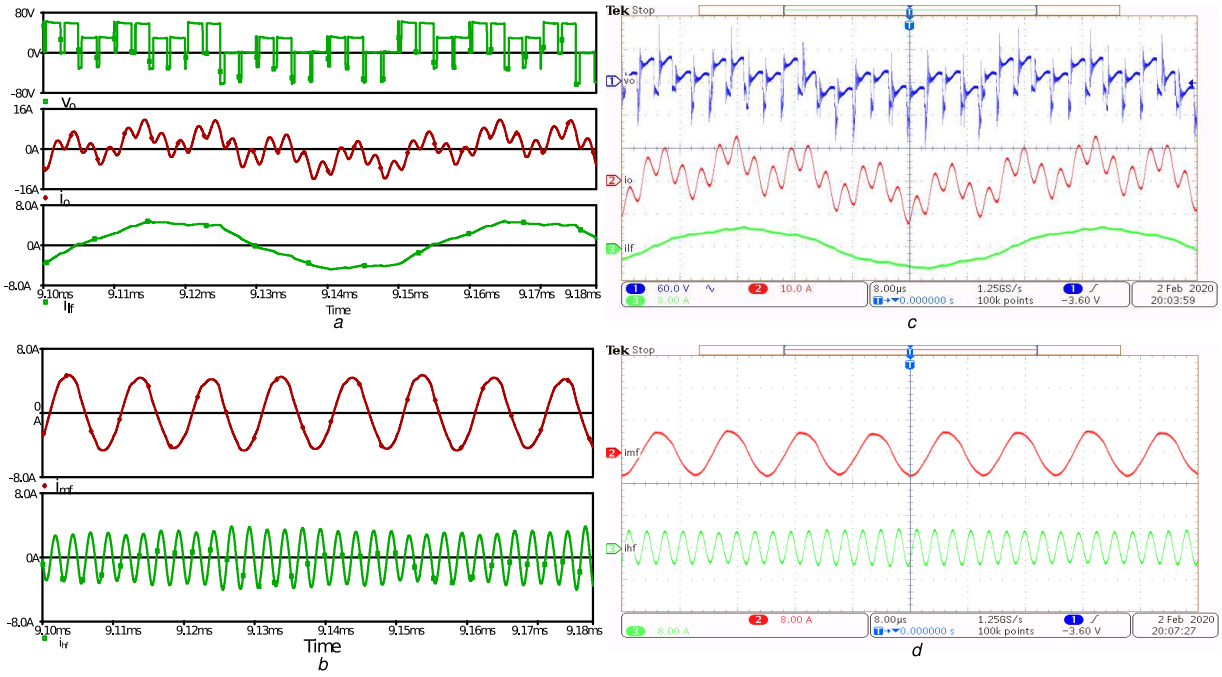

Figure 3.15: Load voltage (v_o), inverter output current (i_o) and load currents at D_l=0.95, D_m=0.95 and D_h=0.2
(a) Simulated waveforms of v_o, i_o and i_{lf}
(b) Simulation waveforms of i_{mf} and i_{hf}
(c) Experimental waveforms of v_o, i_o and i_{lf}
(d) Experimental waveforms of i_{mf} and i_{hf}

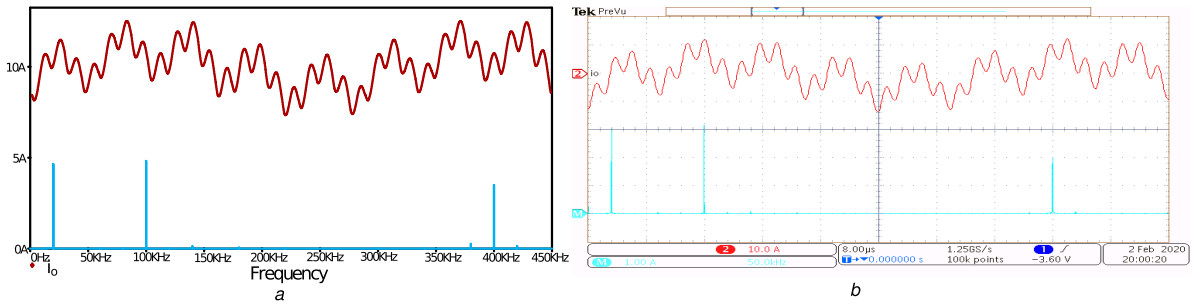

Figure 3.16: Inverter output current i_o and its FFT at D_l=0.95, D_m=0.95 and D_h=0.2
(a) Simulated waveforms
(b) Experimental waveforms

iron, steel, and aluminium are kept over respective IH coils. Iron, steel, and aluminium vessels, which are most commonly used in cooking applications, are selected for experimentation. These different vessel loads are resonated at frequencies of 18.4 kHz, 98 kHz and 395 kHz respectively with corresponding switching frequencies of 20 kHz, 100 kHz and 400 kHz respectively. ADC control is used for independent control of each load power.

Fig. 3.9 shows the simulation and experimental waveforms corresponding to equal duty

cycles of D_l=0.95, D_m=0.95 and D_h=0.95. (Fig. 3.9a) shows simulation waveforms of load voltage, inverter output current, and low-frequency current. (Fig. 3.9b) shows simulation waveforms of medium and high-frequency load currents. (Fig. 3.9c and d) show the corresponding experimental waveforms. (Fig. 3.10a and b) show respectively FFTs of simulated and experimental inverter output current at D_l=0.95, D_m=0.95 and D_h=0.95. It is observed that this current contains only low, medium and high-frequency components with RMS values of I_{lf}=3 A, I_{mf}=3.2 A and I_{hf}=4.72 A. It is also observed that the experimental and simulation results are in good agreement with each other. (Fig. 3.11) shows the simulation and experimental waveforms corresponding to duty cycles of D_l=0.2, D_m=0.95 and D_h=0.95. (Fig. 3.11a) shows simulation waveforms of load voltage, inverter output current, and low-frequency current.(Fig. 3.11b)

Table 3.1: Parameters of hardware prototype

Parameter	**Value**
DC Voltage source-1 (V_{dc1})	30 V
DC Voltage source-2 (V_{dc2})	30 V
Iron vessel equivalent inductance at low frequency (L_{1lf})	88.6 μH
Iron vessel equivalent resistance at Low frequency (R_{1lf})	2.87 Ω
Resonant capacitor at Low frequency (C_{1r})	0.96 μF
Steel vessel equivalent inductance at Medium frequency (L_{2mf})	62.45 μH
Steel vessel equivalent resistance at Medium frequency (R_{2mf})	2.9 Ω
Resonant capacitor at Medium frequency (C_{2r})	0.044 μF
Aluminium vessel equivalent inductance at high frequency (L_{3hf})	50.7 μH
Aluminium vessel equivalent resistance at High frequency (R_{3hf})	3.6 Ω
High frequency vessel resonant capacitor (C_{3r})	0.321 nF
Low switching frequency (f_l)	20 kHz
Iron load resonant frequency (f_{rl})	18.5 kHz
Medium switching frequency (f_m)	100 kHz
Steel load resonant frequency (f_{rm})	98 kHz
High switching frequency (f_h)	400 kHz
Aluminium load resonant frequency (f_{rh})	398 kHz
Mosfets used	IRFB4227pbf
Rdson	19 mΩ
DSP Controller	TMS320F28379D

shows simulation waveforms of medium and high-frequency load currents.(Fig. 3.11c and d)show the corresponding experimental waveforms. (Fig. 3.12a and b) show respectively FFTs of simulated and experimental inverter output current at D_l=0.2, D_m=0.95 and D_h=0.95. It is observed that the low-frequency load current is reduced to I_{lf}=1.7 A whereas medium and high frequency load currents remain at the same values of I_{mf}=3.2 A and I_{hf}=4.72 A. This indicates independent load control, as the reduction in low-frequency duty cycle, decreases only low-frequency load current whereas the other load currents remain unaffected. It is also observed that the experimental and simulation results are in good agreement with each other. (Fig. 3.13) shows the simulation and experimental waveforms corresponding to duty cycles of D_l=0.95, D_m=0.2 and D_h=0.95. (Fig. 3.13a) shows simulation waveforms of load voltage, inverter output current, and low-frequency current. (Fig. 3.13b) shows simulation waveforms of medium and high frequency load currents. (Fig. 3.13c and d) show the corresponding experimental waveforms. (Fig. 3.14a and b) show respectively FFTs of simulated and experimental inverter output current at D_l=0.95, D_m=0.2 and D_h=0.95. It is observed that the medium frequency load current is reduced to I_{mf}=1.8 A whereas low and high-frequency load currents remain at the same values of I_{lf}=3A and I_{hf}=4.72A. This indicates independent load control and it is also observed that the experimental and simulation results are in good agreement with each other. (Fig. 3.15) shows the simulation and experimental waveforms corresponding to duty cycles of D_l=0.95, D_m=0.95 and D_h=0.2. (Fig. 3.15a) shows simulation waveforms of load voltage, inverter output current, and low-frequency current. (Fig. 3.15b) shows simulation waveforms of medium and high-frequency load currents. (Fig. 3.15c and d)show the corresponding experimental waveforms. (Fig. 3.16a and b) show respectively FFTs of simulated and experimental inverter output current at D_l=0.95, D_m=0.95 and D_h=0.2. It is observed that the high-frequency load current is reduced to I_{hf}=2A whereas low and medium-frequency load currents remain at the same values ofI_{lf}=3A and I_{mf}=3.2A. This indicates independent load control and it is observed that the experimental and simulation results are in good agreement with each other.

3.5 Analysis of results

In the proposed multi IH load cascaded inverter, power control is realized through ADC control. The experimental setup is shown in (Fig. 3.17). Based on the thermal measurement, the temperature variations in different vessels are shown in (Fig. 3.18). From the simulation and experimental results, the output powers of individual loads have been calculated as described in section 2.3.1. The load power variation with ADC control is shown in (Fig. 3.19). (Fig. 3.19a) shows the variation of load powers P_{ol}, P_{om} and P_{oh} with low-frequency duty cycle (D_l) when D_m and D_h are kept constant at 0.95. Now it can be observed that only iron vessel load power (P_{ol})

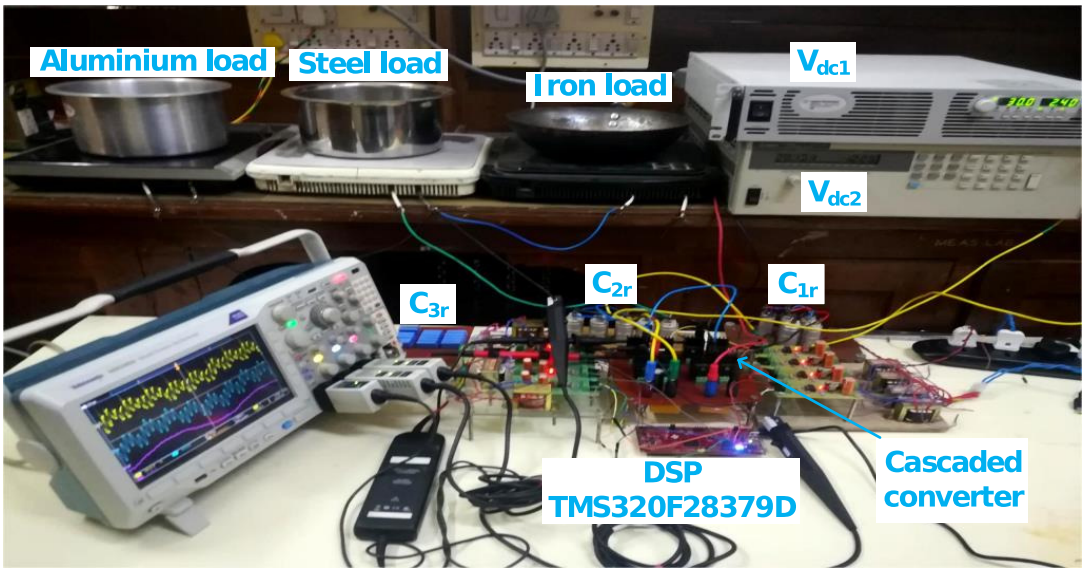

Figure 3.17: Experimental prototype

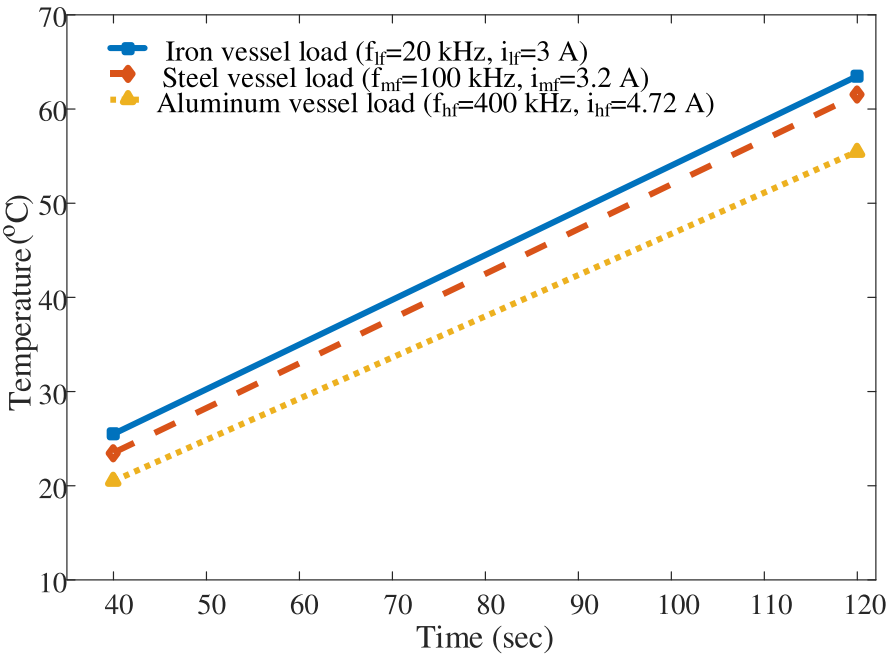

Figure 3.18: Temperature variation in different vessels

is varying while other load powers remain constant. Simulation and experimental results are in good agreement with each other.(Fig. 3.19b) shows the variation of load powers with medium frequency duty cycle (D_m) when D_l and D_h are kept constant at 0.95. It can be observed that only steel vessel load power (P_{om}) is varying while other load powers remain constant. Simulation and experimental results are in good agreement with each other. (Fig. 3.19c) shows the variation of load powers with a high-frequency duty cycle (D_h) when D_l and D_m are kept constant at 0.95. It is observed that only aluminium vessel load power (P_{oh}) is varying while other load powers

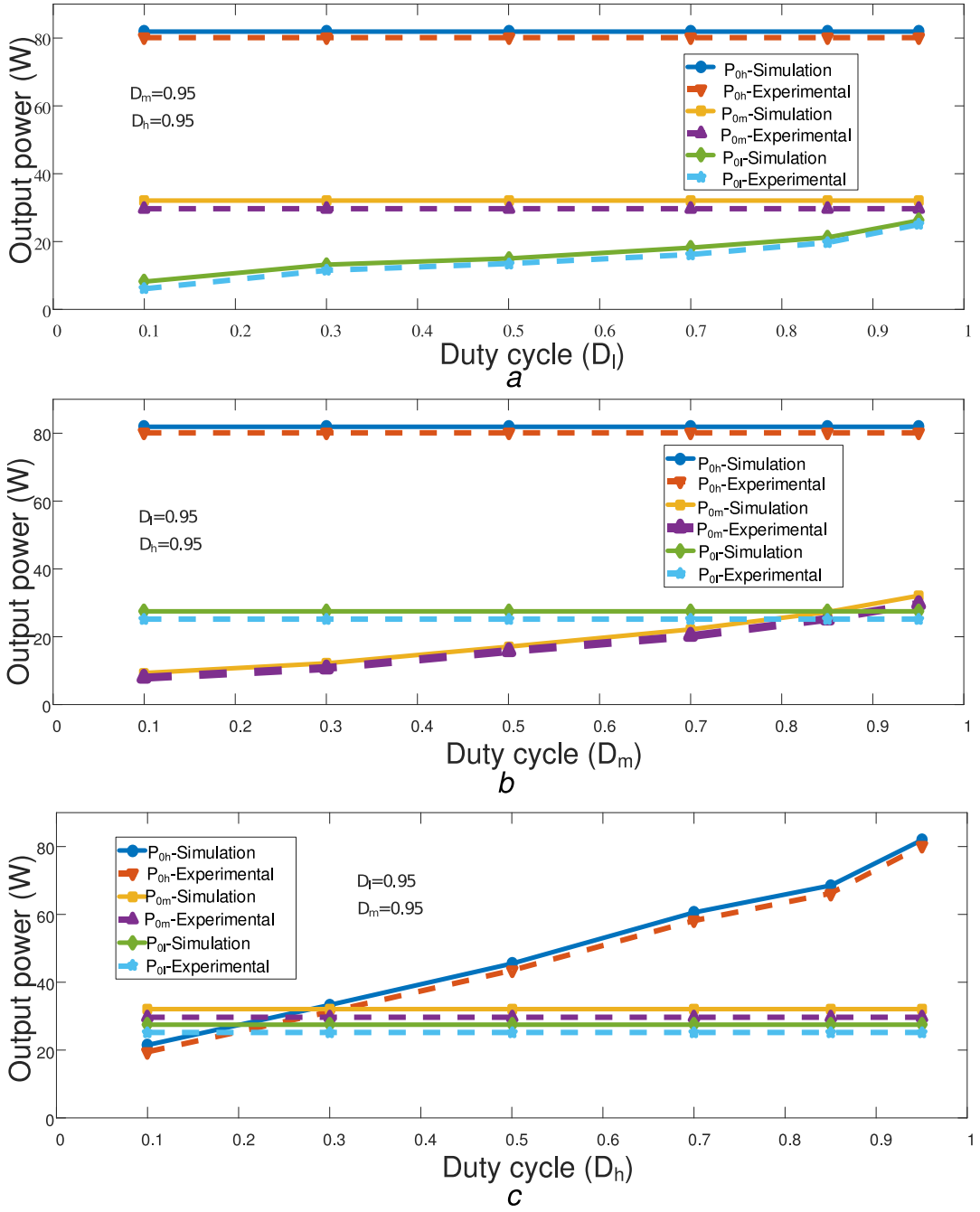

Figure 3.19: Low, Medium and High-Frequency current and power control
(a) Iron vessel power control against D_l
(b) Steel vessel power control against D_m
(c) Aluminium vessel power control against D_h

remain constant. Simulation and experimental results are in good agreement with each other. Hence, independent control of power in iron vessel, steel vessel, and aluminium vessel loads is verified. The total output power (P_o) of the cascaded inverter is the sum of different load powers

as explained. The input power of the cascaded inverter is calculated as below:

$$P_{in} = V_{dc1}I_{dc1} + V_{dc2}I_{dc2} \tag{3.20}$$

where I_{dc1} and I_{dc2} are the input currents of inverter-1 and inverter-2 respectively.

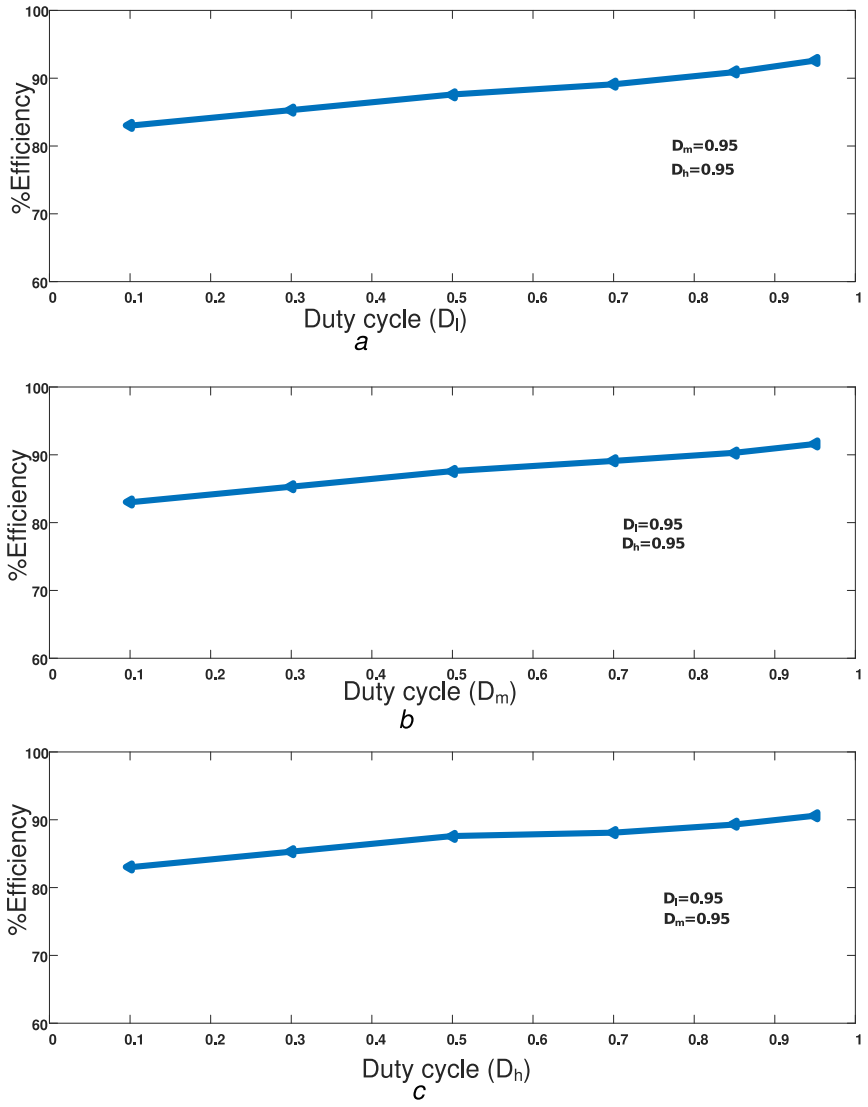

Figure 3.20: Efficiency curves
(a) Overall efficiency vs D_l
(b) Overall efficiency vs D_m
(b) Overall efficiency vs D_h

The overall efficiency of the cascaded inverter is calculated as

$$\eta = \frac{P_o}{P_{in}} \tag{3.21}$$

The efficiency curves are shown in (Fig. 3.20). (Fig. 3.20a) shows the graph of overall efficiency vs low-frequency duty cycle (D_l) when D_m and D_h are kept constant at 0.95. (Fig. 3.20b) shows the graph of overall efficiency vs medium-frequency duty cycle (D_m) when D_l and D_h are kept constant at 0.95. (Fig. 3.20c) shows the graph of overall efficiency vs high-frequency duty cycle (D_h) when D_l and D_m are kept constant at 0.95. From these plots, it can be observed that the overall efficiency increases with the duty cycle of the loads and vary from 85 percent to about 92 percent.

3.6 Conclusions

In this chapter, a multi-load cascaded full-bridge resonant inverter topology has been proposed for different material vessel IH loads. First inverter legs are operated at low and medium frequencies suitable for iron and steel vessels. Second inverter is operated at a high frequency which is suitable for aluminium vessel. Frequencies of 20 kHz, 100 kHz and 400 kHz are used. Independent power control is achieved using asymmetric duty cycle control.Simulation study of the inverter is performed and its results are verified experimentally. Both simulation and experimental results are in good agreement with each other.
The advantages of the proposed inverter configuration are:

i Powers multiple IH loads

ii Suitable for different material vessels

iii Eliminates the use of electro-mechanical switches

iv Low component count

v Overall efficiency is high ($\geq$ 92 %)

vi Independent power control is achieved using asymmetric duty cycle control

vii Proposed scheme can be extended to more than three loads.

The limitation of proposed inverter is the requirement of two DC sources.

Next chapter explains the proposed topology-2, Frequency controlled resonant inverter configuration for different material induction heating applications.

Chapter 4

Frequency Controlled Resonant Inverter configuration for Different Material Induction Heating Applications

Chapter 4

Frequency Controlled Resonant Inverter configuration for Different Material Induction Heating Applications

4.1 Introduction

This chapter proposes frequency controlled resonant inverter configuration suitable for three different material vessel IH application.

In literature, many of the existing multiple-output IH topologies are compatible with ferromagnetic materials only. Non-ferromagnetic material vessels, such as copper and aluminium, cannot be utilised with IH despite their good heating qualities and widespread usage in IC applications. Some converter topologies suitable for vessels made of ferromagnetic and non-ferromagnetic materials have been recently proposed. In [77], a DSP controlled IH system is proposed to heat copper metal pan. In [78] induction heating system is implemented to heat ferromagnetic conductive, non-ferromagnetic conductive and non-ferromagnetic non-conductive materials. Most of the suggested designs have one or many of the following limitations: use of electro-mechanical switches to choose the resonant capacitor combinations, EMI issue, and acoustic noise problems.

This chapter proposes a three-leg resonant inverter that is suitable for three different material vessels. It is capable of powering three different IC loads: iron vessel load, steel vessel load, and aluminium vessel load. These three IC loads are working at their respective resonant frequencies simultaneously. The pulse frequency modulation (PFM) technique is used to regulate the load powers independently. This configuration offers the benefits of independent control, reduced component count, and improved efficiency.

4.2 Three leg multiple load inverter configuration

4.2.1 Circuit description

The proposed three load inverter topology's circuit diagram is shown in (Fig. 4.1). This inverter topology consists of two capacitor C_1, C_2 and six switching devices S_1 to S_6 are Mosfet

switches with body diodes D_1 to D_6 and Lossless snubber capacitors C_{S1}-C_{S6} are connected across switching devices S_1-S_6 respectively to provide ZVS operation. First leg switching devices, S_1 and S_2 are switched at low frequency, f_l to supply iron vessel load. Leg two devices, S_3 and S_4 are operated at medium frequency, f_m to supply steel vessel load and S_5 and S_6 are switched at high frequency, f_h to supply aluminium vessel load. These three different frequency

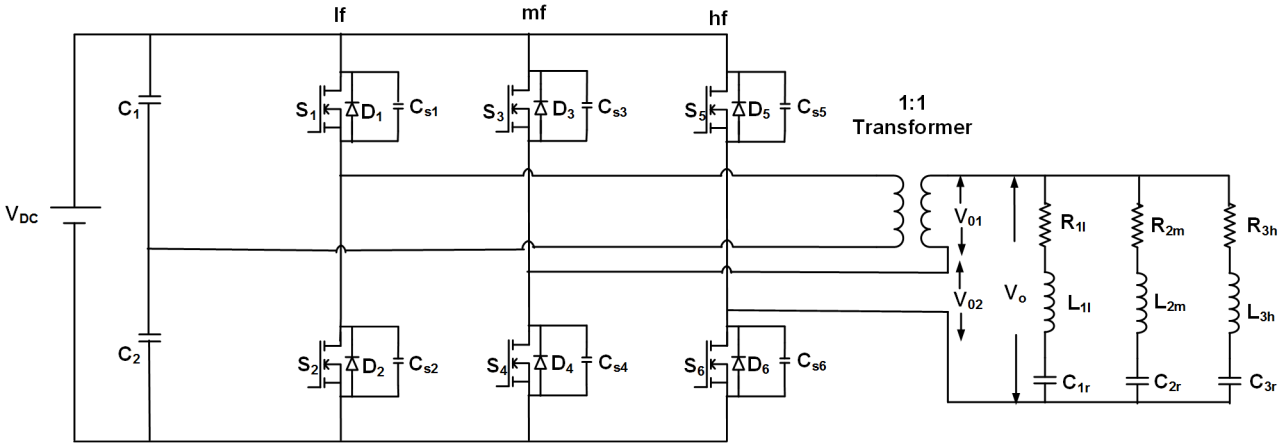

Figure 4.1: Proposed three leg inverter configuration

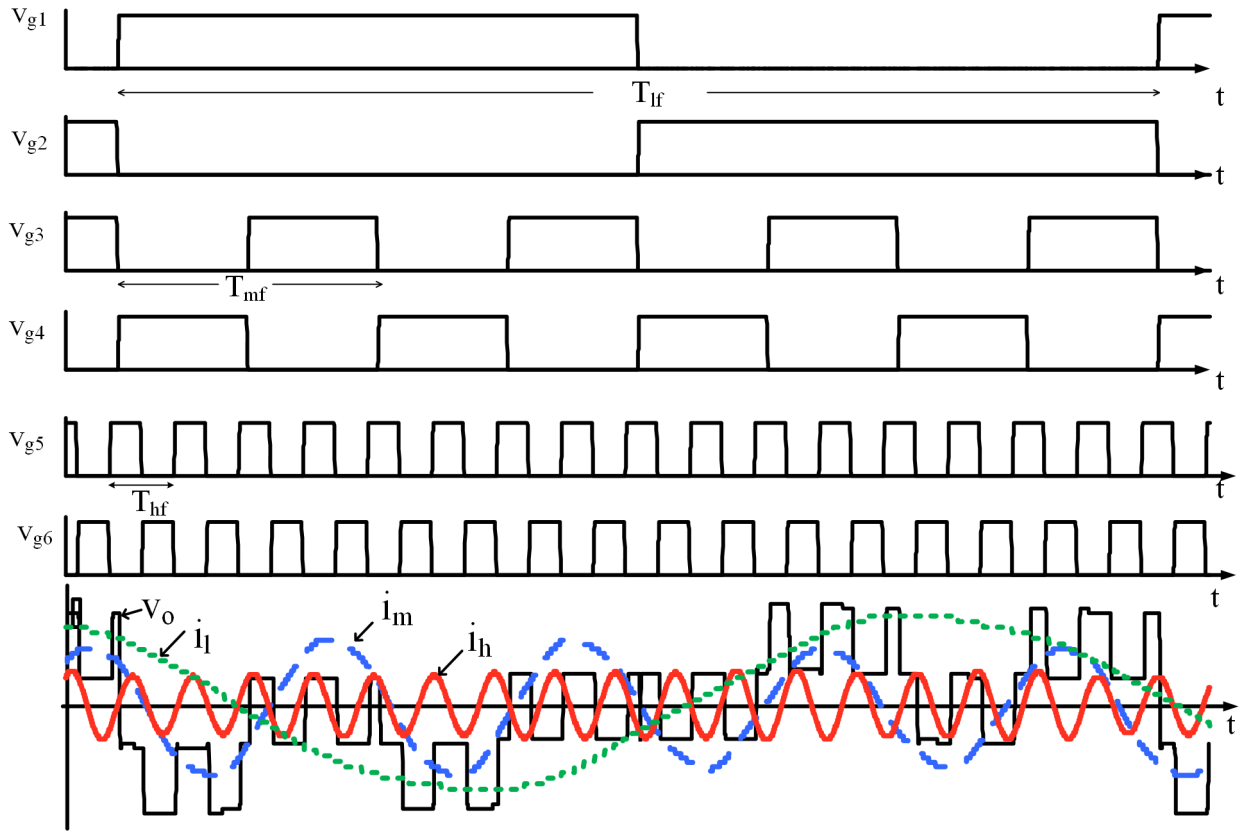

Figure 4.2: Three leg Inverter gate pulses and load voltage and load currents

legs are connected to three IC resonant loads through high frequency 1:1 transformer. Inverters output voltage $v_o = v_{o1}+v_{o2}$ where v_{o1} is transformer secondary terminal voltage and v_{o2} is medium, high frequency legs output voltage. i_o is the total load current of the inverter.

This arrangement supplies power to three burners, each of which is suited to iron, steel and aluminium metal loads. The equivalent resistance and equivalent inductance of an iron metal burner at low frequency, f_l, are R_{1l} and L_{1l} respectively. To resonate this load at low resonant frequency (f_{lr}), an external resonant capacitor C_{r1} is connected in series with load. R_{2m} and L_{2m} are the equivalent resistance and equivalent inductance of a steel metal burner at medium frequency, f_m. C_{r2} is an external resonant capacitor connected in series with load to resonate this load at the medium resonant frequency, f_{mr}. R_{3h} and L_{3h} are the equivalent resistance and equivalent inductance of an aluminium metal burner at high frequency(hf), f_h. An external resonant capacitor C_{r3} is connected in series with load to resonate this load at a high resonant frequency, f_{hr}. i_l, i_m, and i_h are currents flowing through iron, steel, and aluminium metal burner resonant loads, respectively. The switching frequencies for three legs of the inverter are adjusted to f_l= 25 kHz for leg-1 (lf), f_m= 100 kHz for leg-2 (mf) and f_h= 400 kHz for leg-3 (hf), respectively. The inverter switching devices gate pulses, as well as the associated output voltage v_o and different frequency load currents i_l, i_m, and i_h are depicted in (Fig. 4.3). The sum of three distinct frequency load currents is i_o

4.2.2 Inverter legs switching frequency selection

Domestic induction heating loads require alternating current with a high frequency ($\geq$20 kHz). The heat produced in the vessels condenses in a peripheral layer of skin depth ((δ) [79].

Ferromagnetic metal loads have greater resistivity and permeability values. When the vessel is placed on the cooker, the equivalent circuit of the induction cooking load is a series combination of L_{eq} and R_{eq} , where L_{eq} and R_{eq} are the equivalent inductance and resistance. These values vary based on the switching frequency and the material of the vessel used. Three distinct metal vessel IC loads are considered in this arrangement. The first and second IC loads are made of ferromagnetic materials(iron and steel). The third IC load is made of non-ferromagnetic materials(aluminium). The variations of the equivalent circuit parameters L_{eq} and R_{eq} of these three distinct IC loads with inverter operating frequencies are depicted in (Fig. 4.3). (Fig. 4.3a depicts the change of iron load with leg-1 frequency in terms of L_{eq} and R_{eq}. Whereas (Fig. 4.3b) and (Fig. 4.3c) depict the same for steel vessels and aluminium vessels, respectively. According to these frequency characteristics, the iron material vessel load has greater values of L_{eq} and R_{eq} at about 25 kHz. As a result, the switching frequency, f_l, of the iron vessel IC load

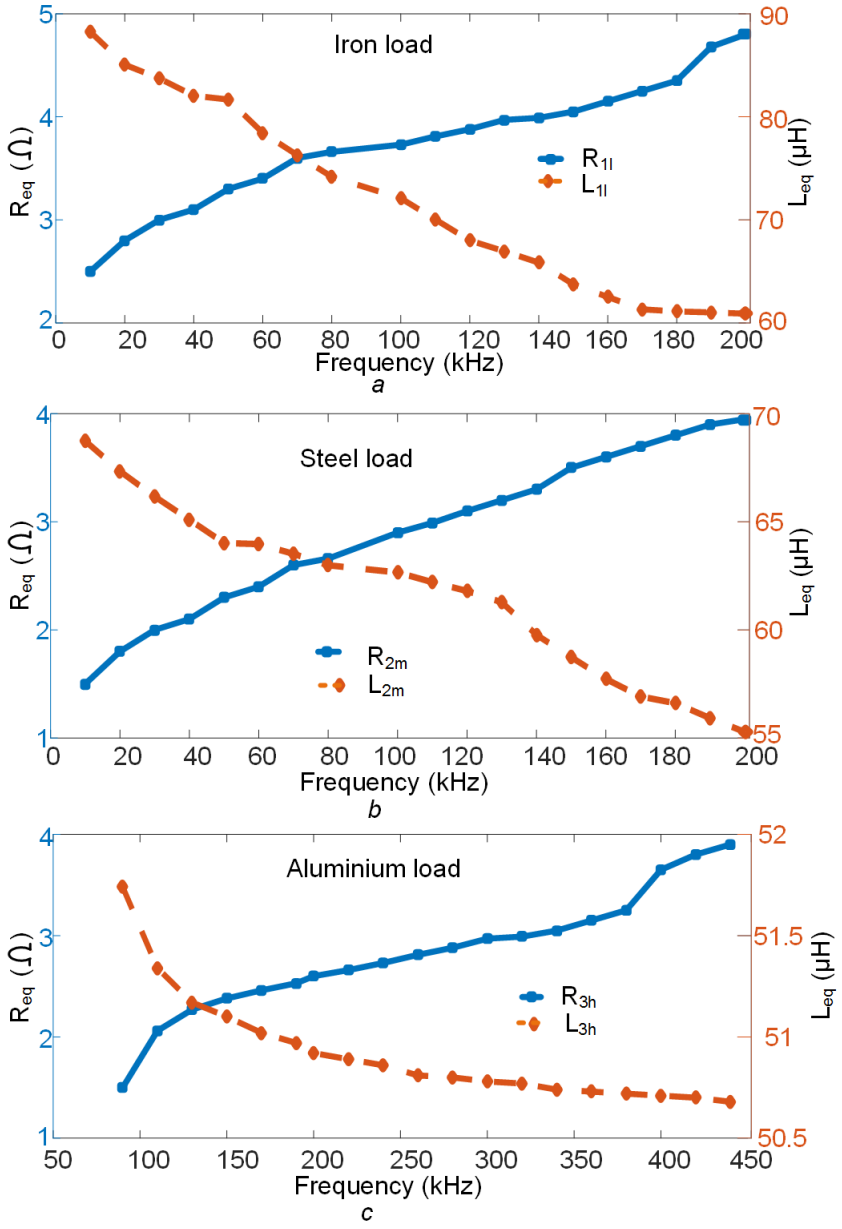

Figure 4.3: Frequency characteristics of different vessel loads
(a) Iron vessel load-1
(b) Steel vessel load-2
(c) Aluminium vessel load-3

is regulated to 25 kHz. At this frequency, steel and aluminium loads have lower L_{eq} and R_{eq} values. Above 80 kHz frequency the equivalent resistance (R_{eq}) of steel vessel load is greater than 2 Ω, and similarly, above 300 kHz frequency the equivalent resistance(R_{eq}) of aluminium vessel load is greater than 2 Ω. As a result, raising the frequency increases the R_{eq} and hence the load output power. The switching frequency of the steel IC load is set to a f_m equal to 100 kHz, while the switching frequency of the aluminium load is set to a f_h equal to 400 kHz. External

resonant capacitors are connected to IC loads to resonate the load at f_r. To get ZVS operation, the $\frac{f_s}{f_r}$ ratio should be set closer to 1.1. As a result, f_{lr}, f_{mr} and f_{hr} are chosen to be 23.5 kHz, 98.2 kHz, and 396 kHz, respectively. The resonant external capacitors are chosen based on the equations for f_{lr}, f_{mr} and f_{hr}, where

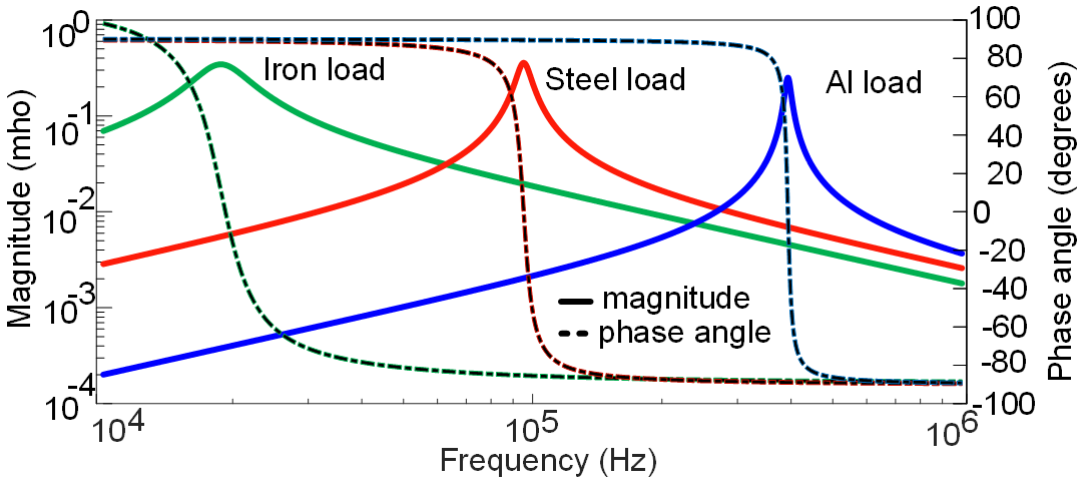

Figure 4.4: Admittance curve

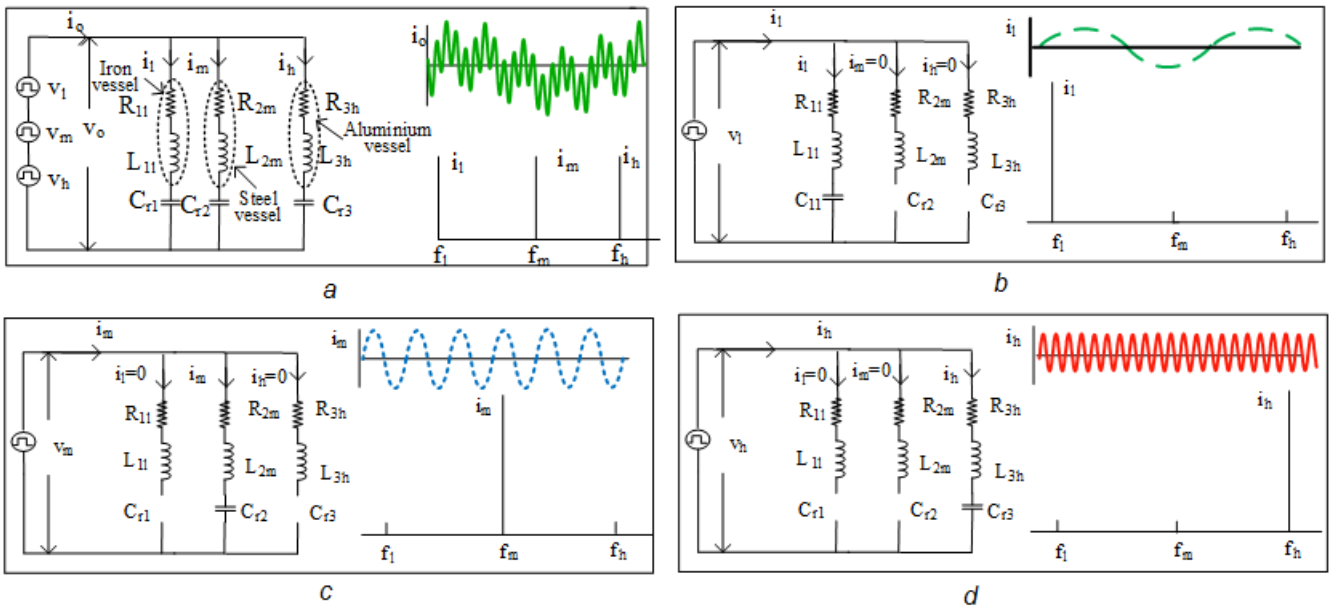

Figure 4.5: Equivalent circuits of the load, load current and their FFTs
(a) Equivalent circuit of multiple frequency inverter, load currents and FFT
(b) Equivalent circuit of load for v_l and load current FFT
(c) Equivalent circuit of load for v_m and load current FFT
(d) Equivalent circuit of load for v_h and load current FFT

$$f_{lr} = \frac{1}{2\pi\sqrt{L_{1l}C_{r1}}}, f_{mr} = \frac{1}{2\pi\sqrt{L_{2m}C_{r2}}} and f_{hr} = \frac{1}{2\pi\sqrt{L_{3h}C_{r3}}} \tag{4.1}$$

respectively. The admittance characteristics of the three domestic IC loads are represented in (Fig. 4.4). It illustrates that the iron vessel, steel vessel, and aluminium vessel resonant loads have the maximum admittance at low-frequency (lf), medium-frequency(mf), and high-frequency(hf) resonant frequency respectively.

4.2.3 Thee-leg inverter operating principle

The total output voltage v_o of the three-leg inverter design is the sum of the transformer secondary terminal voltage v_{o1} and the output voltage v_{o2} of the inverter medium and high-frequency legs. Because the transformer primary terminals are linked to the output of the low-frequency leg and the dc-link capacitor midpoint, it functions as a low-frequency half-bridge inverter and feeds low-frequency voltage to the 1:1 transformer; hence, v_{o1} has a low-frequency component voltage v_l. Similarly v_{o2} is output voltage of medium frequency (mf) and high frequency (hf) legs of the inverter hence v_{o2} is combination of medium frequency and high frequency component of voltages v_m and v_h (Fig. 4.2).

$$v_o = v_{o1} + v_{o2} = v_l + v_m + v_h \tag{4.2}$$

Inverter loads equivalent circuit is shown in Fig. 4.5a. The waveform of the inverter total load current and FFT are also presented. It represents i_o as a sum of low-frequency current i_l, medium-frequency i_m, and high-frequency i_h currents. Fig. 4.5b indicates the behaviour of three IC loads for the low-frequency component of output voltage v_l. At f_l, the external resonant capacitors C_{r2} and C_{r3} have very high reactance and behave as open circuits, thus the i_l does not flow through steel and aluminium vessel loads. The impedance (Z_{1l}) of the iron vessel load is now written as

$$Z_{1l} = R_{1l} + j(X_{L1l} - X_{C1l}) \tag{4.3}$$

where
X_{L1l}=$2\pi f_l L_{1l}$,X_{c1l}=$1/(2\pi f_l C_{r1})$.

However, $X_{L1l}\approx X_{C1l}$ and hence $Z_{1l}\approx R_{1l}$. As a result, at resonance the iron vessel load offers the very low resistance path for i_l , which flows through the iron vessel load.

At f_m, an inductive reactance(L_{1m}) and capacitive reactance (C_{r3}) are extremely high, causing them to behave like open circuits. At resonance Steel vessel load impedance (Z_{2m}) can

be expressed as

$$Z_{2m} = R_{2m} + j(X_{L2m} - X_{Cm2}) \tag{4.4}$$

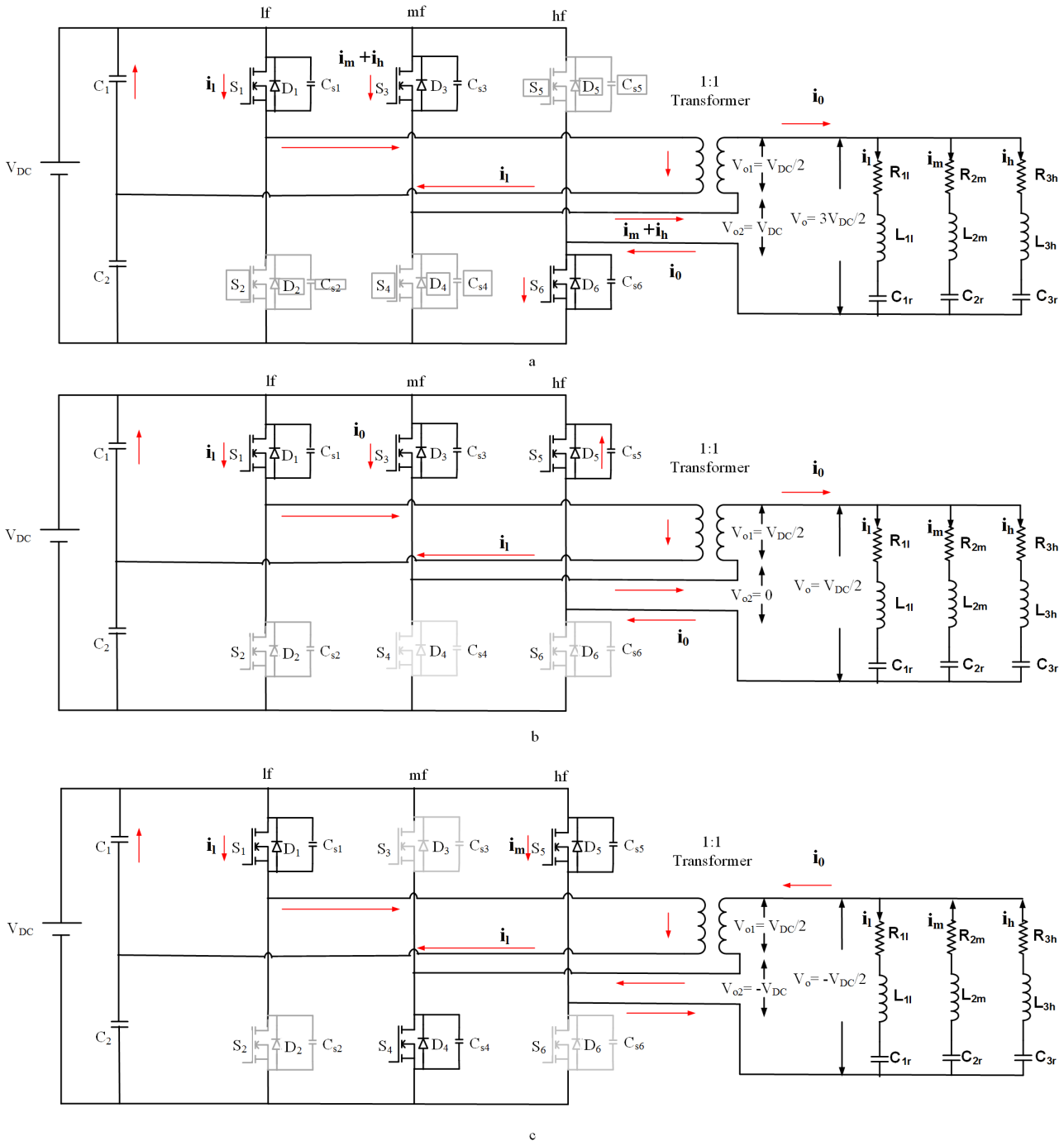

Figure 4.6: Inverter equivalent circuits for mode 1 to mode 3
(a) Mode1 S_1, S_3 and S_6 are ON
(b) Mode2 S_1, S_3 and S_5 are ON
(c) Mode3S_1, S_4 and $S_5$are ON

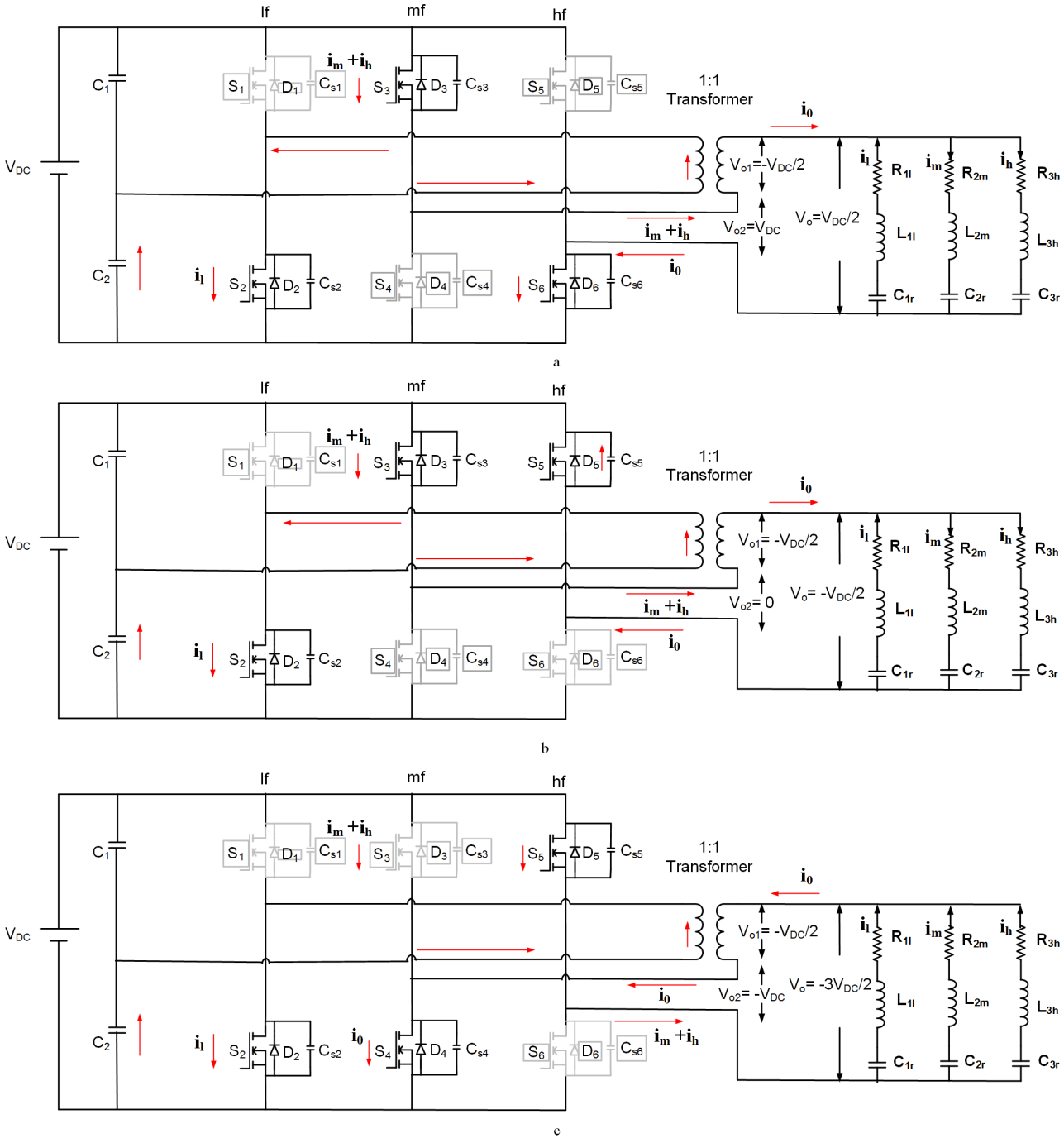

Figure 4.7: inverter equivalent circuits for mode 4 to mode 6
(a) Mode1 S_2, S_3 and S_6 are ON
(b) Mode2 S_2, S_3 and S_5 are ON
(c) Mode3S_2, S_4 and $S_5$are ON

where

X_{L2m}=$2\pi f_m L_{2m}$, and X_{c2m}=$1/(2\pi f_m C_{r2})$

However, $X_{L2m} \approx X_{C2r}$ and hence $Z_{2m} \approx R_{2mf}$. As a result, at resonance the steel vessel load offers very low resistance path for i_m, which flows through the steel vessel load.

At f_h, an inductive reactance (L_{1h}) and capacitive reactance (L_{2h}) are extremely high, and they act like open circuit. The resonant load impedance (Z_{3h}) of an aluminium vessel at high frequency can be written as

$$Z_{3h} = R_{3h} + j(X_{L3h} - X_{C3h}) \tag{4.5}$$

where
$X_{L3h}=2\pi f_h L_{3h}$, and $X_{C3h}=1/(2\pi f_h C_{r2})$

However, $X_{L3h} \approx X_{Cr3}$ and hence $Z_{3h} \approx R_{3h}$. As a result, at resonance, the aluminium vessel load offers the lowest resistance path for the i_h. Hence, a high frequency current(i_h) flows through the aluminium vessel load.

4.2.3.1 Load power control

This multiple-load domestic induction heating (IH) invert total output power is expressed as

$$P_o = P_l + P_m + P_h \tag{4.6}$$

where
P_l = iron vessel load output power $=I_l{}^2 R_{1l}$
P_m = steel vessel load output power $=I_m{}^2 R_{2m}$ and
P_h = aluminium vessel load output power $=I_h{}^2 R_{3h}$

I_l, I_m and I_h are the RMS values of the load currents in an iron vessel load, a steel vessel load, and an aluminium vessel load, respectively. The output powers of these various loads are controlled independently by using the pulse frequency modulation technique.

4.3 Modes of operation

Six distinct modes can be used to illustrate the proposed inverter operation. When the low-frequency leg-1 device S_1 is turned on, three operational modes are explained based on the switching states of the leg-2 and leg-3 devices. Similarly, When the low-frequency leg-1 device S_2 is turned on, three more operational modes are explained. These modes are described below: Mode-1: Switches S_1, S_3, and S_6 are turned on in this mode. (Fig. 4.6a) represents the equivalent equivalent circuit. The output voltages of the transformer secondary terminal voltage and

medium, high frequency legs output voltage of the inverter are $V_1 = V_{dc}/2$ and $V_2 = V_{dc}$, respectively. The total output voltage (v_o) across the different metal loads is the sum of V_{o1} and V_{o2}.

$$v_o = v_{o1} + v_{o2} = \frac{3V_{dc}}{2} \tag{4.7}$$

the instantaneous value of load current

$$i_o(t) = i_{lf}(t) + i_{mf}(t) + i_{hf}(t) \tag{4.8}$$

Mode-2: Switches S_1, S_3, and S_5 are turned on in this mode. Its equivalent circuit is represented in (Fig. 4.6b). The voltages of the transformer secondary terminal voltage and medium, high frequency legs voltages of th inverter are $V_1 = V_{dc}/2$ and $V_2 = 0$. The voltage across the loads is written as

$$v_o = v_{o1} + v_{o2} = \frac{V_{dc}}{2} \tag{4.9}$$

Mode-3: Switches S_1, S_4, and S_5 are turned on in this mode. Its equivalent circuit is presented in (Fig. 4.6c). The output voltages of the transformer secondary terminal voltage and medium, high frequency legs output voltage of th inverter are $V_{o1} = V_{dc}/2$ and $V_{o2} = -V_{dc}$, respectively. The voltage across the loads is defined by the equation

$$v_o = v_{o1} + v_{o2} = -\frac{V_{dc}}{2} \tag{4.10}$$

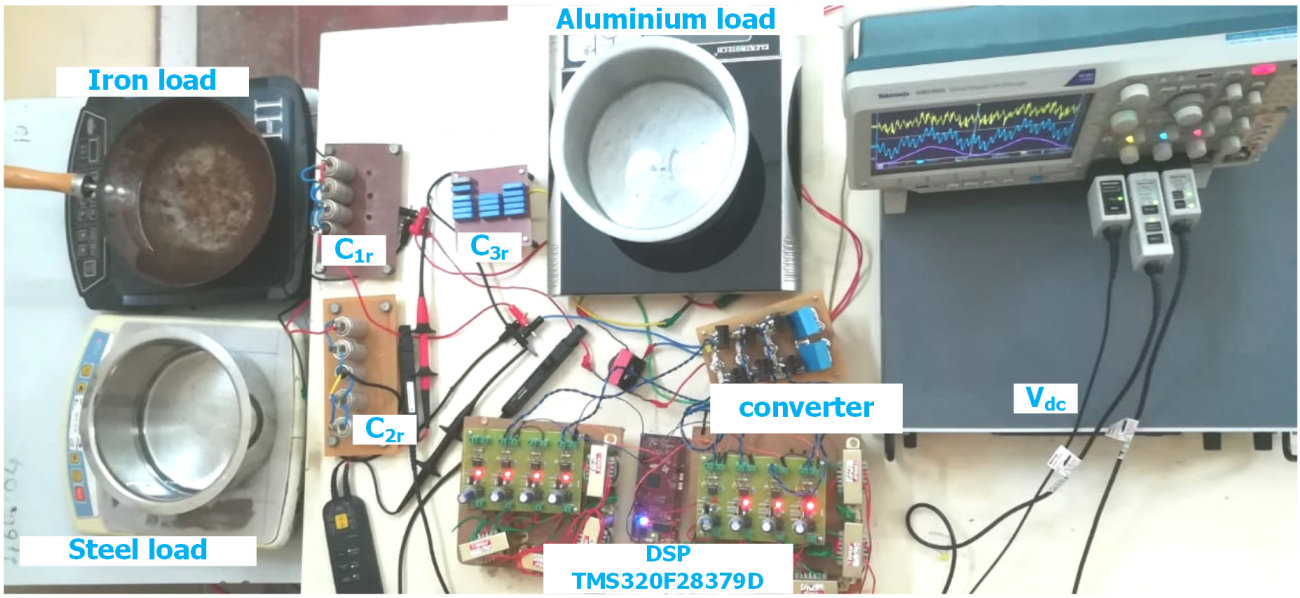

Figure 4.8: Prototype of Experimental setup

When S_2 is turned on, three more operating modes are available, as detailed below.
Mode-4: Switches S_2, S_3, and S_6 are turned on in this mode. Its equivalent circuit is presented in (Fig. 4.7a). The output voltages of the transformer secondary terminal voltage and the medium, high frequency legs output voltage of the inverter are V_{o1} =-V_{dc}/2 and V_{o2} = V_{dc}, respectively. The voltage across the loads is defined by the equation

$$v_o = v_{o1} + v_{o2} = \frac{V_{dc}}{2} \tag{4.11}$$

Mode-5: Switches S_2, S_3, and S_5 are turned on in this mode. The output voltages of the transformer secondary terminal voltage and the inverter's medium and high frequency legs are V_{o1} = - V_{dc}/2 and V_{o2} = 0. The voltage across the loads is defined by the equation

$$v_o = v_{o1} + v_{o2} = -\frac{V_{dc}}{2} \tag{4.12}$$

Table 4.1: Parameters of hardware prototype

Parameter	value
DC Voltage source (V_{DC})	60 V
Iron vessel load equivalent inductance at 25 kHz (L_{1l})	88.6 μH
Iron vessel load equivalent resistance at 25 kHz (R_{1l})	3.3 Ω
Resonant capacitor of load-1 (C_{r1})	0.95 μF
Steel vessel load equivalent inductance at 100 kHz (L_{2m})	63.45 μH
Steel vessel load equivalent resistance at 100 kHz (R_{2m})	3.1 Ω
Resonant capacitor of load-2 (C_{r2})	0.0435 μF
Aluminium vessel load equivalent inductance at 400 kHz (L_{3h})	50.8 μH
Aluminium vessel load equivalent resistance at 400 kHz (R_{3h})	3.7 Ω
Resonant capacitor of load-3 (C_{r3})	0.322 nF
Leg-1 frequency (f_l)	25 kHz
Load-1 resonant frequency (f_{lr})	23.6 kHz
Leg-2 frequency (f_m)	100 kHz
Load-2 resonant frequency (f_{mr})	97.8 kHz
Leg-3 frequency (f_h)	400 kHz
Load-3 resonant frequency (f_{hr})	397.9 kHz
Power mosfets used	IRF300P226
Rdson	40 mΩ
DSP Controller	TMS320F28379D

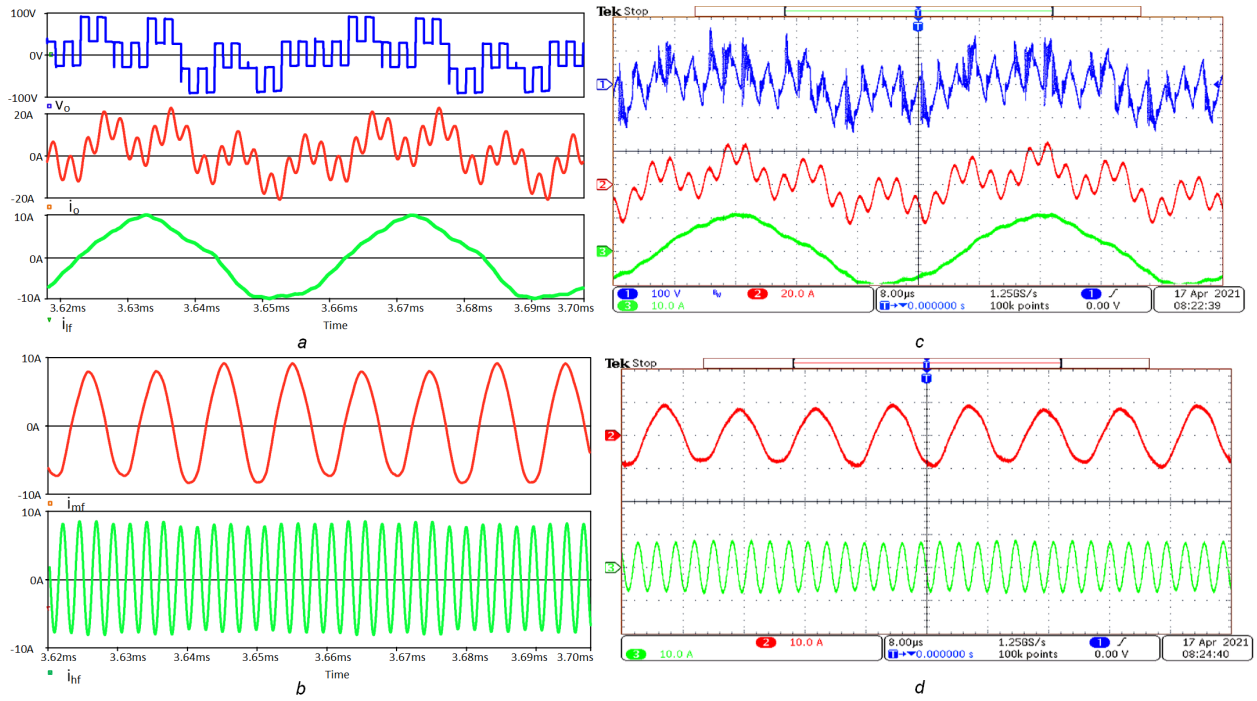

Figure 4.9: Load voltage (v_o), total load current (i_o) and individual load currents at f_l= 25 kHz, f_m= 100 kHz and f_h= 400 kHz
(a) Simulation waveforms of v_o, i_o and i_l
(b) Simulated waveforms of i_m and i_h
(c) Experimental waveforms of v_o, i_o and i_l
(d) Experimental waveforms of i_m and i_h

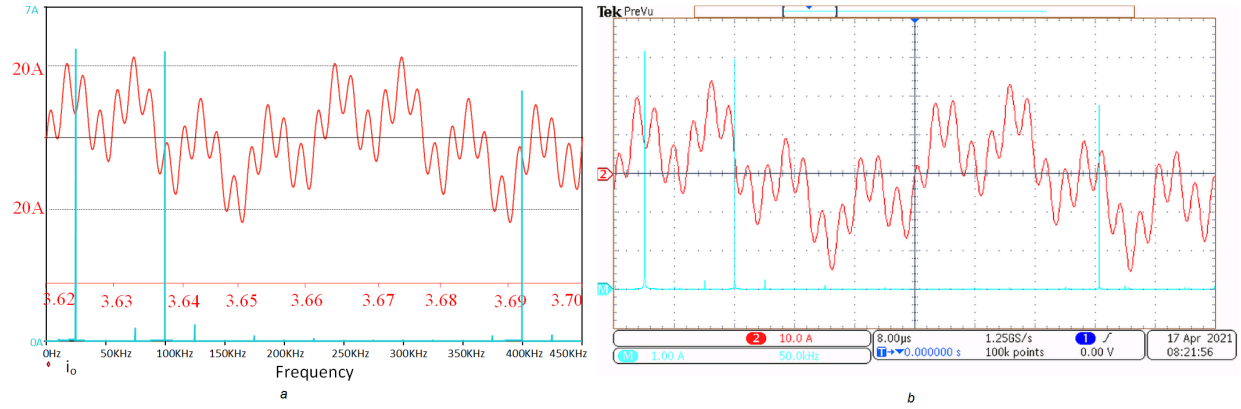

Figure 4.10: Inverter total load current i_o and its FFT at f_l= 25 kHz, f_m= 100 kHz and f_h= 400 kHz
(a) Simulation waveforms
(b) Experimental waveforms

Mode-6: Switches S_2, S_4, and S_5 are turned on in this mode. The output voltages of the transformer secondary terminal voltage and the medium, high frequency legs output voltage of the

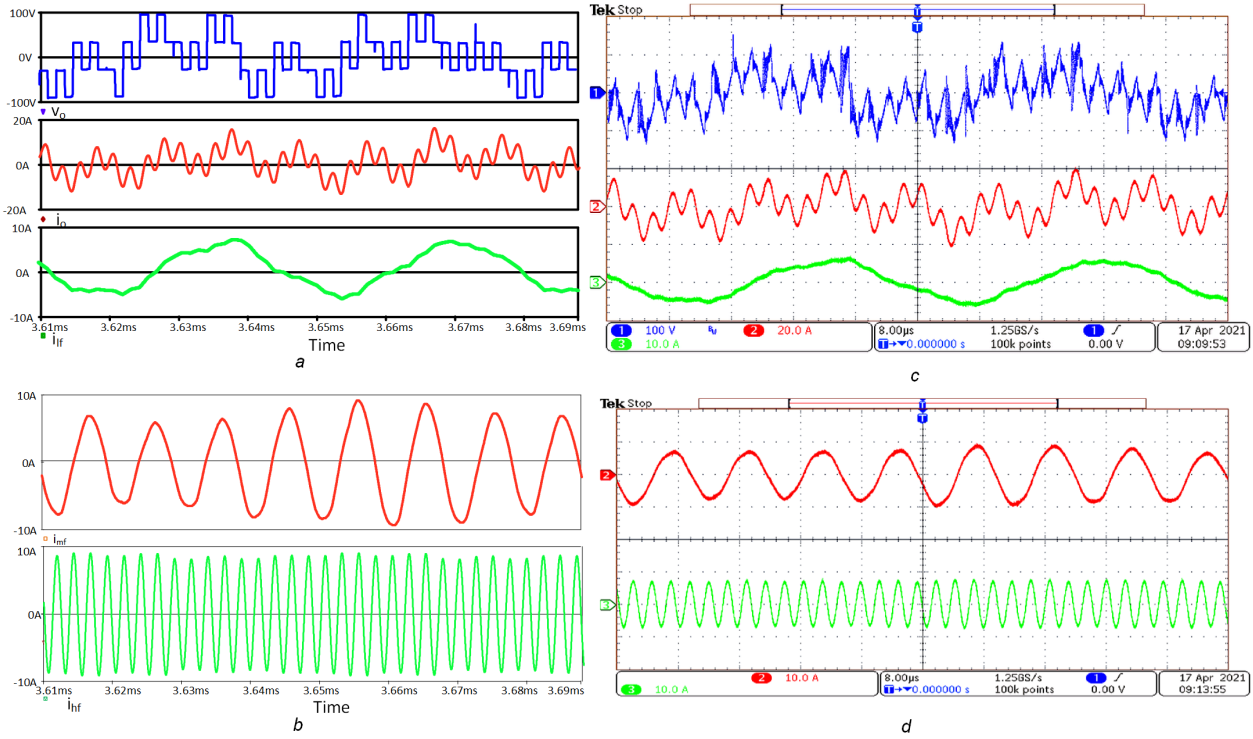

Figure 4.11: Load voltage (v_o), total load current (i_o) and load currents at f_l= 30 kHz, f_m= 100 kHz and f_h= 400 kHz
(a) Simulated waveforms of v_o, i_o and i_l
(b) Simulation waveforms of i_m and i_h
(c) Experimental waveforms of v_o, i_o and i_l
(d) Experimental waveforms of i_m and i_h

inverter areV_{o1} = -V_{dc}/2 and V_{o2} = -V_{dc}, respectively. The voltage across the loads is defined by the equation.

$$v_o = v_{o1} + v_{o2} = -\frac{3V_{dc}}{2} \tag{4.13}$$

4.4 Simulated and experimental results

A 330 W three-leg resonant inverter prototype has been developed for three distinct metal vessel domestic IH applications. Table 5.1 illustrates the circuit parameters. A V_{dc} = 60 V DC voltage is applied for hardware implementation. Domestic IH load characteristics are determined from the load coil side using various metal vessels made of iron material, steel material, and aluminium material that are placed above respective IC coils. The iron metal vessel, steel metal vessel, and aluminium metal vessels, which are widely used in IC applications, are chosen for testing. These various vessels IH loads resonate at frequencies of 23.5 kHz, 98.2 kHz, and 396 kHz, with corresponding switching frequencies of 25 kHz, 100 kHz, and 400 kHz. The

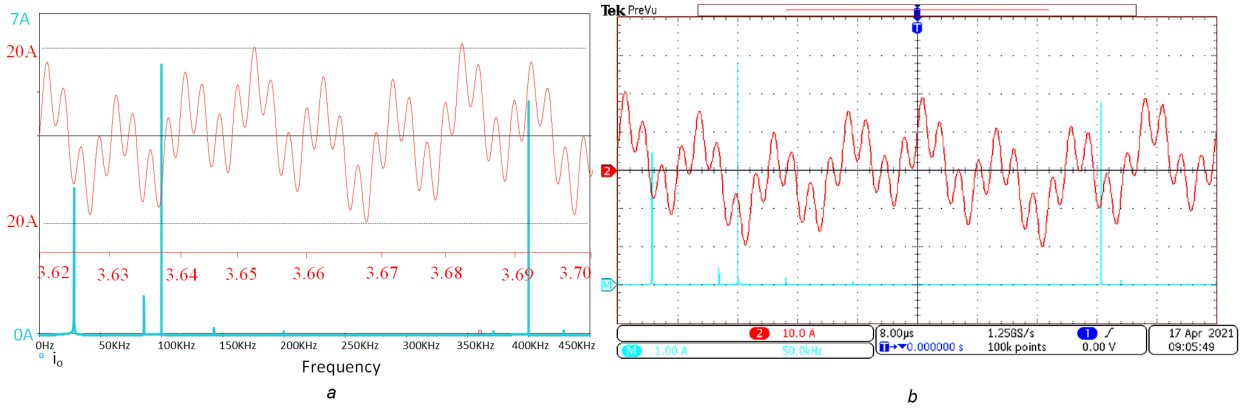

Figure 4.12: Inverter total load current i_o and its FFT f_l= 30 kHz, f_m= 100 kHz and f_h= 400 kHz
(a) Simulation waveforms
(b) experimental waveforms

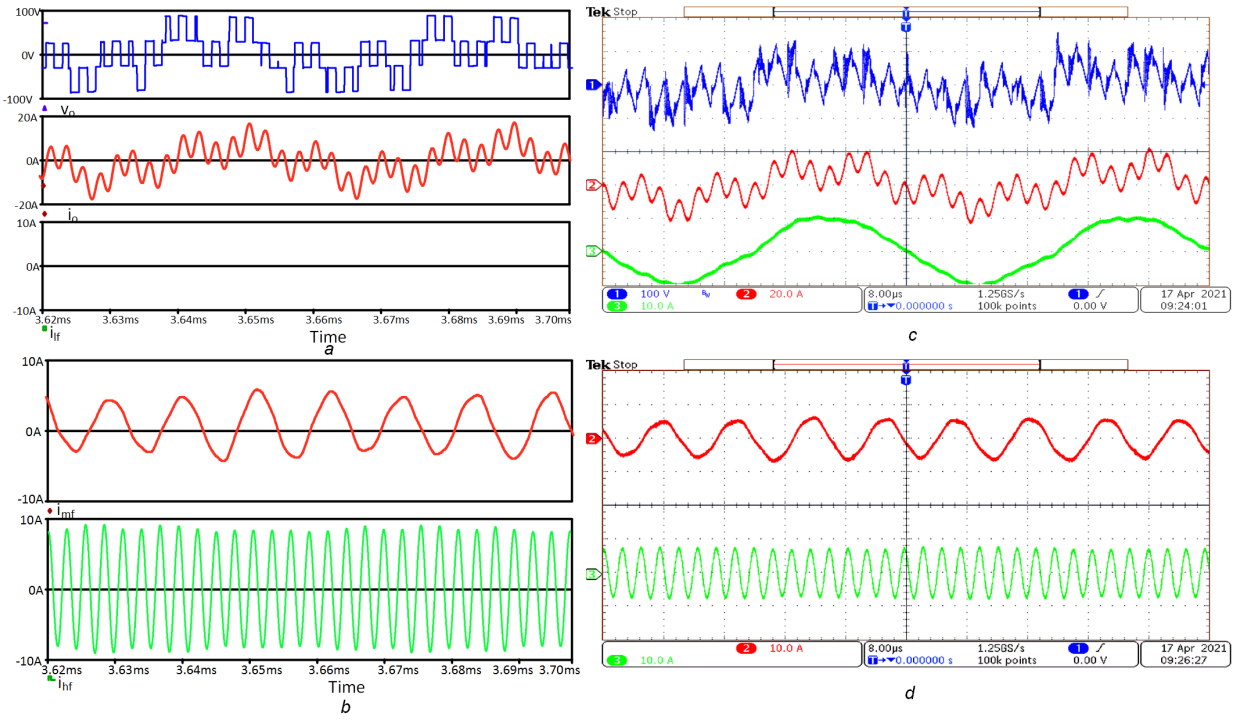

Figure 4.13: Load voltage (v_o), total load current (i_o) and load currents at f_l= 25 kHz, f_m= 105 kHz and f_h= 400 kHz
(a) Simulated waveforms of v_o, i_o and i_l
(b) Simulation waveforms of i_m and i_h
(c) Experimental waveforms of v_o, i_o and i_l
(d) Experimental waveforms of i_m and i_h

pulse frequency modulation method is used to regulate the power of each load independently.

The simulated and experimental waveforms with equal duty cycles of D_l=0.95, D_m=0.95

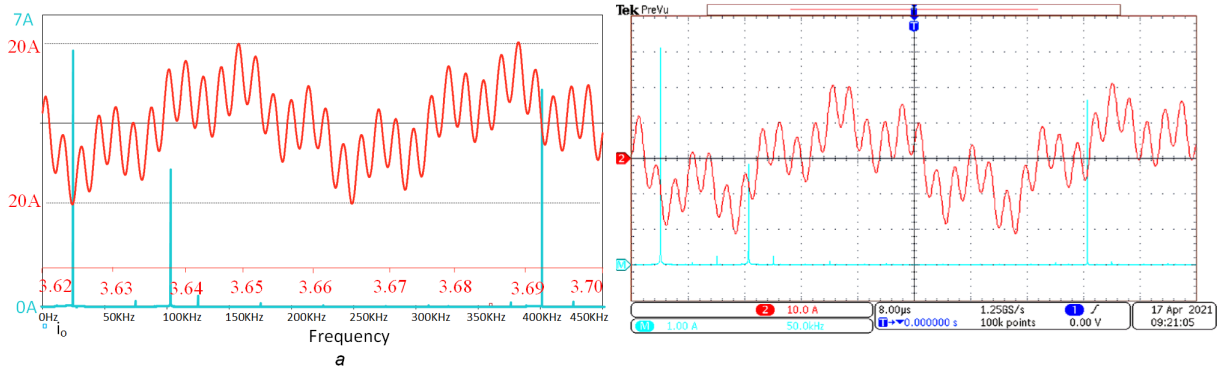

Figure 4.14: Total load current i_o and its FFT at f_l= 25 kHz, f_m= 105 kHz and f_h= 400 kHz
(a) Simulated waveforms
(b) Experimental waveforms

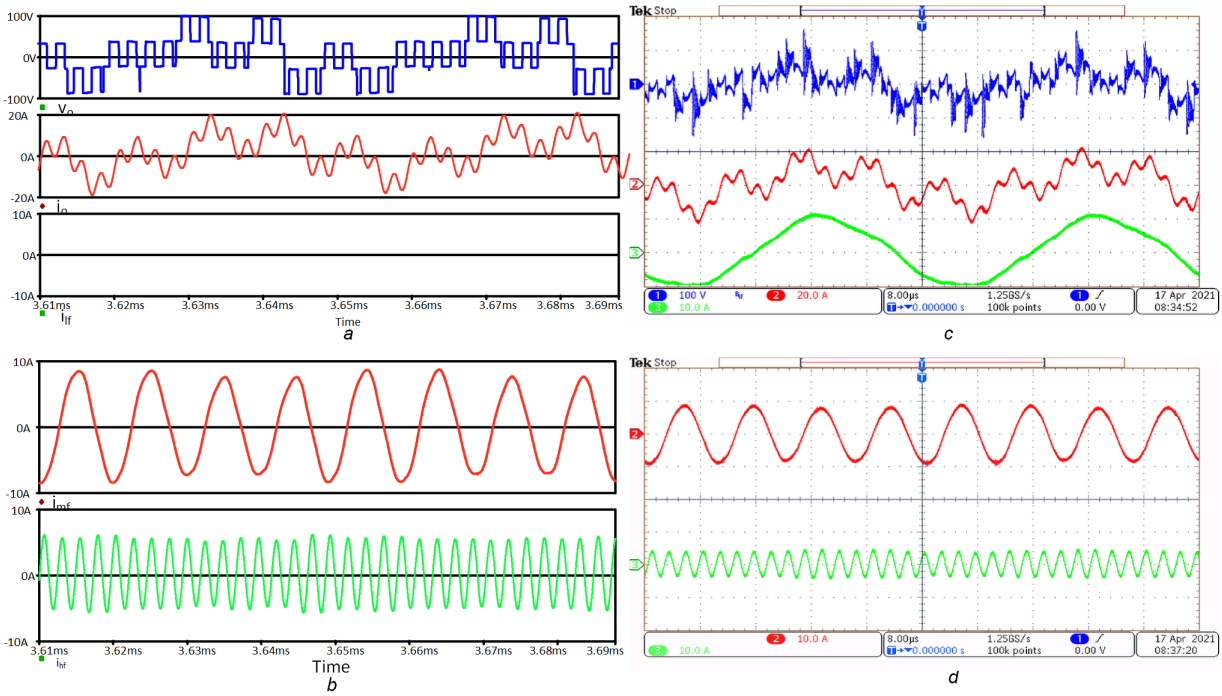

Figure 4.15: Load voltage (v_o), total load current (i_o) and load currents at f_l= 25 kHz, f_m= 100 kHz and f_h= 405 kHz
(a) Simulated waveforms of v_o, i_o and i_l
(b) Simulation waveforms of i_m and i_h
(c) Experimental waveforms of v_o, i_o and i_l
(d) Experimental waveforms of i_m and i_h

and D_h=0.95 are shown in Fig. 4.9. The simulated waveforms of inverter load voltage, output current, and load-1 current are shown in (Fig. 4.9a). The simulated waveforms of load-2 and load-3 currents are shown in (Fig. 4.9b). The comparable experimental waveforms are shown in (Fig. 4.9c and d). (Fig. 4.10a and b) depict FFTs of simulation and experimental inverter

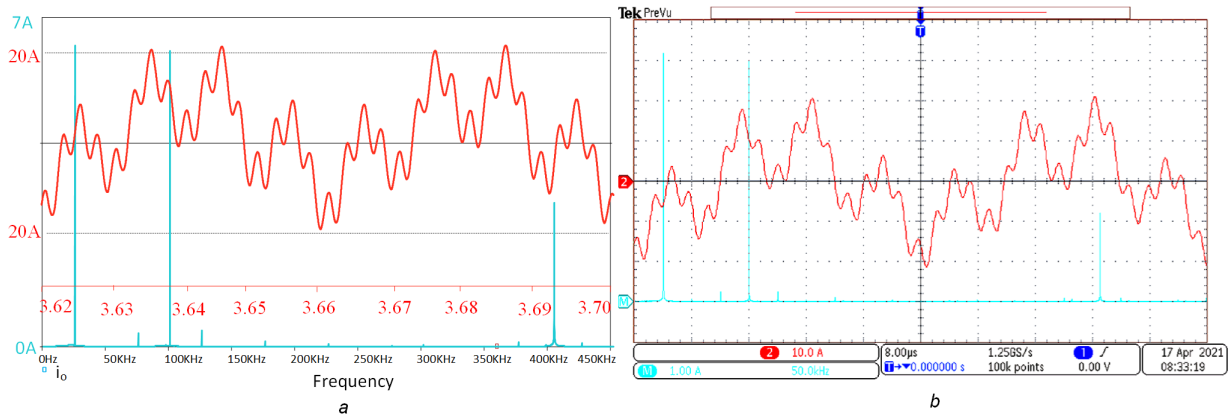

Figure 4.16: Total load current i_o and its FFT at f_l= 25 kHz, f_m= 100 kHz and f_h= 405 kHz
(a) Simulation waveforms
(b) Experimental waveforms

total load current atf_l= 25 kHz, f_m= 100 kHz and f_h=400, respectively. This current is found to have solely low-frequency component current, medium frequency component current, and high-frequency component frequency component current, with RMS values of I_l=6.2 A, I_m=6 A, and I_h=4.9 A.

The simulated and experimental waveforms with inverter leg frequencies off_l=29 kHz, f_m= 100 kHz and f_h= 400 kHz are shown in (Fig. 4.11)). The simulated waveforms of inverter load voltage, output current, and load-1 current are shown in Fig. 4.11a). The simulated waveforms of load-2 and load-3 currents are shown in (Fig. 4.11b). The corresponding experimental waveforms are shown in (Fig. 4.11c and d). (Fig. 4.12a and b) depict FFTs of simulation and experimental inverter total load current at f_l= 29 kHz, f_m= 100 kHz and f_h= 400 kHz, respectively. The load-1 current is decreased to I_l= 3.5, but the load-2 and load-3 currents remains constant at I_m= 6 A and I_h=4.9 A, respectively. As the frequency of leg-1 increases, only the load-1 current increases, while the other load currents remain unchanged.

The simulated and experimental waveforms with inverter leg frequencies of f_l=25 kHz, f_m= 104 kHz and f_h= 400 kHz are shown in (Fig. 4.13). The simulated waveforms of inverter load voltage, output current, and load-1 currents are shown in (Fig. 4.13a). The simulated waveforms of load-2 and load-3 currents are shown in (Fig. 4.13b). The matching experimental waveforms are shown in (Fig. 4.13c and d). (Fig. 4.14a and b) illustrate FFTs of simulation and experimental inverter total current at f_l=25 kHz, f_m= 104 kHz and f_h= 400 kHz, respectively. The load-2 current is decreased to I_m= 2.8 A, but the load-1 and load-3 currents remain unchanged at I_l= 6 A and I_h= 4.9 A, respectively. This implies independent load power control.

The simulated and experimental waveforms with inverter leg frequencies of f_l=25 kHz, f_m= 100 kHz and f_h= 404 kHz are shown in (Fig. 4.15). The simulated waveforms of inverter

load voltage, output current, and load1 current are shown in (Fig. 4.15a). The simulated waveforms of load-2 and load-3 currents are shown in (Fig. 4.15b). The comparable experimental waveforms are shown in (Fig. 4.15c and d). (Fig. 4.16a and b) depict FFTs of simulation and experimental inverter output current at f_l=25 kHz, f_m= 100 kHz and f_h= 400 kHz, respectively. The load-3 current is decreased to I_h= 2.2 A, while the load-1 and load-2 currents remains constant at I_l= 3 Aand I_m= 3.2 A. This implies independent load power control.

4.5 Analysis of obtained from the inverter results

Power control is achieved in the proposed three-leg inverter using the pulse frequency modulation approach (PFM). The output powers of specific loads have been estimated based on simulations and experimental data, as detailed in section load power control 2.3.1. The variation in load power with PFM control is depicted in (Fig. 4.17). The change of load powers (P_l) with low frequency leg frequency control (f_l) while f_m and f_h are maintained constant at their respective frequencies is shown in (Fig. 4.17a). Only the iron vessel load power (P_l) varies, while the other load powers remain constant. The change of load powers with medium frequency leg frequency control (f_m) while f_l and f_h are maintained constant at their respective frequencies is shown in (Fig. 4.17b). Only the steel vessel load power (P_m) varies, while the other load powers remain constant. (Fig. 4.17c) depicts the fluctuation of load powers with a high-frequency (f_h) leg frequency control while f_l and f_m are held constant at their corresponding frequencies. Only the load power of the aluminium vessel (P_h) varies, while the load powers of the other vessels remain constant. As a result, independent power control of iron vessel load, steel vessel load, and aluminium vessel loads is achieved. The total output load power (P_o) of the three-leg inverter configuration is the sum of three different metal vessel load powers described below. The inverter's input power is determined as follows:

$$P_{in} = V_{dc} I_{dc} \tag{4.14}$$

where V_{dc} and I_{dc} are the input voltage and input current of three-leg inverter respectively.

Three-leg inverter overall efficiency is calculated as

$$\eta = \frac{P_o}{P_{in}} \tag{4.15}$$

(Fig. 4.18) depicts the efficiency curves. The curve of overall efficiency (vs) leg-1 frequency (f_l) when f_m and f_h are held constant at 100 kHz and 400 kHz is shown in (Fig. 4.18a). The graph of overall efficiency versus leg-2 frequency (f_m) when f_l and f_h are held constant at 25 kHz and 400 kHz is shown in (Fig. 4.18b). The graph of overall efficiency versus leg-3 frequency (f_h)

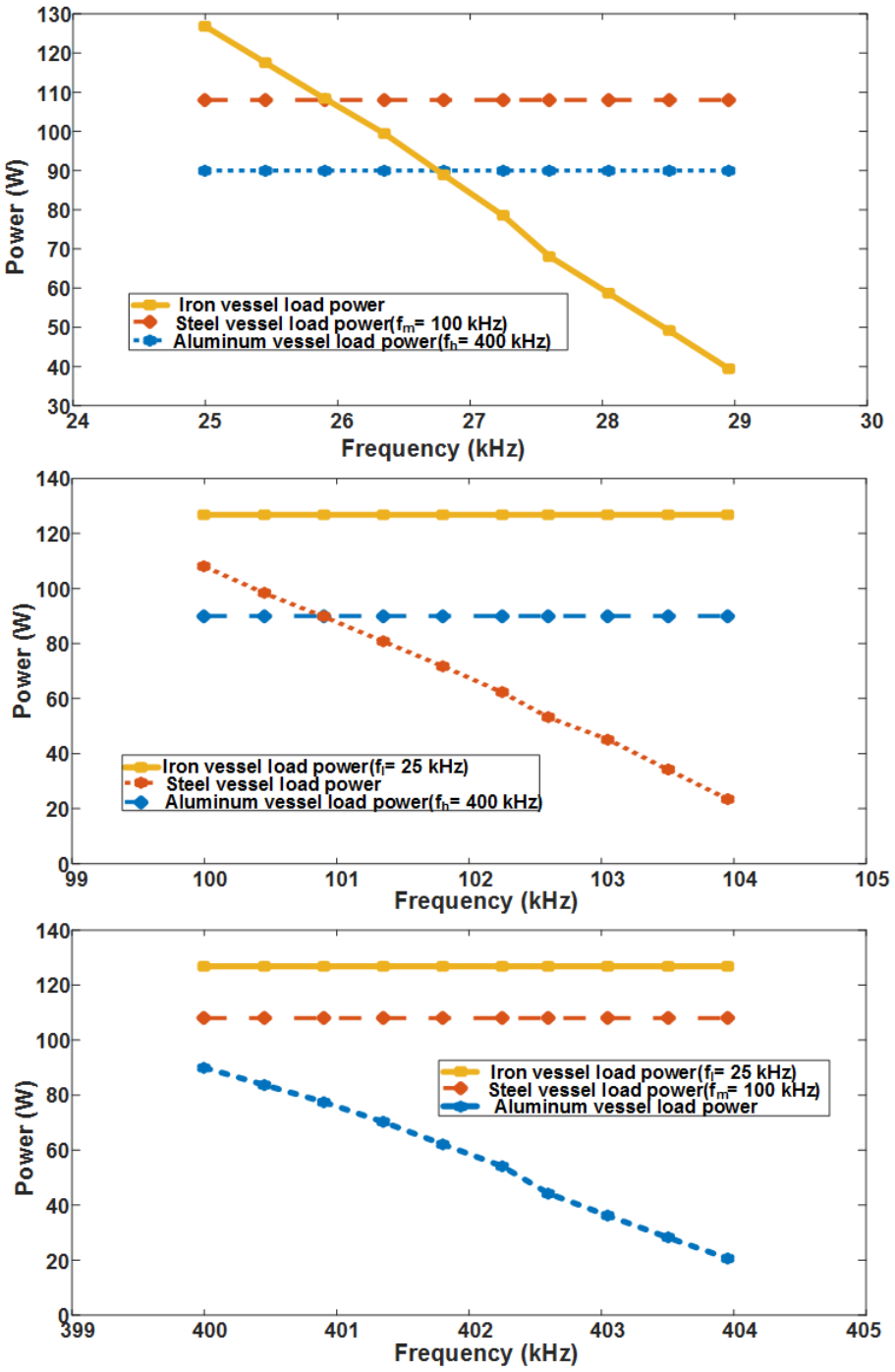

Figure 4.17: Low-frequency (load-1), Medium-frequency (load-2) and High-Frequency (load-3) power control
(a) Load-1 power Vs f_l
(b) Load-2 power Vs f_m
(c) Load-3 Power Vs f_h

when f_l and f_m are held constant at 25 kHz and 100 kHz is shown in (Fig. 4.18c). According to these graphs, total efficiency decreases with leg frequency and varied between 85 and 95

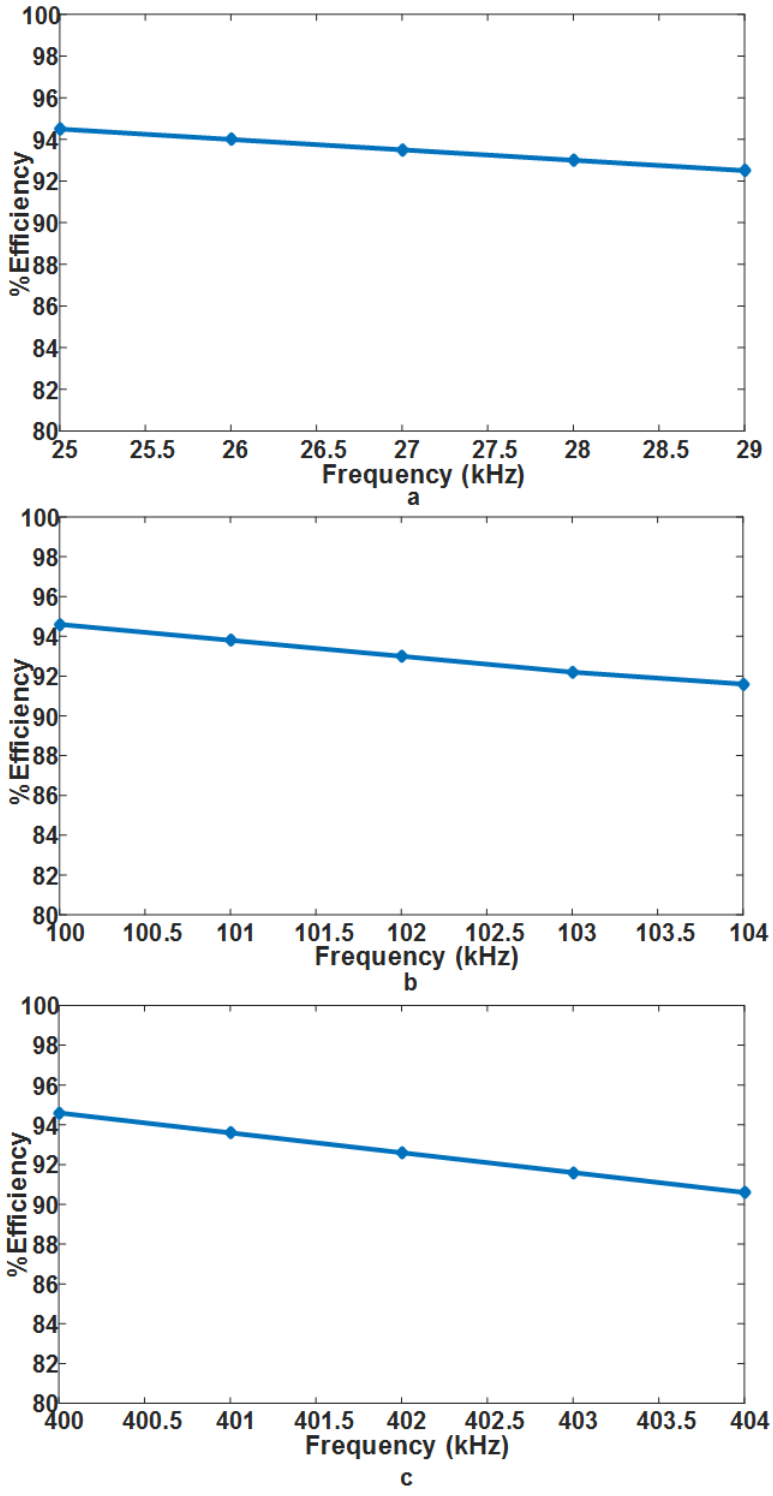

Figure 4.18: Efficiency versus frequency curves
(a) Inverter Efficiency vs f_l
(b) Inverter Efficiency vs f_m
(c) Inverter Efficiency vs f_h

percent.

4.6 Conclusions

A three-output inverter configuration has been proposed to power three different material vessel IH loads. Inverter legs operated at three different frequencies are utilised to power three different material vessel domestic IH loads. Inverter leg-1 operates at a low frequency and is suitable for iron loads, whereas inverter leg-2 operates at a medium frequency and is suitable for steel loads. Inverter leg-3 operates at a high frequency and is suitable for aluminium loads. The three leg switching frequencies are respectively 25 kHz, 100 kHz, and 400 kHz. Pulse frequency modulation approach provides independent power control of the three IH loads. The proposed inverter configuration has been simulated, implemented and a hardware prototype has been built. At full load, the proposed system efficiency is $\geq$94 %. Simulation study of the inverter is performed and its results are verified experimentally. Both simulation and experimental results are in good agreement with each other.

The advantages of the proposed inverter configuration are:

i Suitable for multiple IH loads

ii Suitable for different material vessel domestic induction Cooking

iii Independent power control using pulse frequency control

iv High power conversion efficiency

v Use of only two switching devices per load

vi Eliminates the need for electro-mechanical switches

Hence, it is well suitable for multiple load Induction cooking applications.
Next chapter explains the proposed topology-3, Single-stage pulse frequency controlled ac-ac resonant converter for different material induction cooking applications.

Chapter 5

Single-Stage Pulse Frequency Controlled AC-AC Resonant Converter for Different Material Induction Cooking Applications

Chapter 5

Single-Stage Pulse Frequency Controlled AC-AC Resonant Converter for Different Material Induction Cooking Applications

5.1 Introduction

Most of the IH inverter topologies are based on two stage power conversion which reduces the overall efficiency of the system and increases the size and cost of system. With single stage ac-ac converter these limitations are overcome.

In this chapter, a single-stage AC-AC resonant converter configuration, suitable for IC with different material vessels has been proposed. It is capable of powering multiple-loads of steel and aluminium vessels. Independent power control is achieved through pulse frequency modulation technique. It offers high efficiency, less component count and high power factor. The block diagram of the conventional IC system is shown in Figure. 5.1a. It contains a rectifier for conversion of utility AC supply to DC, a power factor correction unit and separate inverter circuits for each load. The IH loads are of ferromagnetic material. Block diagram of the proposed configuration is shown in Figure. 5.1b, which contains single-stage ac-ac converter which powers steel and aluminium vessels. The IH load equivalent circuit is shown in Figure. 5.1c. R_{eq} is equivalent resistance and L_{eq} is equivalent inductance of the IC load as referred to the coil side.

5.2 Proposed converter configuration

5.2.1 Circuit description

The proposed single-stage resonant converter configuration suitable for two different material vessels is shown in Figure. 5.2. The proposed configuration consists of bridge-less boost rectifier and integrated half-bridge resonant inverter circuit. A boost inductor L_b is connected in series with utility frequency ac supply and a dc-link capacitor C_b is connected across inverter leg to ensure the smooth operation of resonant converter. The voltage across C_b is the

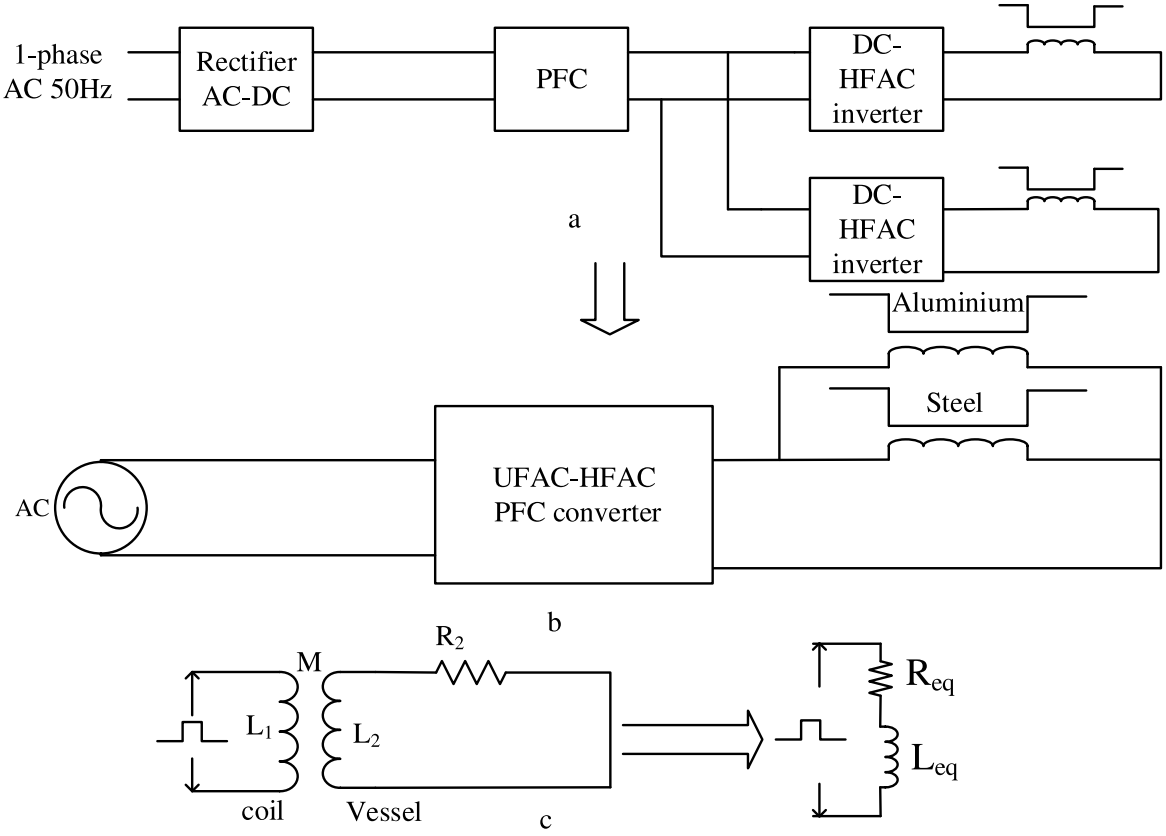

Figure 5.1: Structure of multi-load induction cooking
(a) Two-stage conventional converter
(b) Proposed multi load Single-stage ac-ac converter
(c) Load equivalent circuit

dc-link voltage v_b. The boost inductor L_b contributes to boosting of utility frequency source voltage V_s. Diodes D_l and D_h form the rectifier branch. In this multi-frequency converter, one leg operates at low-frequency l_f which is suitable for a steel vessel and another leg operates at high-frequency h_f which is suitable for an aluminium vessel. Switching devices S_1 and S_2 are connected in low-frequency leg, switching devices S_3 and S_4 are connected in high-frequency leg. Switching pulses of these inverter devices, corresponding output voltage v_o and both vessel load currents i_{lf} and i_{hf} are shown in Figure. 5.3. Low-frequency leg switches S_1 and S_2 are common for both rectification as well as inverter operation. This common leg devices duty cycle (d) is fixed at 0.5 to get maximum voltage across dc-link due to its boost operation. Lossless snubber capacitors C_{s1}-C_{s4} are connected across switching devices S_1-S_4 respectively which help in ZVS operation. D_1-D_4 are anti-parallel diodes of the devices S_1-S_4 respectively. The inverter output voltage is supplied to two IH loads. R_{lf} and L_{lf} are the equivalent resistance and equivalent inductance of steel IH load. C_{rl} is the external resonant capacitor. R_{hf} and L_{hf} are the equivalent inductance and resistance of aluminium IH load and C_{rh} is the external

resonant capacitor. The corresponding resonant frequencies are f_{rl} and f_{rh} respectively. The switching frequencies are selected as f_l=20 kHz and f_h=160 kHz. The admittance curves of two IH resonant loads are shown in Figure. 5.4. As shown in Figure. 5.3, v_o is sum of low and high-frequency voltage components. Low-frequency current i_{lf}, flows through the steel IH load and high frequency current i_{hf} flows through the aluminium IH load.

5.2.2 Selection of switching frequencies

In general, for IH with ferromagnetic material, switching frequency is selected above 20 kHz. The high frequency range is normally selected as 100 kHz - 200 kHz, to limit the inverter switching losses. Characteristics of different IH loads are plotted in Figure. 5.5. Frequency characteristics of steel and aluminium vessel loads are shown in Figure. 5.5a and b. From these figures it is observed that there is a change in inductance and resistance of IH load with frequency. For steel vessel IH load, the switching frequency (f_l) is selected as 20 kHz. From Fig. 5.5b, it is observed that beyond 140 kHz, the equivalent resistance of aluminium vessel IH load increases above 1Ω. Hence, the switching frequency (f_h) is selected as 160 kHz which is an even multiple of low switching frequency (f_l). This frequency ratio of eight will help in independent control of different loads. At switching frequency of 20 kHz, equivalent resistance is 2.2 Ω and equivalent inductance is 68.2 μH for steel vessel IH load. At 160

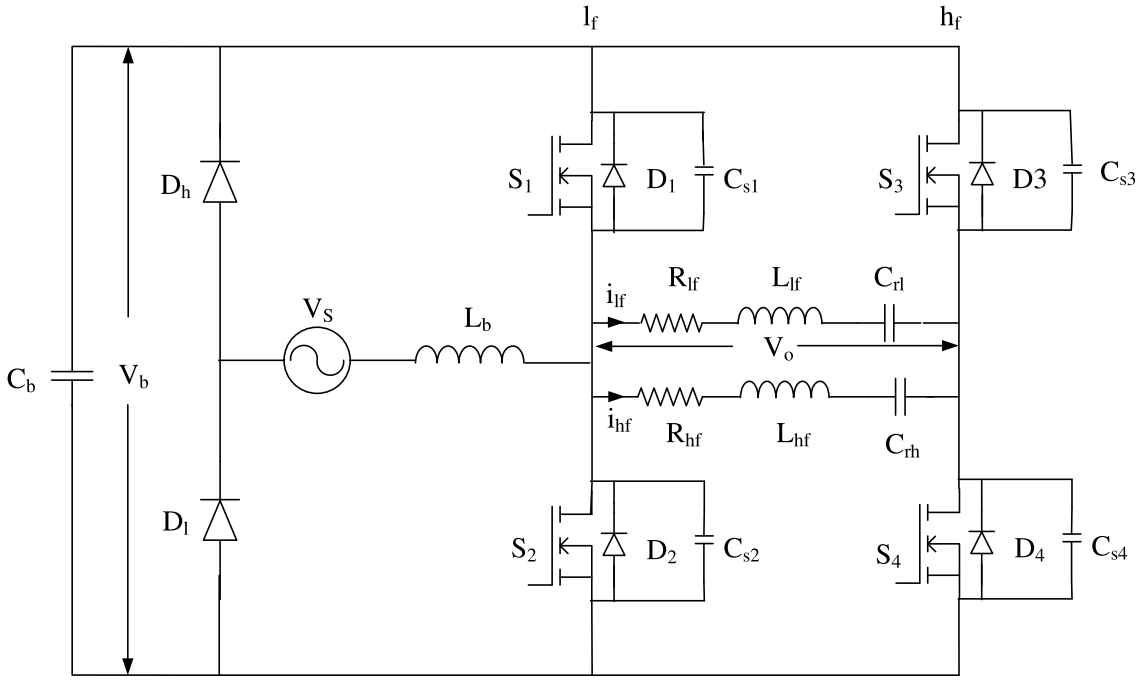

Figure 5.2: Proposed converter configuration

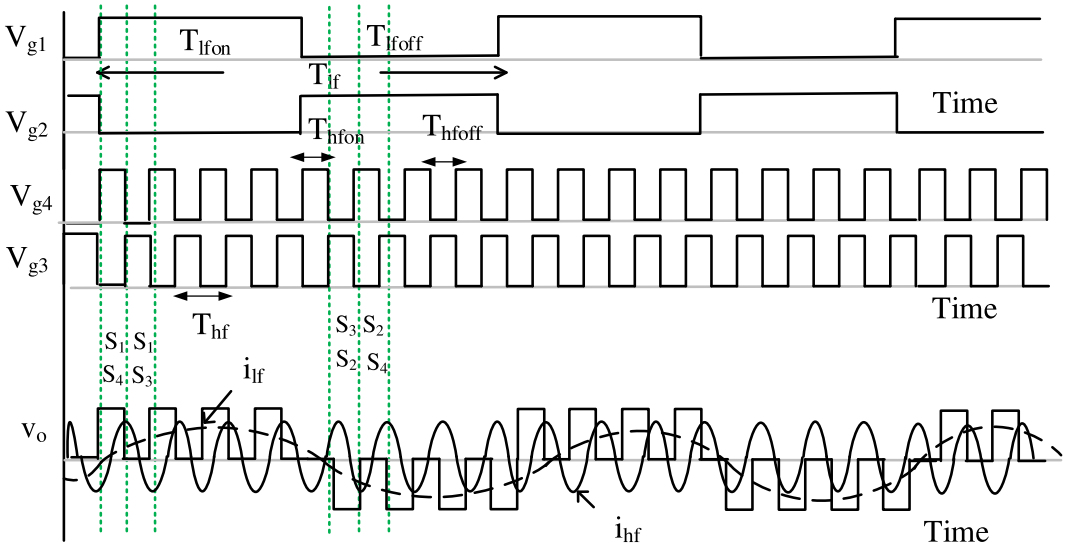

Figure 5.3: Inverter switching pulses and output voltage and load currents

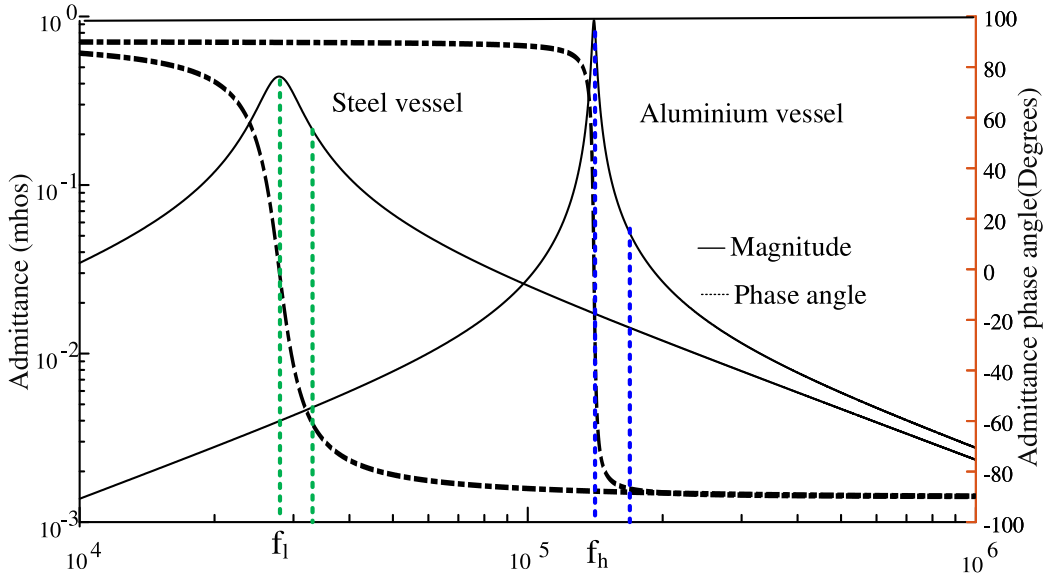

Figure 5.4: Admittance curve

kHz, equivalent resistance is 1.35 Ω and equivalent inductance is 50.7 μH for aluminium vessel IH load. To facilitate ZVS operation, $\frac{f_s}{f_r}$ ratio has to be selected closer to 1.1. Hence f_{rl} and f_{rh} are selected as 18.4 kHz and 158 kHz respectively. The expressions for f_{rl} and f_{rh} are f_{rl}=$\frac{1}{2\Pi\sqrt{L_{lf}C_{rl}}}$ f_{rh}=$\frac{1}{2\Pi\sqrt{L_{hf}C_{rh}}}$ respectively. Admittance characteristics of different IH loads are shown in Figure. 5.4. It shows that steel vessel IH resonant load offers maximum admittance to low frequency current and aluminium vessel IH resonant load offers maximum admittance to high frequency current.

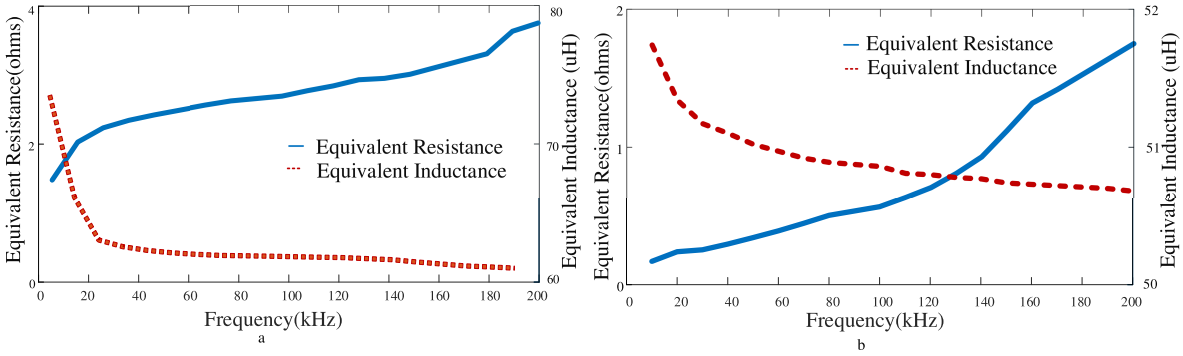

Figure 5.5: IH Load frequency characteristics
(a) Steel vessel
(b) Aluminium vessel

5.2.3 Operating principle

The proposed converter configuration consist of three legs with is the combination of series resonant load inverter and boost converter. In this configuration, as shown in Figure. 5.2, one inverter leg is common for both boost and series inverter operation.
The volt-sec balance across boost inductor L_b,Expression of I_{Lbpeak}.The boost operation is described through equations (5.1)-(5.4) [56]

$$V_s dT_s + (V_s - v_b)(1-d)T_s = 0 \tag{5.1}$$

where T_s is the time period corresponding to the common leg (leg-1) frequency i.e. l_f. Expression of L_b for continuous conduction is

$$L_b > \frac{V_b - v_s}{I_{Lbpeak}}(1-d)T_s \tag{5.2}$$

where

$$I_{Lbpeak} = I_{Lb} + \frac{\Delta I_{Lb}}{2} \tag{5.3}$$

By neglecting the source current ripple, the average value of dc-link voltage v_b can be expressed as

$$v_b = \frac{V_s}{(1-d)} \tag{5.4}$$

From Equation:5.4, it is observed that due to boost operation there is an increase in dc-link voltage v_b which leads to increase in v_o also. Two IH resonant loads are connected across low and high-frequency legs of the inverter.

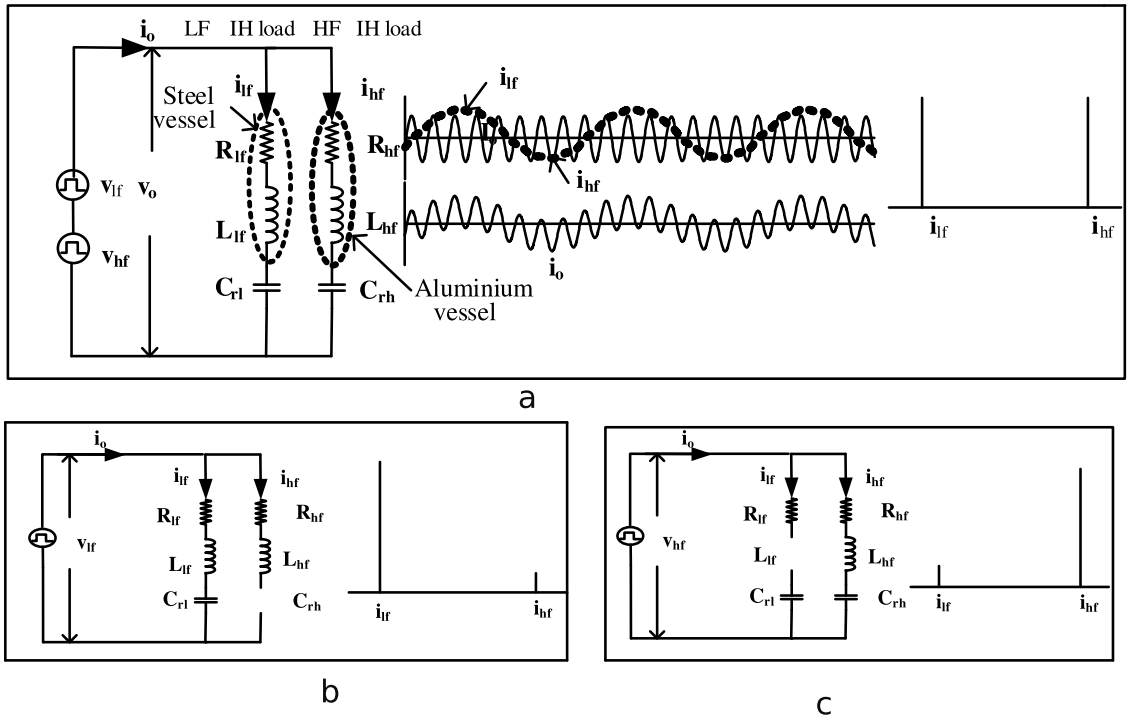

Figure 5.6: Load equivalent circuit, load currents and FFT
(a) Load equivalent circuit of multi-frequency converter, load currents and FFT
(b) Load equivalent circuit for v_{lf} and load current FFT
(c) Load equivalent circuit for v_{hf} and load current FFT

At low-frequency, steel vessel load impedance can be expressed as

$$Z_{eqlf} = R_{lf} + j(X_{Llf} - X_{Clf}) \tag{5.5}$$

where

X_{Llf}=$2\pi f_l L_{lf}$, X_{clf}=$\frac{1}{2\pi f_l C_{rl}}$

At high-frequency, aluminium vessel load impedance can be expressed as

$$Z_{eqhf} = R_{hf} + j(X_{Lhf} - X_{Chf}) \tag{5.6}$$

where

X_{Lhf}=$2\pi f_h L_{hf}$,X_{Chf}=X_{clf}=$\frac{1}{2\pi f_h C_{rh}}$

Inverter output voltage across load v_o is the combination of low and high frequency voltage components, v_{lf} and v_{hf} as shown in Figure. 5.3. Hence v_o can be represented as a series connection of two voltage sources v_{lf} and v_{hf} as shown in Figure. 5.6a.

$$v_0 = v_{lf} + v_{hf} \tag{5.7}$$

Figure. 5.6b shows the load equivalent circuit for low-frequency component of v_o. At f_l, the reactance of C_{rh} is very high and hence it behaves like open circuit. However, the low-frequency load offers low impedance at this frequency and i_{lf} flows through this load as shown in Figure. 5.6b. Figure. 5.6c shows the load equivalent circuit for high-frequency component of v_o. At f_h, the reactance of L_{lf} is very high and hence it behaves as an open circuit. However, the high-frequency load offers low impedance and hence i_{hf} flows through this load as shown in Figure. 5.6c. Hence in response to the output voltage v_o, only a low-frequency current i_{lf} flows through steel vessel load and a high-frequency current i_{hf} flows through aluminium vessel load. Figure. 5.6a. shows the waveforms and FFT of these currents.

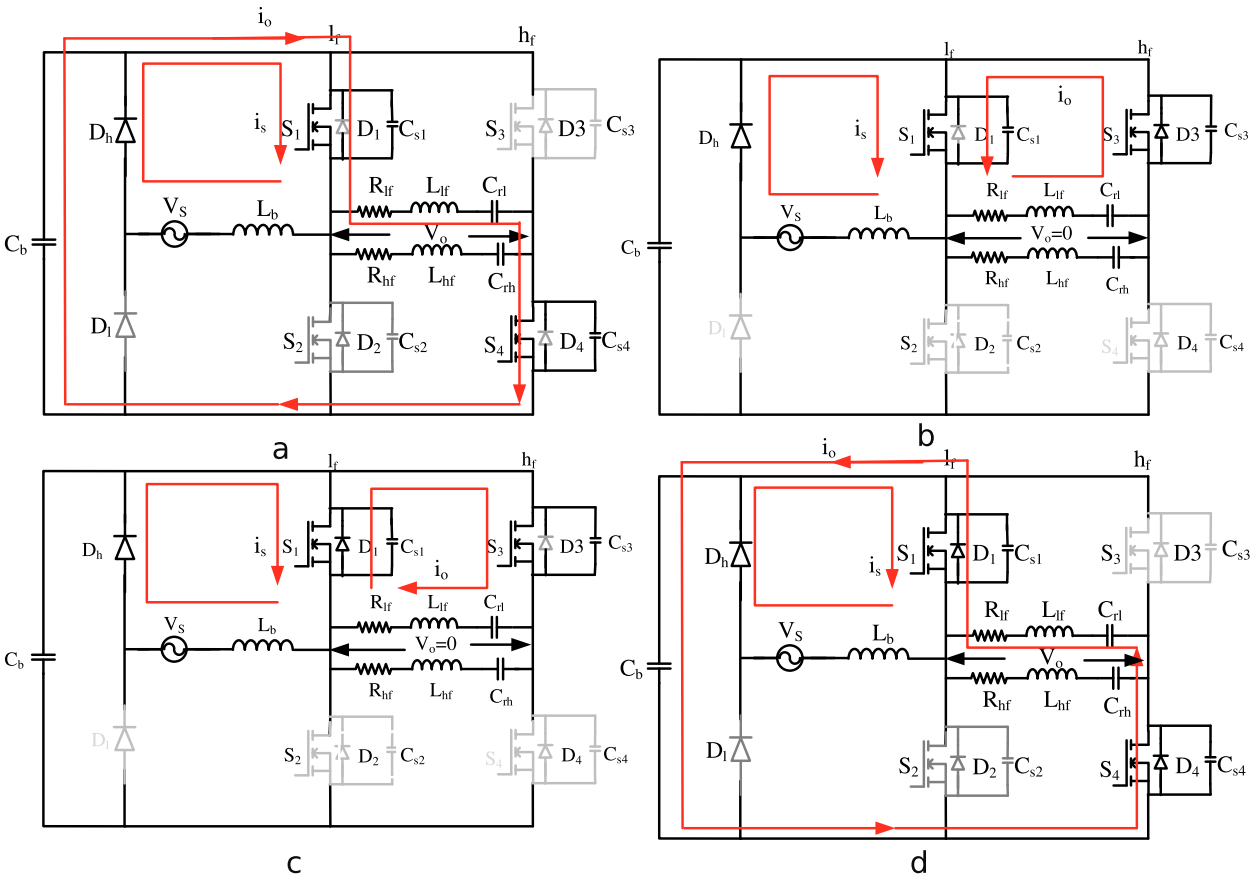

Figure 5.7: Single-stage resonant converter equivalent circuits for mode 1 to mode 4 For $V_s \geq 0$ (positive half cycle)
(a) Mode1 S_1 and S_4 are ON
(b) Mode2 S_1 and S_3 are ON
(c) Mode3 S_3 and S_1 are ON
(d) Mode4 S_4 and S_1 are ON

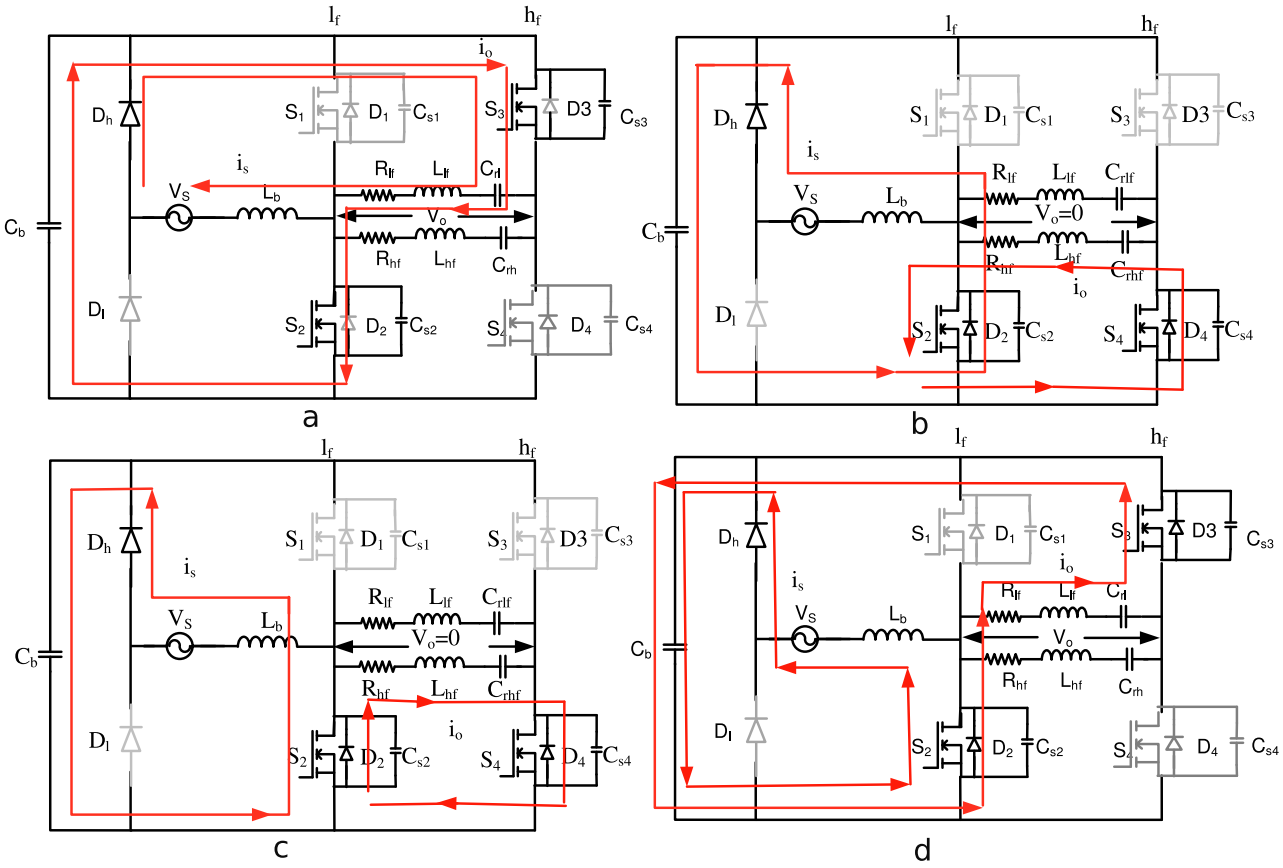

Figure 5.8: Single-stage resonant converter equivalent circuits mode 5 to mode 8 For $V_s \geq 0$ (Positive half cycle)
(a) Mode5 S_3 and S_2 are ON
(b) Mode6 S_4 and S_2 are ON
(c) Mode7 S_2 and S_4 are ON
(d) Mode8 S_2 and S_3 are ON

5.2.4 Output power analysis

The output power to steel vessel is calculated as $I_{lf}{}^2 R_{lf}$, i.e. real power consumption by equivalent resistance of steel vessel load. The output power to aluminium vessel is calculated as $I_{hf}{}^2 R_{hf}$, i.e. real power consumption by equivalent resistance of aluminium vessel load. I_{lf} is RMS value of low frequency current and I_{hf} is RMS values of high frequency currents. The output power(P_o) of the inverter is expressed as

$$P_0 = P_{lf} + P_{hf} \tag{5.8}$$

where

P_{lf} = steel load output power $= I_{lf}{}^2 R_{lf}$

P_{hf} = aluminium load output power =$I_{hf}{}^2 R_{hf}$

5.3 Modes of operation

The proposed converter operation can be described in eight different modes. Modes 1 to 8 are obtained for positive(+ve) half cycle of the utility frequency ac supply voltage and modes 9 to 16 are obtained with negative(-ve) half cycle of the source voltage.

Mode 1:

During this mode, the supply voltage is positive (+ve) and the devices S_1 and S_4 are ON. Figure. 5.7a shows the corresponding equivalent circuit. Source current i_s flows through the path of V_S-D_h-S_1-L_b and boost inductor L_b stores the energy. During this interval, the output current i_o is positive and flows through the path of S_1-load-S_4-C_b. Dc-link capacitor C_b discharges. The inverter output voltage is $+v_b$. Expression for load voltage and load currents are expressed through equations (5.9)-(5.16) [48]

$$v_0 = v_b + v_{crl}(t = 0 \; or \; t_{n-1}) \tag{5.9}$$

$$v_0 = L_{lf}\frac{di_{lf}(t)}{dt} + \frac{1}{C_{rl}}\int i_{lf}(t)dt + v_{crl}(t = 0 \; or \; t_{n-1}) + i_{lf}(t)R_{lf} \tag{5.10}$$

low frequency current

$$i_{lf}(t) = \frac{v_0 - v_{crl}(t = 0 \; or \; t_{n-1})}{\omega_n L_{lf}} e^{-\alpha t}\sin\omega_n t + i_{lf}e^{-\alpha t}(\cos\omega_n t - \frac{\alpha}{\omega_n}\sin\omega_n t) \tag{5.11}$$

$$v_{crl}(t) = v_{crlo} + v_0 - v_{crl}(t = 0\, or\, t_{n-1})(1 - e^{-\alpha t}(\cos\omega_n t - \frac{\alpha}{\omega_n}\sin\omega_n t)) + \frac{i_{lf}(t = 0 \; or \; t_{n-1})}{\omega_n C_{rl}} e^{-\alpha t}\sin\omega_n t \tag{5.12}$$

where

α=$\frac{R_{lf}}{2L_{lf}}$ and ω_n=$\frac{1}{\sqrt{L_{lf}C_{rl}}}$

similarly

$$v_0 = v_b + v_{crh}(t = 0 \; or \; t_{n-1}) \tag{5.13}$$

$$v_0 = L_{hf}\frac{di_{hf}(t)}{dt} + \frac{1}{C_{rh}}\int i_{hf}(t)dt + v_{crh}(t = 0 \; or \; t_{n-1}) + i_{hf}(t)R_{hf} \tag{5.14}$$

low frequency current

$$i_{hf}(t) = \frac{v_0 - v_{crh}(t = 0 \; or \; t_{n-1})}{\omega_n L_{hf}} e^{-\alpha t}\sin\omega_n t + i_{hf}e^{-\alpha t}(\cos\omega_n t - \frac{\alpha}{\omega_n}\sin\omega_n t) \tag{5.15}$$

$$v_{crh}(t) = v_{crho} + v_0 - v_{crh}(t = 0\, or\, t_{n-1})(1 - e^{-\alpha t}(\cos\omega_n t - \frac{\alpha}{\omega_n}\sin\omega_n t)) + \frac{i_{hf}(t = 0\, or\, t_{n-1})}{\omega_n C_{rh}} e^{-\alpha t}\sin\omega_n t \tag{5.16}$$

where
α=$\frac{R_{hf}}{2L_{hf}}$ and ω_n=$\frac{1}{\sqrt{L_{hf}C_{rh}}}$
Hence the instantaneous value of load current

$$i_0(t) = i_{lf}(t) + i_{hf}(t) \tag{5.17}$$

These equation:5.9 to 5.16 are applicable for all remaining modes where the final quantities of previous mode become initial values of the next mode.

At the end of mode-1, i_o becomes positive(+ve).

Mode 2:

During this mode, devices S_1 and S_3 are ON and Figure. 5.7b shows the corresponding equivalent circuit. Source current i_s flows through the path of V_S-D_h-S_1-L_b. The output current is positive and freewheels through S_3 and S_1. Inverter output voltage v_o is zero.

Table 5.1: Parameters of hardware prototype

Parameter	**Value**
AC input voltage (V_s)	40 V (max)
Boost inductor	400 μH
dc-link capacitor	6.8 uF
Low-frequency IC load equivalent inductance (L_{lf})	68.2 μH
Low frequency IC load equivalent resistance (R_{lf})	2.09 Ω
Low frequency load resonant capacitor (C_{rl})	1.205 μF
High-frequency IC load equivalent inductance (L_{hf})	50.737 μH
High frequency IC load equivalent resistance (R_{hf})	1.35 Ω
High frequency load resonant capacitor (C_{rh})	0.0202 μF
Leg-1 switching frequency (f_l)	20 kHz
Low frequency IH load resonant frequency(f_{rl})	18.4 kHz
Leg-2 switching frequency (f_h)	160 kHz
High frequency IH load Resonant frequency (f_{rh})	158 kHz
MOSFETs used	IRFB4227pbf
Rds,on	19 mΩ
Control Board	arduino
Diodes used	VS60EPS
Snubber capacitors	2 nF

Mode 3:
During this mode, devices S_1 and S_3 are ON and Figure. 5.7c shows the corresponding equivalent circuit. Source current i_s flows through the path of V_S-D_h-S_1-L_b. The output current is negative and flowing through D_1,S_3 and load. The load voltage v_o is zero.
Mode 4:
During this mode, devices S_1 and S_4 are ON. Figure. 5.7d shows the corresponding equivalent circuit. Source current i_s flows through the path of V_S-D_h-S_1-L_b and boost inductor L_b stores the energy. During this interval, the output current i_o is negative and flows through the path of S_4-load-S_1-C_b and dc-link capacitor C_b charges. The inverter output voltage is $+v_b$.
Mode 5:
During this mode, the supply voltage is positive and the devices S_2 and S_3 are ON and Figure. 5.8a shows the corresponding equivalent circuit. Source current i_s flows through the path of V_s-D_h-S_3-load-L_b and boost inductor L_b releases magnetic energy to load. Dc-link capacitor C_b discharges through S_3,load,S_2. The inverter output voltage is -v_b and i_o is negative.
Mode 6:
During this mode, devices S_2 and S_4 are ON and Figure. 5.8b shows the corresponding equivalent circuit. Source current i_s flows through the path of V_s-D_h-C_b-S_2-L_b. i_o is negative and flows through the path of load-S_2-D_4. Dc-link capacitor C_b is charging. Inverter output voltage v_o is zero.
Mode 7:
During this mode, devices S_2 and S_4 are ON and Figure. 5.8c shows corresponding equivalent circuit. Source current i_s flows through the path of V_s-D_h-C_b-S_2-L_b. i_o is positive and flows through the path of load-S_4-D_2. Dc-link capacitor C_b discharges. Inverter output voltage v_o is zero.
Mode 8:
During this mode, devices S_2 and S_3 are ON and Figure. 5.8d shows corresponding equivalent circuit. Source current i_s flows through the path of V_s-D_h-C_b-S_2-L_b. i_o is positive and flows through the path of load-S_3-C_b-S_2. Dc-link capacitor C_b charges. The inverter output voltage is -v_b.

During the supply voltage negative half cycle ($V_s < 0$), the operation consists of 8 modes which are similar to that of the modes existing for the positive half cycle with changes in conducting elements due to polarity reversal. D_h is off and D_l is on during this negative half cycle.

5.4 Simulation and experimental results

A 316 W prototype of a single-stage resonant converter has been implemented for induction cooking with two different material vessels. The implemented prototype is shown in Figure. 5.9. The converter circuit parameters are described in Table 5.1. The AC input voltage V_s = 40 V (max) and frequency f=50 Hz. The load parameters are measured from the coil side with the practical domestic cooking vessels of steel and aluminium kept over the IH coils. Switching frequencies of converter legs 1 and 2 are selected as 20 kHz and 160 kHz respectively. The low and high resonant frequencies are set as 18.4 kHz and 158 kHz respectively by using suitable values of resonant capacitors. The simulation and experimental results at different switching frequencies are shown in (Figure. 5.10 to Figure. 5.16). Figure. 5.10 shows the simulated and experimental results of source voltage (V_s), source current (i_s), inverter output voltage v_o, low frequency output current i_{lf}, high frequency output current i_{hf} at f_l=20 kHz and f_h=160 kHz. The simulated and experimental results are in good agreement with each other. Figure. 5.10a and b show respectively, simulated and experimental waveforms of V_s and i_s. From these waveforms it can be observed that supply voltage V_s and current i_s are in phase and the proposed converter operates at unity power factor. Figure. 5.10c and d show respectively simulated and experimental waveforms of v_o, i_{lf} and i_{hf}. Figure. 5.11a and b show the simulated and experimental waveforms of dc-link voltage v_b at f_l=20 kHz and f_h=160 kHz. It is observed that the peak value of the dc-link voltage is 80 V when the peak value of source volt-

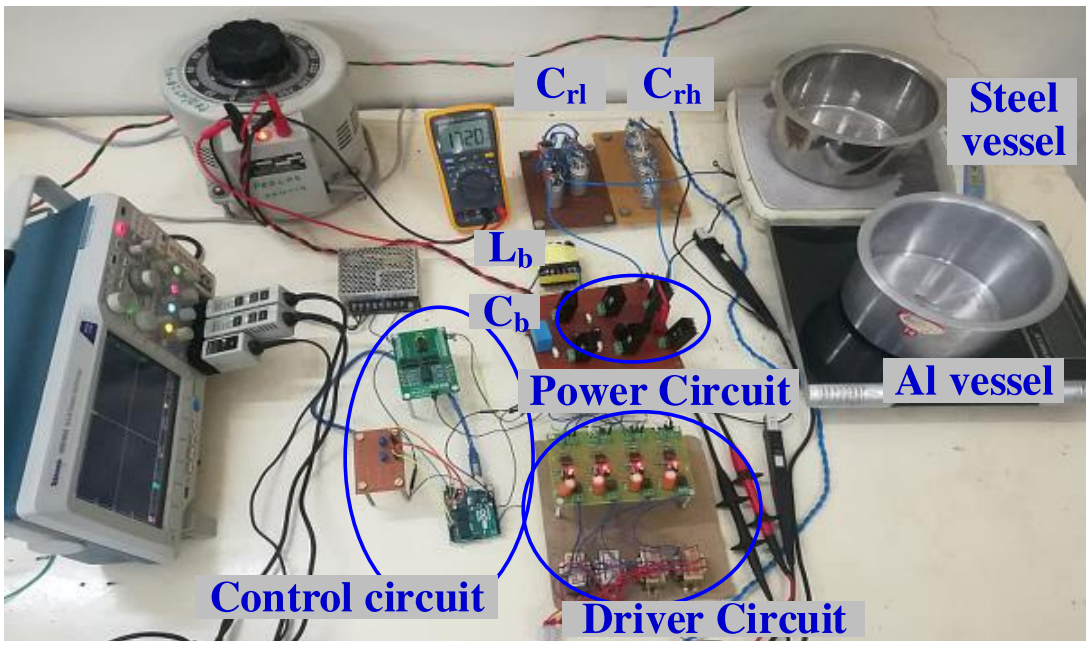

Figure 5.9: Prototype of Experimental setup

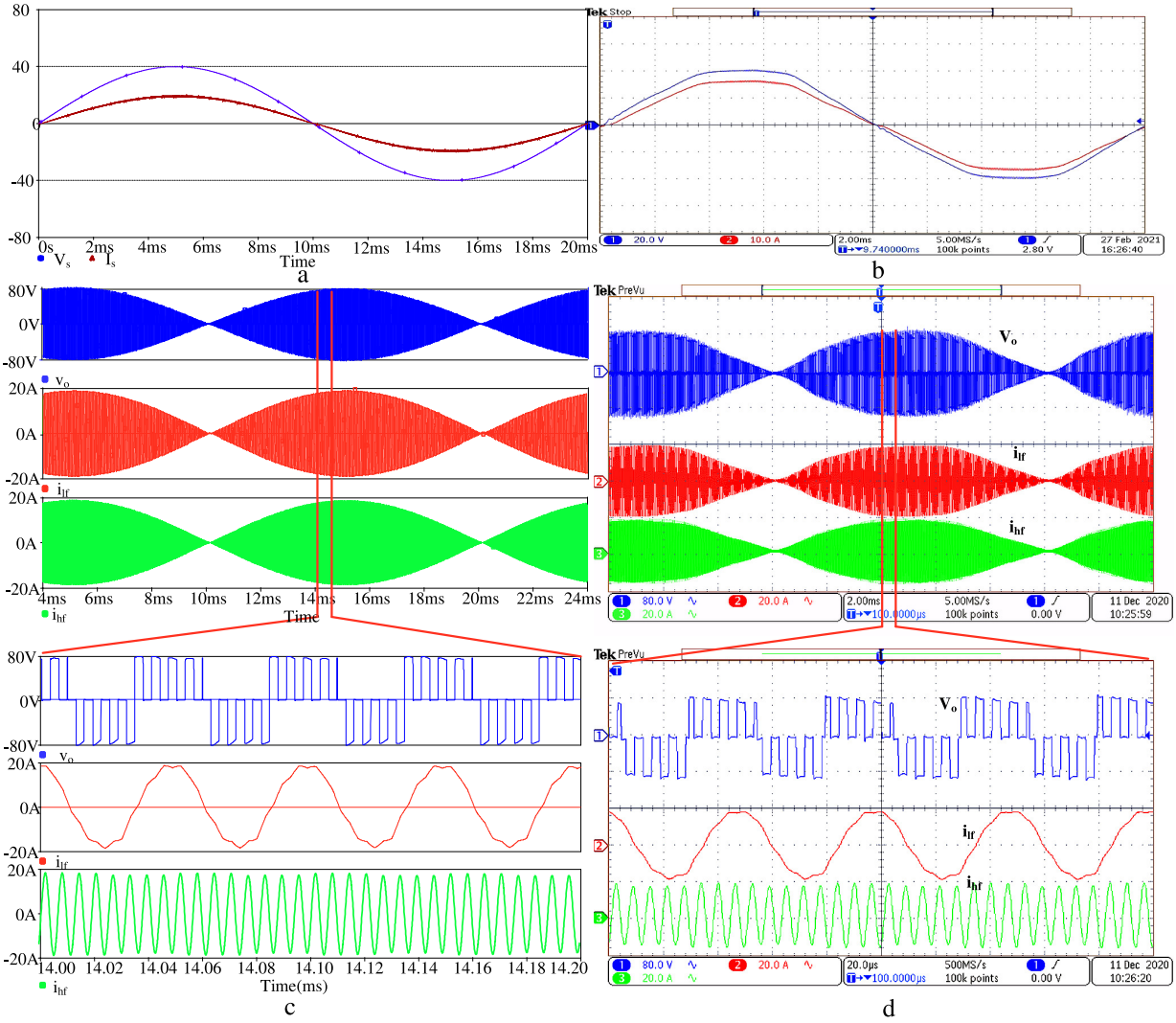

Figure 5.10: Simulated and experimental waveforms of V_s, i_s, v_o, i_{lf} and i_{hf}
(a) Simulated waveforms of source voltage and source current
(b) Experimental waveforms of source voltage and source current
(c) Simulated waveforms of output voltage, low and high-frequency load currents at f_l=20 kHz and at f_h=160 kHz
(d) Experimental waveforms of load voltage, low and high-frequency load currents at f_l=20 kHz and at f_h=160 kHz

age is 40 V, which indicates the boost operation of the converter. Figure. 5.12 shows simulated and experimental waveforms of total output load current i_o and its FFT with f_l=20 kHz and f_h=160 kHz. Fig. 5.12a show simulated waveforms of total output load current i_o and its FFT. Fig. 5.12b show experimental waveforms of total output load current i_o and its FFT. Figure. 5.13 and Figure. 5.14 shows simulated and experimental waveforms of individual load currents FFT with f_l=20 kHz and f_h=160 kHz. Figure. 5.13a show simulated waveforms of low frequency load current i_{lf} and its FFT, Figure. 5.13b show experimental waveforms of low frequency load

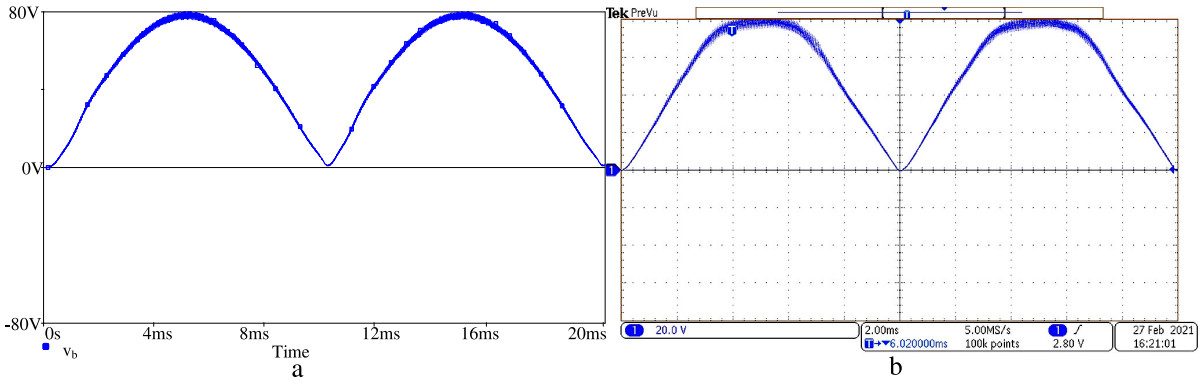

Figure 5.11: Simulated and experimental waveforms dc-link capacitor Voltage
(a) Simulated waveform of dc-link capacitor voltage
(b) Experimental waveform of dc-link capacitor voltage

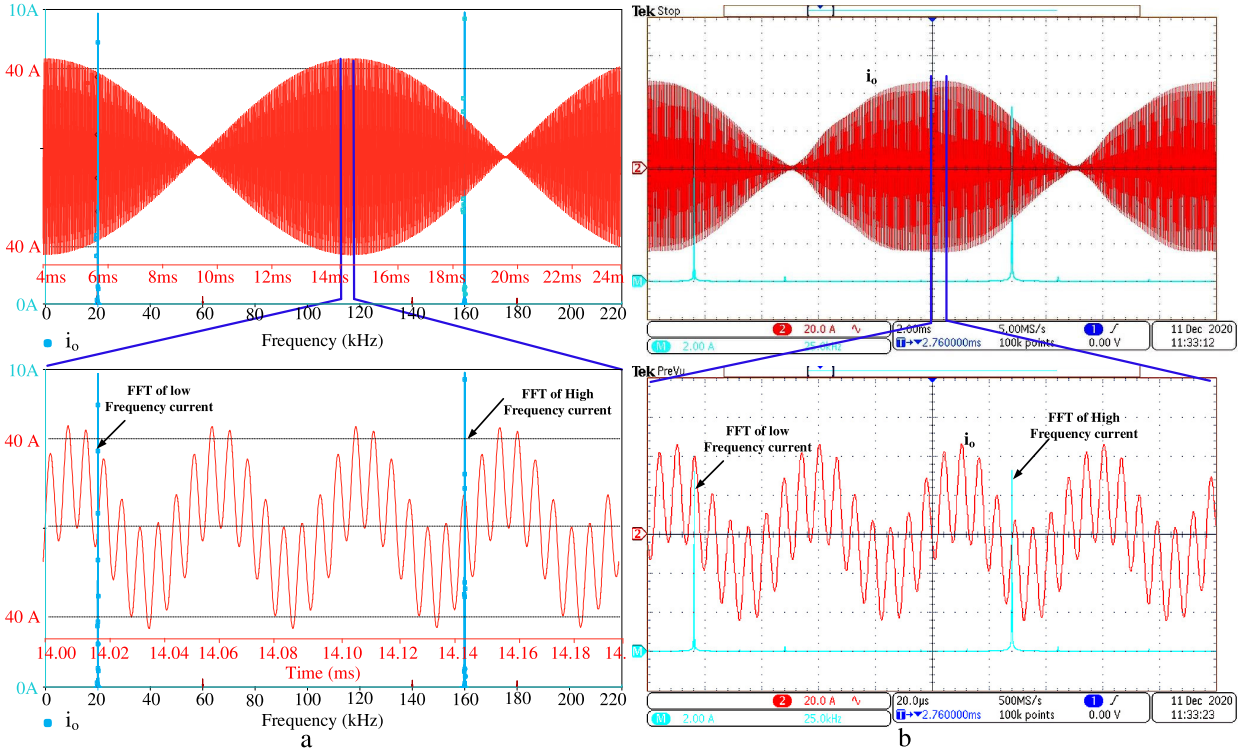

Figure 5.12: Simulated and experimental waveforms of i_o, and its FFTs for f_l=20 kHz and f_h=160 kHz
(a) Simulated waveform of total output current and its FFT
(b) Experimental waveform of total output current and its FFT

current i_{lf} and its FFT, Figure. 5.14a show simulation waveforms of high frequency load current i_{hf}. Figure. 5.14b show experimental waveforms of high frequency load current i_{hf}. From these figures, it is observed that inverter output current contains only low and high-frequency

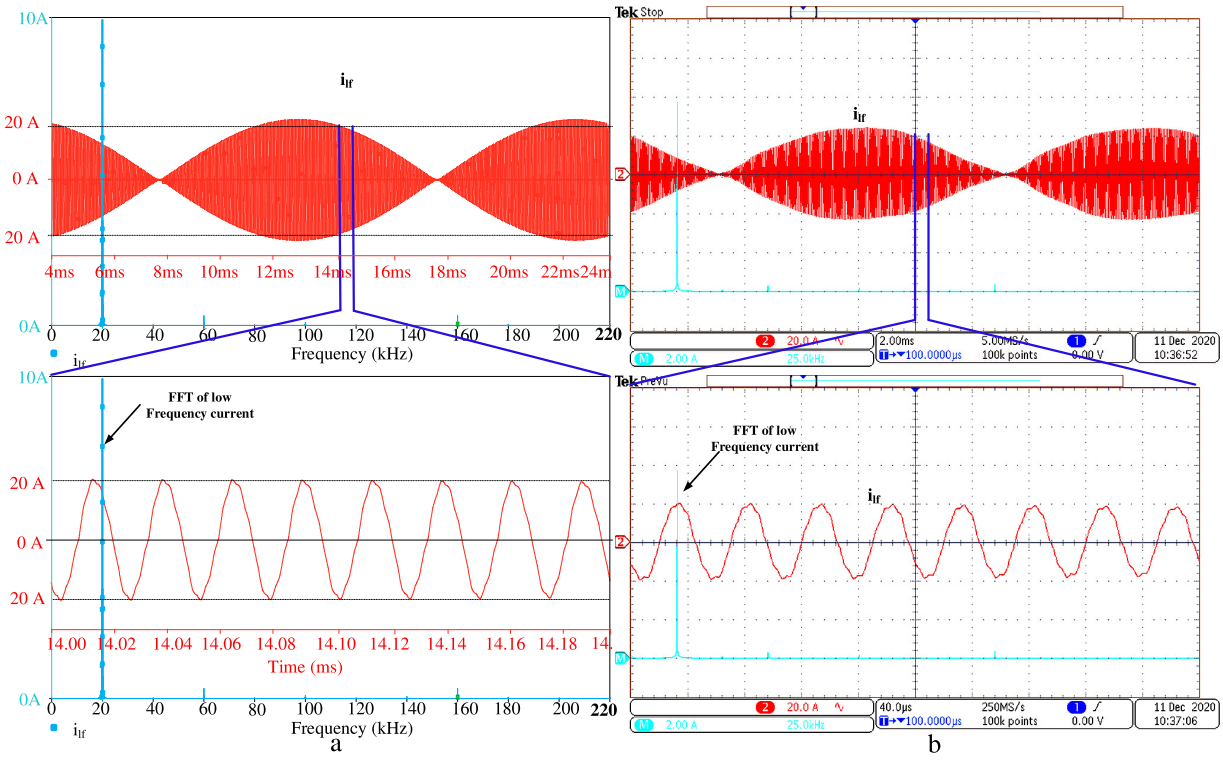

Figure 5.13: Simulated and experimental waveforms of i_{lf} and its FFTs for f_l=20 kHz
(a) Simulated waveform of low frequency load current and its FFT
(b) Experimental waveform of low frequency load current and its FFT

components of current and the respective frequency current component flows through the corresponding IH load. The low-frequency current component flows through the steel vessel IH load and high-frequency current component flows through the aluminium vessel IH load. From FFTs, it is observed that low-frequency IH load RMS current is i_{lf} = 9.6 A and the same for high-frequency IH load is i_{hf} = 9.56 A. Output power control is achieved using pulse frequency control. Figure. 5.15 and Figure. 5.16 show the simulated and experimental waveforms of total output current i_o and its FFT for different combinations of f_l and f_h. Figure. 5.15a and b show simulation and experimental waveforms of i_o and its FFT at f_l=25 kHz and f_h=160 kHz. It is observed that low-frequency load RMS current is reduced to I_{lf}=4.2 A and high-frequency load RMS current remains unchanged at I_{hf} =9.56 A as only low switching frequency is increased. Figure. 5.16a and b show simulated and experimental waveforms of i_o and its FFT at f_l=20 kHz and f_l=165 kHz. From these figures it can be observed that high-frequency load RMS current is reduced to I_{hf}=4.2 A and low-frequency load RMS current remains at the rated value of I_{lf} =9.6 A. These results depict independent load power control. Low and high-frequency output powers (P_{lf} and P_{hf}) are controlled by varying corresponding switching frequency. The above results are tabulated in Table 5.2. The simulated and experimental results are in good agreement with

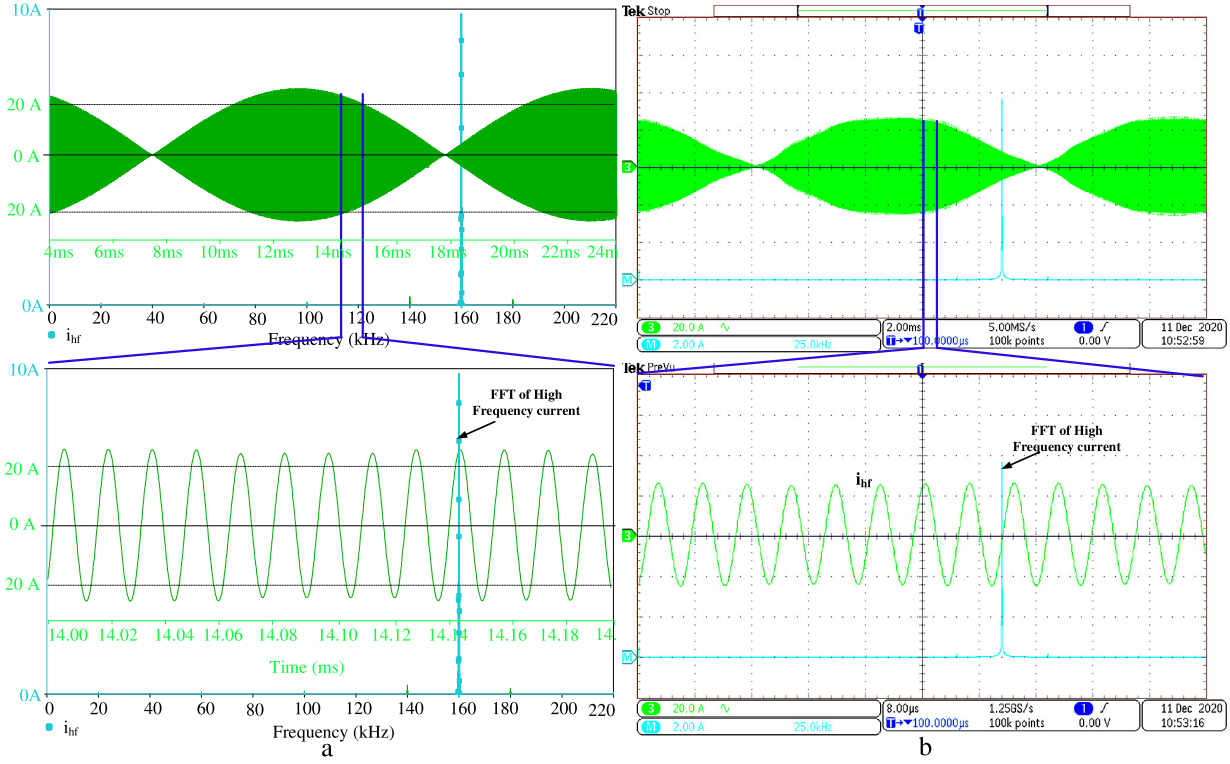

Figure 5.14: Simulated and experimental waveforms of i_{hf} and its FFTs for f_h=160 kHz
(a) Simulated waveform of high frequency load current and its FFT
(b) Experimental waveform of high frequency load current and its FFT

each other. Hence, the proposed converter provides a single stage AC-AC converter with unity power factor, boost operation, multi-frequency output and independent output power control.

5.5 Analysis of results and converter efficiency

In the proposed single-stage AC-AC converter, power control is obtained through pulse frequency control. Figure. 5.17 shows low and high-frequency output currents and power control with frequency. Figure. 5.17a shows the variation of simulated and experimental load currents with variation of low switching frequency of leg-1 devices. Figure. 5.17c shows the low and high-frequency IH load powers with variation of the low switching frequency of leg-1 devices. It can be observed that the low-frequency load current and corresponding output power i.e., of steel vessel decrease with increase in low switching frequency. The corresponding high-frequency components remain constant. Figure. 5.17b shows the variation of simulated and experimental load currents with variation of high switching frequency of leg-2 devices. Figure. 5.17d shows the low and high-frequency IH load powers with variation of high switching frequency of leg-2 devices. It can be observed that the high-frequency load current and corre-

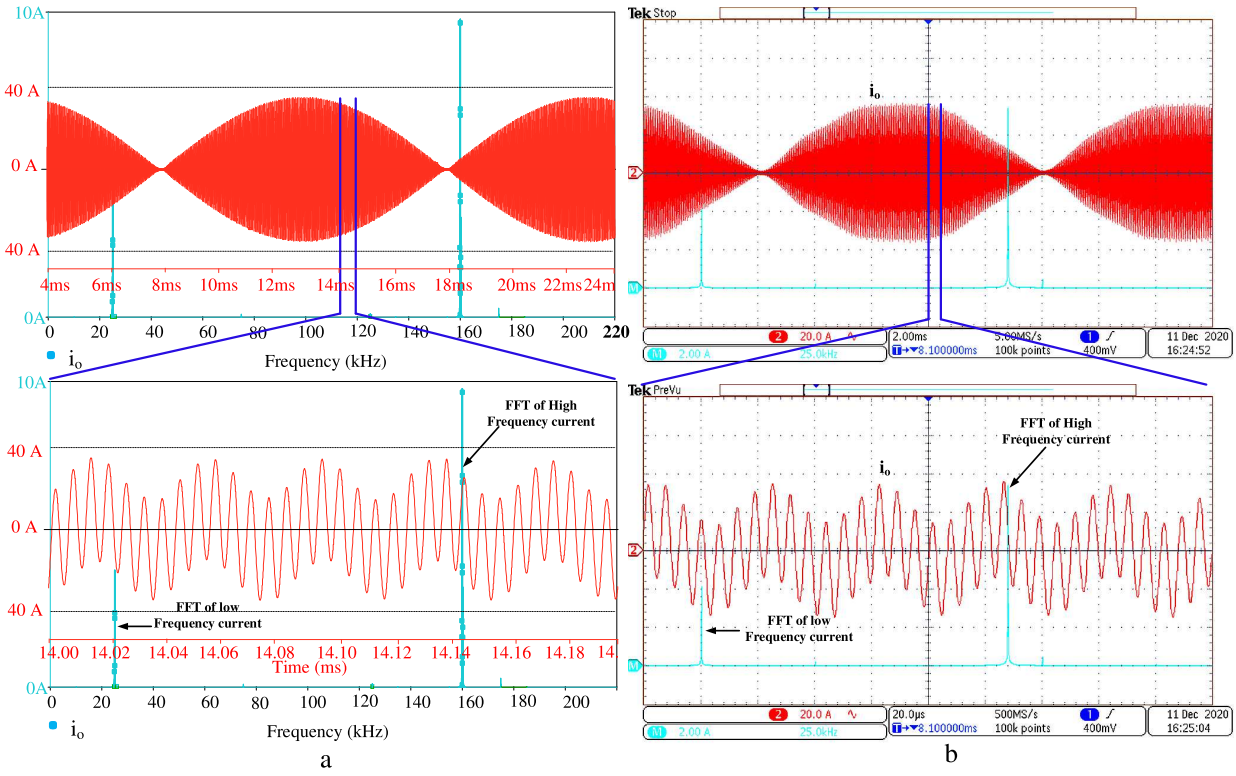

Figure 5.15: Simulated and experimental waveforms of i_o, and its FFTs for f_l=25 kHz and f_h=160 kHz
(a) Simulated waveform of total output current and it FFT at f_l=25 kHz and f_h=160 kHz
(b) Experimental waveform of total output current and it FFT at f_l=25 kHz and f_h=160 kHz

sponding power i.e., of aluminium vessel IH load power decreases with increase in high switching frequency, where the corresponding low-frequency components remain constant. These characteristics prove the independent power control of both low and high frequency vessel loads with pulse frequency modulation. The simulated and experimental results are also in good agreement. Hence the proposed inverter is suitable for heating steel and aluminium vessels simultaneously with independent control. The low and high frequency output powers are obtained using equations (5.18) and (5.19)

$$P_{lf} = V_{olf,rms} I_{olf,rms} \cos\phi_{olf} \approx I_{lf}^2 R_{lf} \tag{5.18}$$

$$P_{hf} = V_{ohf,rms} I_{ohf,rms} \cos\phi_{ohf} \approx I_{hf}^2 R_{hf} \tag{5.19}$$

The total output power is the sum of output powers of steel vessel load (P_{lf}) and aluminium vessel load (P_{hf}).

$$P_0 = P_{lf} + P_{hf} \tag{5.20}$$

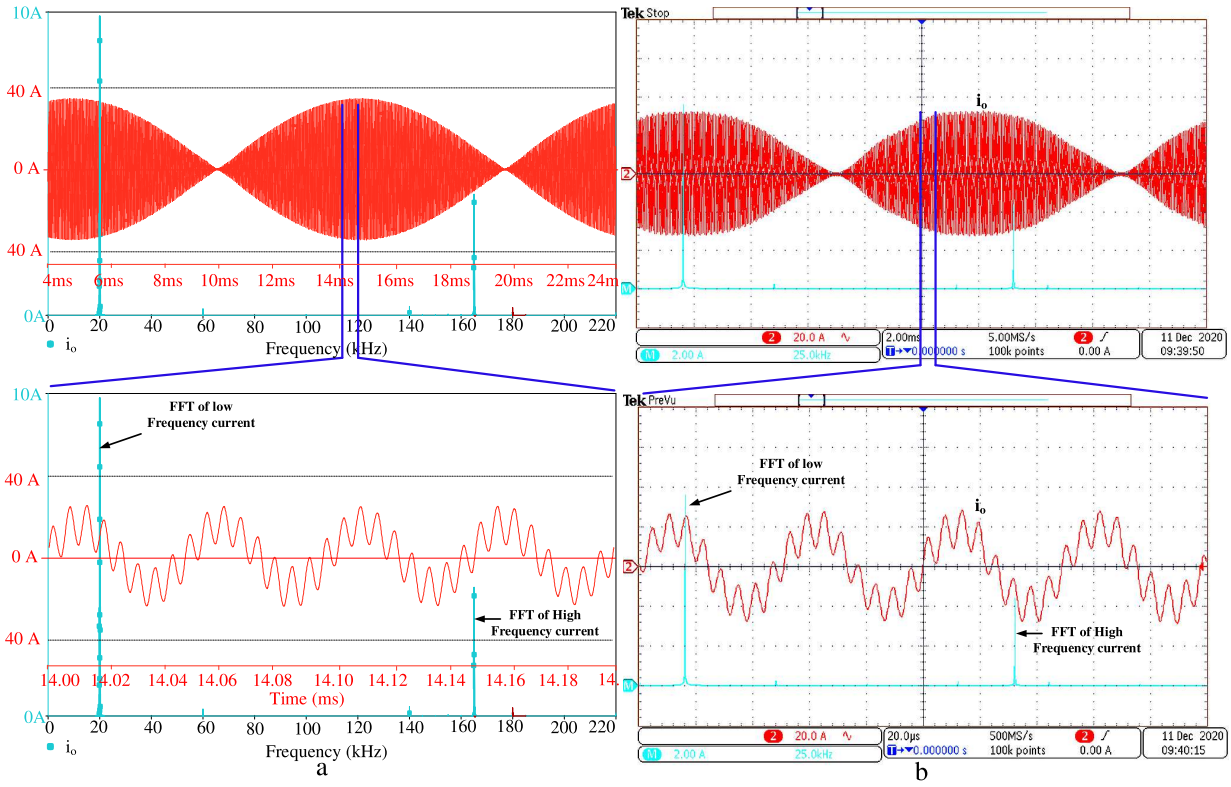

Figure 5.16: Simulated and experimental waveforms of i_o, and its FFTs for f_l=20 kHz and f_h=165 kHz
(a) Simulated waveform of total output current and it FFT at f_l=20 kHz and f_h=165 kHz
(b) Experimental waveform of total output current and it FFT at f_l=20 kHz and f_h=165 kHz

The input power of the converter is calculated (Equation:5.21) as product of RMS input voltage (V_s,rms) and RMS input current (I_s,rms) of the converter as the power factor is closer to unity.

$$P_{in} = V_{s,rms} I_{s,rms} \cos\phi_{in} \approx V_{s,rms} I_{s,rms} \tag{5.21}$$

Overall converter efficiency is calculated as

$$\eta = \frac{P_o}{P_{in}} \tag{5.22}$$

The overall efficiency vs low and high switching frequencies are shown in Figure. 5.18a and b respectively. The overall efficiency of the proposed converter topology remains significantly high for both switching frequency variations. Thermal images of steel and aluminium vessels at different load currents are shown in Figures. 19 and 20. Thermal imager (CHAUVIN ARNOUX-C.A1950) has been used. Thermal images of steel vessel at low frequency currents of 4 A, 5 A, 6.92 A are shown in Figure. 5.19a, b and c respectively. However these

Table 5.2: Output power and efficiency for different combinations of f_l and f_h

V_s (V)	P_{in} (W)	f_l (kHz)	f_h(kHz)	P_{lf} (W)	P_{hf}(W)	P_o(W)	Efficiency
40	340	20	160	192.6	123.4	316	93.2%
40	173.2	25	160	37	123.4	160.4	92.5%
40	235	20	165	192.6	23.8	216.4	92.2%

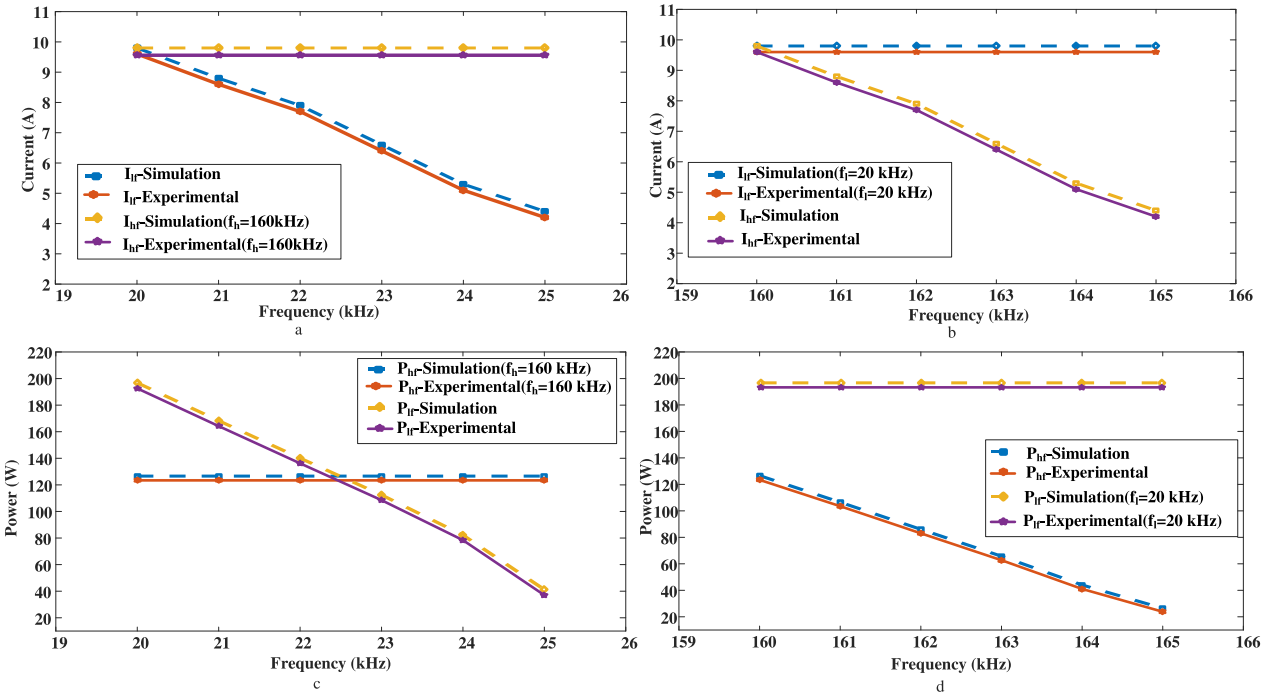

Figure 5.17: Low and high frequency output current and power control
(a) Load current variation with f_l
(b) Load current variation with f_h
(c) Load power variation with f_l
(d) Load power variation with f_h

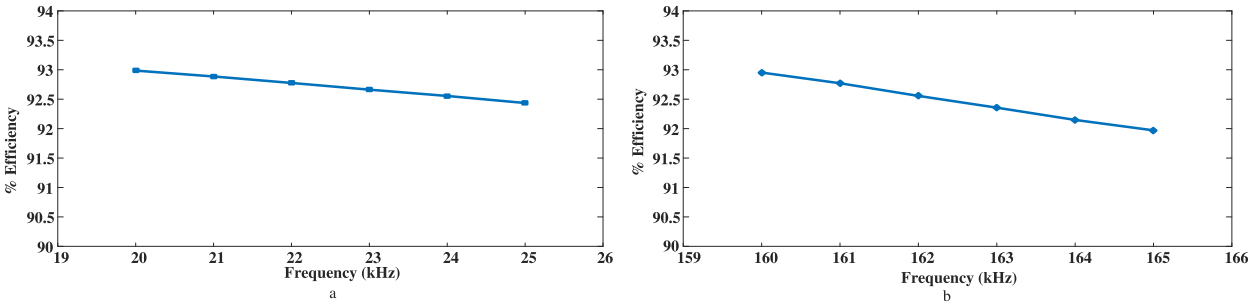

Figure 5.18: Efficiency curves
(a) Efficiency vs low frequency (f_l)
(b) Efficiency vs high frequency (f_h)

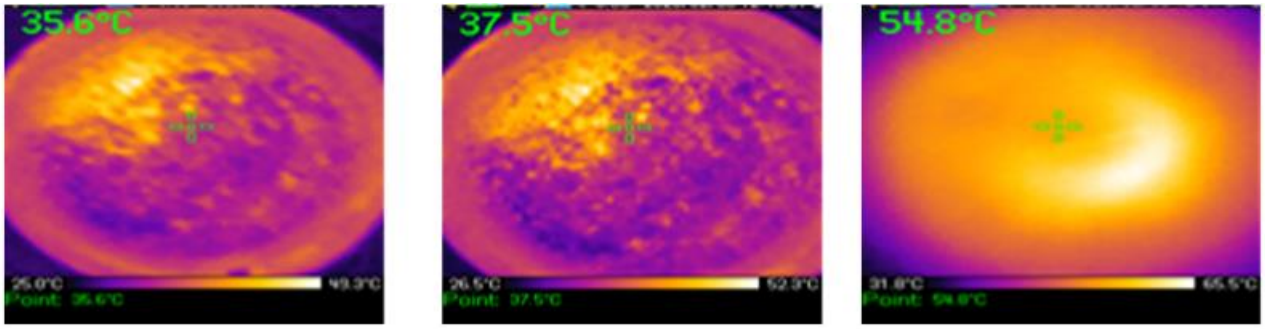

Figure 5.19: Steel vessel thermal images at f_l=20 kHz
(a) i_{lfrms}= 4 A
(b) i_{lfrms}= 5 A
(c) i_{lfrms}= 6.92 A

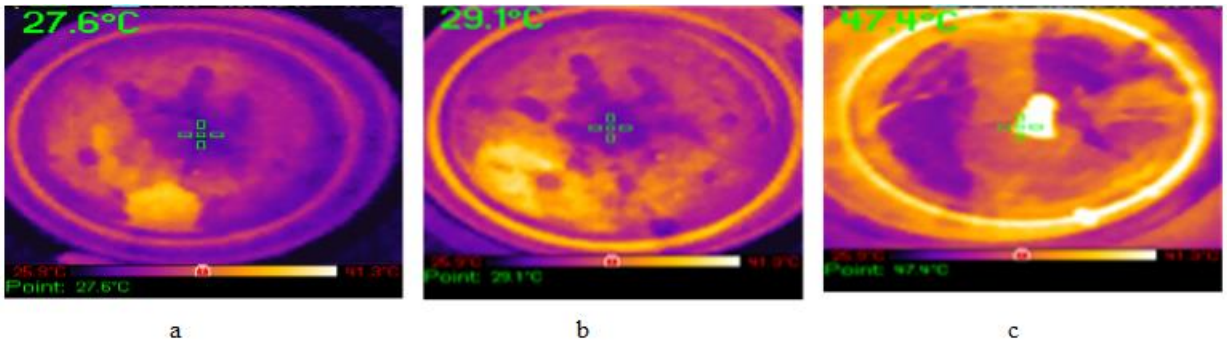

Figure 5.20: Aluminium vessel thermal images at f_h=160 kHz
(a) i_{hfrms} = 4 A
(b) i_{hfrms} = 5 A
(c) i_{hfrms} = 6.96 A

low frequency currents cannot generate heat in aluminium vessel due to its lower values of permeability and equivalent resistance. Hence the proposed inverter configuration powers the aluminium vessel load with high frequency currents. Thermal images of aluminium vessel at high frequency currents of 4 A, 5 A, 6.96 A are shown in Figure. 5.20a, b and c respectively. From these figures, it is observed that aluminium vessel also gets heated and hence the proposed converter configuration is suitable for both steel and aluminium vessels.

5.6 Conclusions

In this chapter a single-stage ac-ac resonant converter for different material induction cooking applications has been proposed and implemented. Inverter legs are operated at two different frequencies suitable for two different material cooking vessels. The low frequency leg

is common for both rectification and inversion operation. Low frequency of 20 kHz is used for steel vessel and high frequency of 160 kHz is used for aluminium vessel. Independent output power control is achieved by pulse frequency control. The number of switching devices is two per load. In this configuration, overall efficiency of >93% is achieved at full load. Output power control is achieved using pulse frequency control modulation technique. Simulation study of the inverter is performed and its results are verified experimentally. Both simulation and experimental results are in good agreement with each other.
The advantages of the proposed inverter configuration are listed below:

i Eliminates the rectifier bridge

ii Achieved boost operation and high power factor

iii Suitable for two IH loads

iv Reduces the size of reactive components

v Suitable for different material vessel domestic induction Cooking

vi Independent power control is achieved using pulse frequency modulation

vii High power conversion efficiency

viii Uses only two switching devices per load

ix Eliminates the use electro-mechanical switches

Next chapter presents the conclusions and scope for future work.

Chapter 6

Conclusions and Scope for Future work

Chapter 6

Conclusions and Scope for Future work

6.1 Conclusions

Multi-load induction heating, different material induction heating and single stage ac-ac resonant converter for induction cooking applicatons have been studied. Three different inverter configurations for different material IH have been proposed. A thorough analysis, design, implementation and comparison of the proposed IH topologies is performed.

6.1.1 Summary of Important findings

The following conclusions have been arrived from the research work.

6.1.1.1 Proposed inverter configuration-1 (Cascaded Full-bridge Resonant Inverter)

Cascaded full-bridge resonant inverter topology is proposed for different material vessel IH loads. First inverter legs are operated at low and medium frequencies suitable for iron and steel vessels. Second inverter is operated at high frequency suitable for aluminium vessel. Frequencies of 20 kHz, 100 kHz and 400 kHz are used. Independent power control is achieved using asymmetric duty cycle control. The proposed inverter topology is designed, simulated and hardware prototype is implemented. Simulation and experimental results are in good agreement with each other.

This topology provides the following advantages compared with the existing multiple load IH inverter topologies:

- Suitable for different material vessels
- Eliminates the use of electro-mechanical switches
- Reduced device count (8 devices per 3 loads)
- Simple control technique

- Ability to power multiple loads with equal or unequal voltages/wattages
- Reduced switching losses due to soft-switching
- High overall efficiency ($\geq$ 92 %)
- Independent power control with asymmetric duty cycle control
- Proposed scheme can be extended to more than three loads
  The limitation of this inverter topology is the requirement of two DC sources.

6.1.1.2 Proposed inverter configuration-2 (Frequency controlled three leg resonant inverter)

The three-output inverter topology has been designed and tested to power both ferromagnetic and non-ferromagnetic vessels. The inverter's three distinct frequency legs are utilised to power three different material vessel domestic IH loads. Inverter leg-1 operates at a low frequency and is suitable for iron loads, whereas Inverter leg-2 operates at a medium frequency and is suitable for steel vessel IC loads. Inverter leg-3 operates at a high frequency, making it ideal for IC loads in aluminium vessels. The leg frequencies are 25 kHz, 100 kHz, and 400 kHz. Variable-frequency control is implemented with a DSP controller. It provides independent power control of the three IH loads. The proposed inverter topology is designed, simulated and hardware prototype is implemented. Simulation and experimental results are in good agreement with each other.

This topology provides the following advantages compared to the existing multiple load IH inverter topologies:

- Suitable for different material vessels
- Eliminates the use electro-mechanical switches
- Reduced device count (2 devices per load)
- Compact in size
- Simple control technique
- Ability to power multiple loads with a single DC source
- Reduced switching losses due to soft-switching
- Higher overall efficiency ($\geq$ 94 %)

- Independent power control is achieved using pulse frequency modulation technique.
- Proposed scheme can be extended to more than three loads by adding additional inverter legs

6.1.1.3 Proposed inverter configuration-3 (Single stage ac-ac resonant converter)

A single-stage ac-ac resonant converter has been proposed for different material induction cooking applications. Inverter legs are operated at two different frequencies suitable for two different material cooking vessels. The low frequency leg is common for both rectification and inversion operation. Low frequency of 20 kHz is used for steel vessel and high frequency of 160 kHz is used for aluminium vessel. Independent output power control is achieved using pulse frequency control. The number of switching devices is two per load. In this configuration, overall efficiency of >93% is achieved at full load. Output power control is achieved using pulse frequency control modulation technique. The salient features of the proposed converter are: Suitability for different material IH loads, single stage AC-AC conversion, boost operation, high power factor, independent power control, soft switching operation and high efficiency. Simulation study of the inverter is performed and its results are verified experimentally. Both simulation and experimental results are in good agreement with each other.

Table 6.1: Advantages of proposed configuration-3 (Single-stage AC-AC converter) over existing IH converter topologies

Advantages over existing two-stage IH converters :	**Advantages over existing multi-load single-stage AC-AC converters:**
• Single power conversion stage and hence reduced component count and increased efficiency • Boost operation is possible • Reduced device density because of higher switching frequency • Soft switching across all devices including auxiliary circuit devices • Ability to power different material vessel induction cooking loads	• Better device utilization factor • Able to handle multiple load • Higher efficiency • Simple control • Ability to power different material vessel induction cooking loads

Table 6.2: Comparison between proposed three resonant converter configurations

Configuration\ Feature	**Configuration-1**	**Configuration-2**	**Configuration-3**
Source	2 DC	DC	AC
Power factor correction	Not applicable	Not applicable	Yes
Multiple load capability	Yes	Yes	Yes
Different material vessel heating capability	Yes	Yes	Yes
No.of loads	3	3	2
Independent power control	Yes	Yes	Yes
No.of inverter legs	4	3	2
Boost operation	No	No	Yes
No. of Switching devices per load	Medium	Low	Low
Power control	ADC	PFM	PFM
Switching Frequency (kHz)	20, 100 and 400	25, 100 and 400	20 and 160
Resonant Frequency (kHz)	19.5 ,98.5 and 398	23.5, 98.5 and 396	19.8 and 158
Rating of IH load	Load1: 26 W Load2: 30 W Load3: 82 W	Load1: 128.5 W, Load2: 115.5 W Load3: 85.25 W	Load1: 193 W Load2: 123 W
Overall Efficiency (%)	92	93	94
Need of electro mechanical switch	No	No	No
Key Features	Different material vessel IC, Independent control and High efficiency	Different material vessel IC, Independent control, High efficiency and Reduced component count	Different material vessel IC, Independent control, Single-stage ac-ac conversion Reduced component count, High efficiency, Power factor correction, Boost operation
Application	Three different material vessel IC (Iron, Steel and Al)	Three different material vessel IC (Iron, Steel and Al)	Two different material vessel IC (Steel and Al)

6.1.2 Comparison of the proposed converter configurations

A relative comparison of the three proposed innverter configurations is shown in Table 6.2. Both configuration-1 and configuration-2 are suitable for three different material vessel IH applications. Iron, steel and aluminium vessel loads are used. In configuration-1 two full-bridge inverters are used with cascaded connection. It also uses two isolated DC sources. ADC control is used. This configuration provides independent power control and high efficiency. Only limitation is the requirement of two DC sources. In configuration-2, a three leg inverter based topology is used, and hence number of switching devices is reduced by two compared to configuration-1. This configuration uses a high frequency 1:1 transformer. PFM control is used. This configuration provides the advantages of independent load control, reduced component count and high efficiency. In configuration-3, a single-stage ac-ac converter based topology is proposed which is suitable for two different material vessel IH applications. It eliminates the need for diode bridge rectifier and hence provides reduced component count and high efficiency.

PFM control is used. This configuration provides advantages of single stage ac-ac conversion, high power factor, dc-link voltage boost operation, low component count, independent power control and high efficiency. All the three proposed converter configurations are suitable for different material IH applications.

6.2 Suggestions for Future Research

As an extension to the current research work, there is scope for exploring further for a prospective researcher:

- Small signal analysis of all the proposed inverter configurations can be carried out.
- Closed loop control can be implemented for power regulation for different IH loads.
- Proposed configurations can be further analysed with the aim of reduction of component count.

Bibliography

Bibliography

[1] S. Semiatin, *Elements of induction heating: design, control, and applications*. Asm International, 1988.

[2] G. H. Brown, C. N. Hoyler, R. A. Bierwirth *et al.*, "Theory and application of radio-frequency heating." *Theory and application of radio-frequency heating.*, 1947.

[3] V. Rudnev, D. Loveless, and R. L. Cook, *Handbook of induction heating*. CRC press, 2017.

[4] E. Plumed, J. Acero, I. Lope, and J. M. Burdío, "Design methodology of high performance domestic induction heating systems under worktop," *IET Power Electronics*, 2019.

[5] O. Lucía, P. Maussion, E. J. Dede, and J. M. Burdío, "Induction heating technology and its applications: past developments, current technology, and future challenges," *IEEE Transactions on industrial electronics*, vol. 61, no. 5, pp. 2509–2520, 2013.

[6] E. Dede, V. Esteve, J. González, J. García, E. Maset, and D. Ramirez, "A 12 kW/250 kHz series resonant converter for induction heating," *Transactions of the South African Institute of Electrical Engineers*, vol. 1, no. 86, pp. 45–48, 1995.

[7] M. Salem, A. Jusoh, N. R. N. Idris, and I. Alhamrouni, "Performance study of series resonant converter using zero voltage switching," in *2014 IEEE Conference on Energy Conversion (CENCON)*. IEEE, 2014, pp. 96–100.

[8] E. Dede, J. Jordan, J. Gonzalez, J. Linares, V. Esteve, and E. Maset, "Conception and design of a parallel resonant converter for induction heating," in *[Proceedings] APEC'91: Sixth Annual Applied Power Electronics Conference and Exhibition*. IEEE, 1991, pp. 38–44.

[9] E. Laithwaite, "The influence of Michael Faraday on power engineering," *Power Engineering Journal*, vol. 5, no. 5, pp. 209–219, 1991.

[10] L. Meng, K. W. E. Cheng, and K. W. Chan, "Systematic approach to high-power and energy-efficient industrial induction cooker system: circuit design, control strategy, and

prototype evaluation," *IEEE transactions on power electronics*, vol. 26, no. 12, pp. 3754–3765, 2011.

[11] P. R. Stauffer, T. C. Cetas, and R. C. Jones, "Magnetic induction heating of ferromagnetic implants for inducing localized hyperthermia in deep-seated tumors," *IEEE Transactions on Biomedical Engineering*, no. 2, pp. 235–251, 1984.

[12] S. Llorente, F. Monterde, J. Burdio, and J. Acero, "A comparative study of resonant inverter topologies used in induction cookers," in *APEC. Seventeenth Annual IEEE Applied Power Electronics Conference and Exposition (Cat. No. 02CH37335)*, vol. 2. IEEE, 2002, pp. 1168–1174.

[13] F. P. Dawson and P. Jain, "A comparison of load commutated inverter systems for induction heating and melting applications," *IEEE transactions on power electronics*, vol. 6, no. 3, pp. 430–441, 1991.

[14] J. Acero, P. J. Hernandez, J. M. Burdio, R. Alonso, and L. Barragdan, "Simple resistance calculation in litz-wire planar windings for induction cooking appliances," *IEEE Transactions on magnetics*, vol. 41, no. 4, pp. 1280–1288, 2005.

[15] M. Kim, H.-P. Park, and J.-H. Jung, "Practical design methodology of IH and IPT dual-functional apparatus," *IEEE Transactions on Power Electronics*, vol. 35, no. 9, pp. 8897–8901, 2020.

[16] A. Shenkman, B. Axelrod, and Y. Berkovich, "Single-switch AC-AC converter with high power factor and soft commutation for induction heating applications," *IEE Proceedings-Electric Power Applications*, vol. 148, no. 6, pp. 469–474, 2001.

[17] I. Hirota, H. Omori, K. A. Chandra, and M. Nakaoka, "Practical evaluations of single-ended load-resonant inverter using application-specific IGBT and driver IC for induction-heating appliance," in *Proceedings of 1995 International Conference on Power Electronics and Drive Systems. PEDS 95*. IEEE, 1995, pp. 531–537.

[18] H. W. Koertzen, J. D. Van Wyk, and J. A. Ferreira, "Design of the half-bridge, series resonant converter for induction cooking," in *Proceedings of PESC'95-Power Electronics Specialist Conference*, vol. 2. IEEE, 1995, pp. 729–735.

[19] M. Kamli, S. Yamamoto, and M. Abe, "A 50-150 kHz half-bridge inverter for induction heating applications," *IEEE Transactions on Industrial Electronics*, vol. 43, no. 1, pp. 163–172, 1996.

[20] O. Lucia, J. M. Burdio, I. Millan, J. Acero, and L. A. Barragan, "Efficiency-oriented design of ZVS half-bridge series resonant inverter with variable frequency duty cycle control," *IEEE Transactions on Power Electronics*, vol. 25, no. 7, pp. 1671–1674, 2010.

[21] R. L. Steigerwald, "A comparison of half-bridge resonant converter topologies," *IEEE transactions on Power Electronics*, vol. 3, no. 2, pp. 174–182, 1988.

[22] H. Sarnago, O. Lucia, A. Mediano, and J. M. Burdio, "Analytical model of the half-bridge series resonant inverter for improved power conversion efficiency and performance," *IEEE Transactions on Power Electronics*, vol. 30, no. 8, pp. 4128–4143, 2014.

[23] S. M. W. Ahmed, M. Eissa, M. Edress, and T. S. Abdel-Hameed, "Experimental investigation of full bridge series resonant inverters for induction-heating cooking appliances," in *2009 4th IEEE Conference on Industrial Electronics and Applications*. IEEE, 2009, pp. 3327–3332.

[24] E. J. Dede, J. V. Gonzalez, J. A. Linares, J. Jordan, D. Ramirez, and P. Rueda, "25-kW/50-kHz generator for induction heating," *IEEE transactions on industrial electronics*, vol. 38, no. 3, pp. 203–209, 1991.

[25] T. Mishima, S. Sakamoto, and C. Ide, "ZVS phase-shift PWM-controlled single-stage boost full-bridge AC–AC converter for high-frequency induction heating applications," *IEEE Transactions on Industrial Electronics*, vol. 64, no. 3, pp. 2054–2061, 2016.

[26] H. Koertzen, J. Ferreria, and J. Van Wyk, "A comparative study of single switch induction heating converters using novel component effectivity concepts," in *PESC'92 Record. 23rd Annual IEEE Power Electronics Specialists Conference*. IEEE, 1992, pp. 298–305.

[27] J. A. Sabate, *Zero-voltage switched resonant and PWM converters: design-oriented analysis and performance evaluation*. Virginia Polytechnic Institute and State University, 1994.

[28] T. Ahmed, K. Ogura, S. Chandhaket, and M. Nakaoka, "Asymmetrical duty cycle controlled edge resonant soft switching high frequency inverter for consumer electromagnetic induction fluid heater," *Automatica, ATKAAF*, vol. 44, no. 1-2, pp. 21–26, 2003.

[29] J. M. Burdio, L. A. Barragan, F. Monterde, D. Navarro, and J. Acero, "Asymmetrical voltage-cancellation control for full-bridge series resonant inverters," *IEEE transactions on power electronics*, vol. 19, no. 2, pp. 461–469, 2004.

[30] M. K. Kazimierczuk and M. K. Jutty, "Fixed-frequency phase-controlled full-bridge resonant converter with a series load," *IEEE transactions on power electronics*, vol. 10, no. 1, pp. 9–18, 1995.

[31] H.-J. Chiu, Y.-K. Lo, T.-P. Lee, C.-C. Chuang, and S.-C. Mou, "A single-stage phase-shifted full-bridge AC/DC converter with variable frequency control," *International Journal of Circuit Theory and Applications*, vol. 38, no. 8, pp. 867–879, 2010.

[32] H. Ogiwara, M. Itoi, and M. Nakaoka, "PWM-controlled soft-switching SEPP high-frequency inverter for induction-heating applications," *IEE Proceedings-Electric Power Applications*, vol. 151, no. 4, pp. 404–413, 2004.

[33] Y.-S. Kwon, S.-B. Yoo, and D.-S. Hyun, "Half-bridge series resonant inverter for induction heating applications with load-adaptive PFM control strategy," in *APEC'99. Fourteenth Annual Applied Power Electronics Conference and Exposition. 1999 Conference Proceedings (Cat. No. 99CH36285)*, vol. 1. IEEE, 1999, pp. 575–581.

[34] T. Isobe, K. Usuki, N. Arai, T. Kitahara, K. Fukutani, and R. Shimada, "Variable frequency induction heating using magnetic energy recovery switch (MERS)," in *2008 IEEE Power Electronics Specialists Conference*. IEEE, 2008, pp. 2139–2145.

[35] V. Esteve, J. Jordan, E. Sanchis-Kilders, E. J. Dede, E. Maset, J. B. Ejea, and A. Ferreres, "Enhanced pulse-density-modulated power control for high-frequency induction heating inverters," *IEEE Transactions on Industrial Electronics*, vol. 62, no. 11, pp. 6905–6914, 2015.

[36] J. Shen, H. Ma, W. Yan, J. Hui, and L. Wu, "PDM and PSM hybrid power control of a series-resonant inverter for induction heating applications," in *2006 1ST IEEE Conference on Industrial Electronics and Applications*. IEEE, 2006, pp. 1–6.

[37] P. Herasymenko, "Combined PS-PDM control method for voltage-source seriesresonant inverter," *Przegląd Elektrotechniczny*, vol. 1, no. 5, pp. 42–47, 2021.

[38] N. A. Ahmed, "High-frequency soft-switching ac conversion circuit with dual-mode PWM/PDM control strategy for high-power IH applications," *IEEE transactions on industrial electronics*, vol. 58, no. 4, pp. 1440–1448, 2010.

[39] L. A. Barragán, D. Navarro, J. Acero, I. Urriza, and J. M. Burdío, "FPGA implementation of a switching frequency modulation circuit for EMI reduction in resonant inverters for

induction heating appliances," *IEEE Transactions on Industrial Electronics*, vol. 55, no. 1, pp. 11–20, 2008.

[40] Ó. Lucia, L. A. Barragan, J. M. Burdio, O. Jimenez, D. Navarro, and I. Urriza, "A versatile power electronics test-bench architecture applied to domestic induction heating," *IEEE Transactions on Industrial Electronics*, vol. 58, no. 3, pp. 998–1007, 2010.

[41] O. Lucia, J. M. Burdio, I. Millan, J. Acero, and D. Puyal, "Load-adaptive control algorithm of half-bridge series resonant inverter for domestic induction heating," *IEEE transactions on industrial electronics*, vol. 56, no. 8, pp. 3106–3116, 2009.

[42] F. Forest, E. Labouré, F. Costa, and J. Y. Gaspard, "Principle of a multi-load/single converter system for low power induction heating," *IEEE Transactions on Power Electronics*, vol. 15, no. 2, pp. 223–230, 2000.

[43] J. M. Burdio, F. Monterde, J. R. Garcia, L. A. Barragan, and A. Martinez, "A two-output series-resonant inverter for induction-heating cooking appliances," *IEEE Transactions on Power Electronics*, vol. 20, no. 4, pp. 815–822, 2005.

[44] L. Meng, K. W. E. Cheng, and S. L. Ho, "Multicoils design for induction cookers with applying switched exciting method," *IEEE transactions on magnetics*, vol. 48, no. 11, pp. 4503–4506, 2012.

[45] H. Sarnago, P. Guillén, J. M. Burdío, and O. Lucia, "Multiple-output ZVS resonant inverter architecture for flexible induction heating appliances," *IEEE Access*, vol. 7, pp. 157 046–157 056, 2019.

[46] O. Lucia, C. Carretero, J. M. Burdio, J. Acero, and F. Almazan, "Multiple-output resonant matrix converter for multiple induction heaters," *IEEE Transactions on Industry Applications*, vol. 48, no. 4, pp. 1387–1396, 2012.

[47] D. Vijaya Bhaskar, N. Vishwanathan, T. Maity, and S. Porpandiselvi, "A three-output inverter for induction cooking application with independent control," *EPE Journal*, vol. 28, no. 2, pp. 89–99, 2018.

[48] S. K. Papani, V. Neti, and B. K. Murthy, "Dual frequency inverter configuration for multiple-load induction cooking application," *IET Power Electronics*, vol. 8, no. 4, pp. 591–601, 2015.

[49] H. Sarnago, A. Mediano, and O. Lucia, "High efficiency ac-ac power electronic converter applied to domestic induction heating," *IEEE transactions on Power Electronics*, vol. 27, no. 8, pp. 3676–3684, 2012.

[50] H. Sarnago, O. Lucia, A. Mediano, and J. M. Burdio, "A class-E direct ac-ac converter with multicycle modulation for induction heating systems," *IEEE Transactions on Industrial Electronics*, vol. 61, no. 5, pp. 2521–2530, 2013.

[51] H. Sarnago, O. Lucía, A. Mediano, and J. M. Burdio, "Efficient and cost-effective ZCS direct AC–AC resonant converter for induction heating," *IEEE Transactions on Industrial Electronics*, vol. 61, no. 5, pp. 2546–2555, 2013.

[52] H. Sarnago, O. Lucia, A. Mediano, and J. M. Burdio, "Direct AC–AC resonant boost converter for efficient domestic induction heating applications," *IEEE Transactions on Power Electronics*, vol. 29, no. 3, pp. 1128–1139, 2013.

[53] T. Mishima, Y. Nakagawa, and M. Nakaoka, "A bridgeless BHB ZVS-PWM AC–AC converter for high-frequency induction heating applications," *IEEE Transactions on Industry Applications*, vol. 51, no. 4, pp. 3304–3315, 2015.

[54] R. C. M. Gomes, M. A. Vitorino, D. A. Acevedo-Bueno, and M. B. de Rossiter Corrêa, "Multiphase resonant inverter with coupled coils for AC–AC induction heating application," *IEEE Transactions on Industry Applications*, vol. 56, no. 1, pp. 551–560, 2019.

[55] S.-W. Lee and H.-L. Do, "Efficient bridgeless PFC converter with reduced voltage stress," *International Journal of Circuit Theory and Applications*, vol. 44, no. 7, pp. 1455–1467, 2016.

[56] H. Sarnago, O. Lucia, A. Mediano, and J. M. Burdio, "Design and implementation of a high-efficiency multiple-output resonant converter for induction heating applications featuring wide bandgap devices," *IEEE Transactions on Power Electronics*, vol. 29, no. 5, pp. 2539–2549, 2013.

[57] H.-P. Park and J.-H. Jung, "Load-adaptive modulation of a series-resonant inverter for all-metal induction heating applications," *IEEE Transactions on Industrial Electronics*, vol. 65, no. 9, pp. 6983–6993, 2018.

[58] I. Millan, D. Puyal, J. Burdio, J. Acero, and S. Llorente, "Resonant inverter topology for all-metal domestic induction heating," in *2007 IEEE International Symposium on Industrial Electronics*. IEEE, 2007, pp. 913–918.

[59] D. Wetz, D. Landen, S. Satapathy, and D. Surls, "Inductive heating of materials for the study of high temperature mechanical properties," *IEEE Transactions on Dielectrics and Electrical Insulation*, vol. 18, no. 4, pp. 1342–1351, 2011.

[60] T. Hirokawa, E. Hiraki, T. Tanaka, M. Okamoto, and M. Nakaoka, "The practical evaluations of time-sharing high-frequency resonant soft-switching inverter for all metal IH cooking appliances," in *IECON 2012-38th Annual Conference on IEEE Industrial Electronics Society*. IEEE, 2012, pp. 3302–3307.

[61] T. Hirokawa, M. Okamoto, E. Hiraki, T. Tanaka, and M. Nakaoka, "A novel type time-sharing high-frequency resonant soft-switching inverter for all metal IH cooking appliances," in *IECON 2011-37th Annual Conference of the IEEE Industrial Electronics Society*. IEEE, 2011, pp. 2526–2532.

[62] H. Yonemori and M. Kobayashi, "On the heating characteristic and magnetic flux of a double-coil drive type induction heating cooker," in *IECON 2006-32nd Annual Conference on IEEE Industrial Electronics*. IEEE, 2006, pp. 2488–2493.

[63] W. Han, K. Chau, C. Jiang, and W. Liu, "All-metal domestic induction heating using single-frequency double-layer coils," *IEEE Transactions on Magnetics*, vol. 54, no. 11, pp. 1–5, 2018.

[64] I. Millan, J. Burdío, J. Acero, O. Lucía, and S. Llorente, "Series resonant inverter with selective harmonic operation applied to all-metal domestic induction heating," *IET Power Electronics*, vol. 4, no. 5, pp. 587–592, 2011.

[65] W. Han, K. T. Chau, W. Liu, X. Tian, and H. Wang, "A dual-resonant topology-reconfigurable inverter for all-metal induction heating," *IEEE Journal of Emerging and Selected Topics in Power Electronics*, 2021.

[66] S. Shuvo, E. Hossain, T. Islam, A. Akib, S. Padmanaban, and M. Z. R. Khan, "Design and hardware implementation considerations of modified multilevel cascaded H-bridge inverter for photovoltaic system," *Ieee Access*, vol. 7, pp. 16 504–16 524, 2019.

[67] J. Rodriguez, J.-S. Lai, and F. Z. Peng, "Multilevel inverters: a survey of topologies, controls, and applications," *IEEE Transactions on industrial electronics*, vol. 49, no. 4, pp. 724–738, 2002.

[68] R. Choudhary, H. M. Suryawanshi, G. G. Talapur, M. A. Chaudhari, and A. B. Shitole, "Modified cascaded multi-level inverter structure with reduced voltage stress across h-bridge for high voltage application," *Electric Power Components and Systems*, vol. 46, no. 6, pp. 659–672, 2018.

[69] J. Liu, K. Cheng, and Y. Ye, "A cascaded multilevel inverter based on switched-capacitor for high-frequency AC power distribution system," *IEEE Transactions on Power Electronics*, vol. 29, no. 8, pp. 4219–4230, 2013.

[70] K. Corzine and Y. Familiant, "A new cascaded multilevel h-bridge drive," *IEEE Transactions on power electronics*, vol. 17, no. 1, pp. 125–131, 2002.

[71] B. A. P. Shalini and S. Sethuraman, "Cascaded multilevel inverter for industrial applications," in *International Conference on Advances in Information Technology and Mobile Communication*. Springer, 2012, pp. 339–344.

[72] Y. Li, R. Mai, M. Yang, and Z. He, "Cascaded multi-level inverter based IPT systems for high power applications," *Journal of Power Electronics*, vol. 15, no. 6, pp. 1508–1516, 2015.

[73] B. Diong, S. Basireddy, K. Corzine, and Y. Familiant, "Multilevel inverters with equal or unequal sources for dual-frequency induction heating," in *Nineteenth Annual IEEE Applied Power Electronics Conference and Exposition, 2004. APEC'04.*, vol. 2. IEEE, 2004, pp. 825–831.

[74] B. Diong, S. Basireddy, and K. Corzine, "Multilevel converter-based dual-frequency induction heating power supply," in *IECON'03. 29th Annual Conference of the IEEE Industrial Electronics Society (IEEE Cat. No. 03CH37468)*, vol. 2. IEEE, 2003, pp. 1992–1997.

[75] L. Qingfeng, W. Huamin, and L. Zhaoxia, "Discuss on the application of multilevel inverter in high frequency induction heating power supply," in *TENCON 2006-2006 IEEE Region 10 Conference*. IEEE, 2006, pp. 1–4.

[76] S. Porpandiselvi and N. Vishwanathan, "Inverter configuration for simultaneous dual frequency induction hardening with independent control," *EPE Journal*, vol. 23, no. 1, pp. 13–20, 2013.

[77] M.-S. Huang, C.-C. Liao, Z.-F. Li, Z.-R. Shih, and H.-W. Hsueh, "Quantitative design and implementation of an induction cooker for a copper pan," *IEEE Access*, vol. 9, pp. 5105–5118, 2020.

[78] W. Han, K. Chau, and W. Lam, "All-utensil domestic induction heating system," *Energy Conversion and Management*, vol. 195, pp. 1035–1043, 2019.

[79] T. Tanaka, "A new induction cooking range for heating any kind of metal vessels," *IEEE Transactions on Consumer Electronics*, vol. 35, no. 3, pp. 635–641, 1989.

Appendix

Publications

SCI International Journal Publications:

[1] Srinivas Khatroth and Porpandiselvi Shunmugam , "**Single-stage pulse frequency controlled AC-AC resonant converter for different material vessel induction cooking applications**," in *International Journal of Circuit Theory and Applications*, vol. 49, no. 9, pp. 2865-2884, 13 04 2021.
doi: 10.1002/cta.3042.

[2] Srinivas Khatroth and Porpandiselvi Shunmugam , "**Cascaded full-bridge resonant inverter configuration for different material vessel induction cooking**," in *IET Power Electronics*, vol. 13, no. 19, pp. 4428-4438, 30 12 2020.
doi: 10.1049/iet-pel.2020.0728.

Journals Communicated:

[1] Srinivas Khatroth and Porpandiselvi Shunmugam, " **Frequency Controlled Multi-Load Resonant Inverter for Different Material Induction Heating Applications**," in *International Journal of Circuit Theory and Applications*.

Conference Presentations:

[1] Srinivas K and Porpandiselvi S and P Sharath"**Pulse Frequency Controlled Resonant Inverter for Different Material Induction Cooking Loads**," in *2018 3rd International Conference on Inventive Computation Technologies (ICICT)*, pp. 744-748, 12 3 2018.
doi: 10.1109/ICICT43934.2018.9034275.

[2] Srinivas Khatroth and Porpandiselvi S and N Vishwanathan, **"Three-load Cyclic Controlled Single-Stage AC-AC Resonant Converter for Induction Cooking Applications"**, *2021 IEEE 2nd International Conference on Smart Technologies for Power, Energy and Control (STPEC)*, pp. 1-6,, 22 12 2021.
doi: 10.1109/STPEC52385.2021.9718631.

Curriculum - Vitae

Name	:	K Srinivas
Date of Birth	:	22^{nd} *August* 1985
Marital Statue	:	Married
Gender	:	Male
Contact number	:	+91 7893497136
Email id	:	srinukhitu@student.nitw.ac.in

Academic Qualifications:

Program	Institute	% of Marks	Year
M.Tech. (Control System)	National Institute of Technology Kurukshetra	7.48(CGPA)	2010
B.Tech. (EEE)	PRRM College of Engg.&technology Shabad	60.15	2007